Fall 2014

Crustal thickness and Vp/Vs beneath the Western United States: Constraints from stacking of receiver functions

Uranbaigal Purevsuren

CRUSTAL THICKNESS AND Vp/Vs BENEATH THE WESTERN UNITED STATES: CONSTRAINTS FROM STACKING OF RECEIVER FUNCTIONS

by

URANBAIGAL PUREVSUREN

A DISSERTATION

Presented to the Faculty of the Graduate School of the

MISSOURI UNIVERSITY OF SCIENCE AND TECHNOLOGY

In Partial Fulfillment of the Requirements for the Degree

DOCTOR OF PHILOSOPHY

in

GEOLOGY AND GEOPHYSICS

2014

Approved
Stephen S. Gao, Advisor
Kelly H. Liu, Advisor
Andreas Eckert
Kevin Mickus
Wan Yang

ABSTRACT

This study investigates crustal characteristics beneath the western United States. Crustal parameters, including crustal thickness (*H*), mean *Vp/Vs*, and the sharpness of the Moho as quantified by the amplitude of the P-to-S converted phases from the Moho, are measured at a total of 1000 permanent and portable broadband seismic stations using over 150,000 receiver functions recorded between 1988 and 2012. The study area is composed of a diverse set of tectonic provinces formed by a series of tectonic events, and is thus ideal for investigating crustal formation and modification by different tectonic processes. The resulting crustal thickness varies from 21 km in the Pacific Border to 57 km beneath the Rocky Mountains, with a mean thickness of 38.5±1.8 km. The *Vp/Vs* varies from 1.70 in the Great Plains to 1.90 in the Columbia River Basalt Group (north Columbia Plateau), with a mean value of 1.77±0.014. We explore relationship between crustal thickness, Vp/Vs, surface elevation, and the age of the crust, and find no positive relationship between crustal thickness and *Vp/Vs*. In addition, no clear connections between the *Vp/Vs* and the crustal age are found. High *Vp/Vs* and relatively low *R* values are observed at locations with crustal partial melts inferred by seismic tomography, such as Yellowstone, the eastern Snake River Plain, and the southeastern portion of the Rio Grande Rift. Moreover, secondary arrivals that arrive before the P-to-S conversion from the Moho and probably reflect the top of the so-called 7.xx layer, are observed beneath the Cheyenne Belt, boundary of Snake River Plain and Basin Range, as well as beneath the Wyoming craton, Colorado Plateau, and Delaware Basin.

ACKNOWLEDGMENTS

I would like to extend a great appreciation to my co-advisors, Drs. Stephen S. Gao and Kelly H. Liu, for their continuous support, guidance, and encouragement in developing my research abilities. I would also like to thank the Geology and Geophysics Program for funding my research and teaching assistantships. My appreciation goes to Dr. Kevin Mickus for his wonderful advice, and encouragement for doing my research.

I would also like to thank the rest of my advisory committee, Drs. Andreas Eckert and Wan Yang for their input, advice and patience in my research. I am thankful to Dr. Obo-Ikuenobe Franca for her generous heart. My appreciation goes to the staff members in the Department of Geological Sciences and Engineering, especially Paula Cochran for always willing to assist.

Last but definitely not least, I would like to thank my loving husband, Munkhjargal Namsraijav, and our wonderful kids, Zolboo, Khuslen, and Maraljin, for their most passionate and never ending support of my pursuit for higher and better education.

TABLE OF CONTENTS

LIST OF ILLUSTRATIONS

Figure Page

LIST OF TABLES

Table Page

NOMENCLATURE

Symbol	Description
Vp	Primary wave (compressional wave) velocity
Vs	Secondary wave (shear wave) velocity
ϕ	The ratio between Vp and Vs ($\phi = Vp/Vs$)
σ	Poisson's ratio: $\sigma=0.5[1-1/(\phi^2-1)$
H	Crustal thickness
R	Stacking amplitude of the converted Moho phases
RF	Receiver function
Ga	Billion years
Ma	Million years
PmS	Direct converted phase
PPms and PSmS	Crustal reverberations (multiples)
$t_1^{(i,j)}$	Moveout of PmS
$t_2^{(i,j)}$	Moveout of PPmS
$t_3^{(i,j)}$	Moveout of PSmS
w_1, w_2, and w_3	Weighting factors for PmS, PPmS, and PSmS

1. INTRODUCTION

Over the past several decades, a great deal of progress has been made toward understanding the nature and evolution of the different tectonic provinces within the western United States. In spite of the numerous studies, the crust beneath the western US and its properties are still not well understood. The western portion of the US offers the best region for acquiring detailed and reliable seismological information because it has an almost evenly spaced (approximately 70 km) seismic network with a great number of modern, broadband, digital seismographs (Figure 1.1). Additionally, more recent studies have clearly shown that the physical properties of the crust beneath the area vary notably among the tectonic provinces. In this study, the receiver function method is applied to study the spatial variations of crustal thickness and its properties which includes Vp/Vs and sharpness of the Moho (R).

1.1. IMPORTANCE OF RELIABLY DETERMINING CRUSTAL PROPERTIES

Numerous seismic refraction, potential field, and passive seismic investigations over the past several decades have demonstrated that determining crustal thickness, Vp/Vs, and Moho sharpness accurately is essential to understanding the evolution of tectonic regimes within the Earth's crust (Braile et al., 1974, 1982; Brown et al., 1979; Catchings & Mooney, 1988a, 1988b; Allmendinger et al., 1983; Blümling & Prodehl, 1983; Mooney et al., 1998; Gao et al., 2004; Cox & Keller, 2010; Eagar et al., 2011; Gilbert, 2012; Keller, 2013).

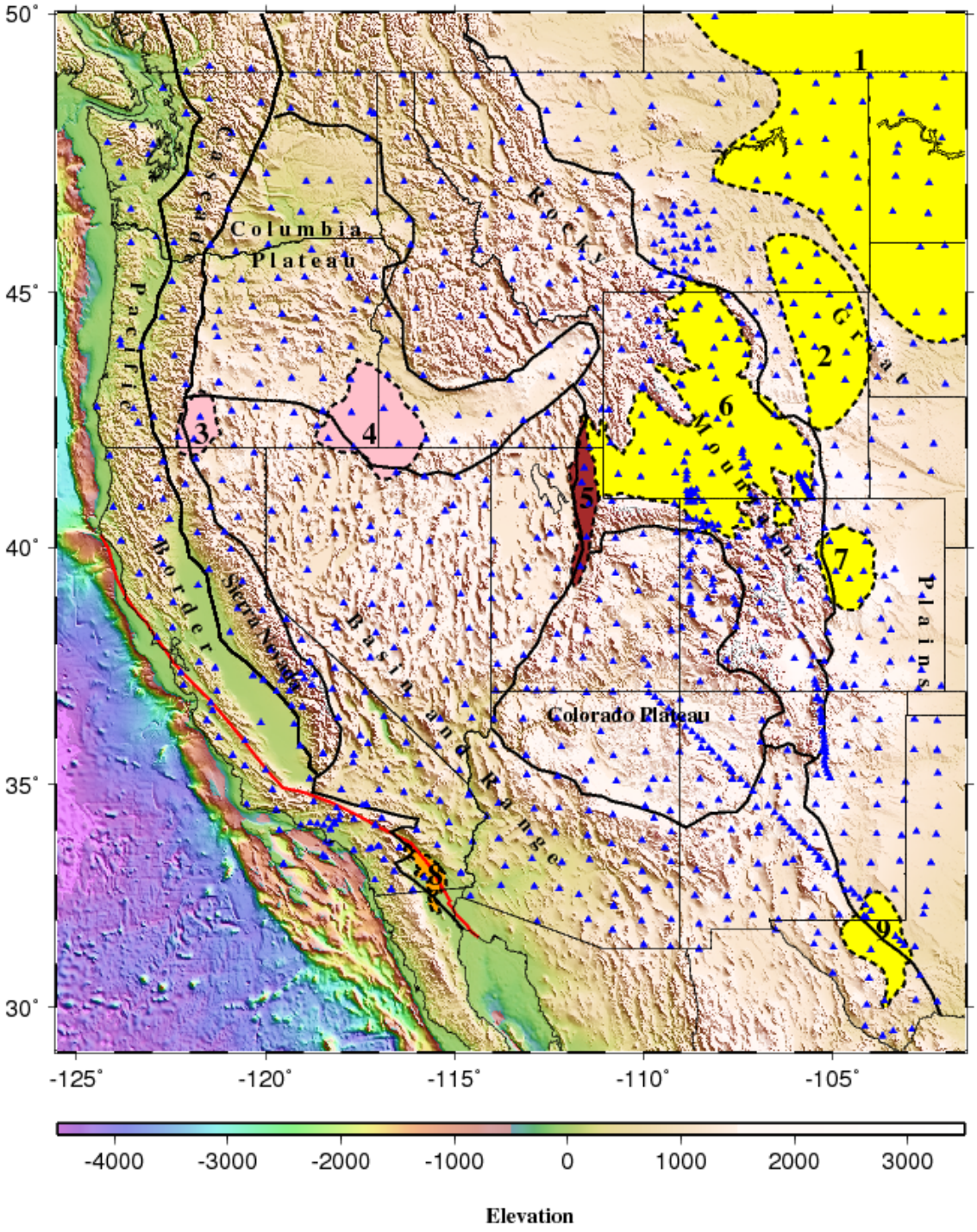

Figure 1.1. Major tectonic provinces and location of seismic stations used in the study. Blue triangles represent seismic stations and bold black lines denote boundaries of major tectonic provinces. The red line shows the San Andreas Fault, and dashed black lines represent boundaries of other tectonic features discussed in the text: 1- Williston Basin, 2- Powder River Basin, 3- Modoc Plateau, 4- Owyhee Plateau, 5- Wasatch Front, 6- Wyoming Basins, 7- Denver Basin, 8- Salton Trough, and 9- Delaware Basin.

In addition to crustal thickness, crustal Vp/Vs (Zhu & Kanamori, 2000), and the sharpness of the Moho (Nair et al., 2006; Liu & Gao, 2010) provide important additional constraints on crustal formation, structure, and evolution. Moreover, knowledge of crustal structure is a prerequisite for acquiring accurate information on the nature of the Earth's interior, below the Moho discontinuity (Anderson, 1989). Although knowledge of the crustal structure has improved significantly over the last several decades, both the origin and evolution of the crust remain an unsettled topic among researchers (Rudnick, 1995; Kearey & Vine, 1996).

1.1.1 Crustal Thickness. Previous studies indicate that crustal thickness values vary in different tectonic provinces (Table 1.1). Thickening of the crust may occur for a variety of reasons, including tectonic deformation, thermal expansion, addition of surface volcanic products, emplacement of magmatic intrusions at depth within the crust, and sedimentation (Bird, 1984; Yang & Liu, 2009). Crustal thickness decreases with age in the orogen. Thickening of the crust beneath orogen occurs primarily in the lower crust due to the lower crustal layer behaves in a ductile manner during deformation (Condie, 2011). Crustal thinning occurs by internal crustal process including lithospheric cooling or phase change, ductile flowage, subcrustal erosion, surface erosion following thermal uplift, injection of dense material, collapse of magma chambers, and lateral movements such as rifting and transverse shearing (Green, 1977; Heacock, 1977; Wernicke et al., 1988; Buck, 1991; Thybo & Nielsen, 2008).

Table 1.1. Average crustal thickness of major tectonic provinces (Mooney et al., 1998)

Province	Crustal thickness	
	Mean (km)	Standard Deviation (km)
Shield	40.77	7.04
Orogen	42.66	10.56
Arc	31.33	8.27
Platform	38.96	7.03
Extended Crust	30.54	6.03
Forearc	26.78	7.88

1.1.2 Vp/Vs. The *Vp/Vs* value provides information on both crustal composition and evolution (Zhu & Kanamori, 2000; Nair et al., 2006; Liu & Gao, 2010). The *Vp/Vs* has been proven by laboratory experiments and seismic reflection/refraction surveys (Kern, 1982; Tarkov & Vavakin, 1982; Holbrook et al., 1988; Zandt & Ammon, 1995; Christensen, 1996) to be more useful than *Vp* or *Vs* alone. This ratio is significant to study crustal properties and it depends strongly on the mean rheology. It is thus often used to describe the nature of the crust (Holbrook et al., 1988; Christensen & Mooney, 1995). The *Vp/Vs* is related to the better known Poisson's ratio $\sigma=0.5[1-1/(\phi^2-1)]$, where $\phi^2 = Vp/Vs$. The value increases if the silica content is low, while it increases if the Fe and Mg content is increased (Christensen & Fountain, 1975; Zandt & Ammon, 1995; Christensen, 1996). Tarkov and Vavakin (1982) demonstrated that the *Vp/Vs* for granitic rocks is 1.71. It is 1.78 for andesitic rocks and 1.87 for basaltic rocks. In general, an average *Vp/Vs* within the crust is 1.78. It has a range from 1.74 in the upper crust and

1.81 in the lower crust (Christensen, 1996). It is clear that *Vp/Vs* increases with crustal composition changing from felsic to mafic. Moreover, fluid content and partial melt play an important role on the *Vp/Vs*. Large *Vp/Vs* values (>1.87) are related usually to extensive crustal melting (Chevrot & van der Hilst, 2000; Reed et al., 2014).

The study of Zandt and Ammon (1995) concluded that the average *Vp/Vs* value of crust has a good correlation with crustal type. The *Vp/Vs* values in Precambrian shield are consistently high with an average of 1.84±0.005 and in platforms, the average is about 1.78±0.01 (Zandt & Ammon, 1995; Christensen, 1996). In Mesozoic-Cenozoic orogens, however, *Vp/Vs* is lower (1.73±0.01), but more variable, reflecting some combination of lithologic and thermal differences in the young orogenic crust (Zandt & Ammon, 1995; Christensen, 1996). Additionally, the *Vp/Vs* increases within the rift that corresponded by a mafic crust beneath the extension area (Daly et al., 2008). In the vicinity of subduction zones, the *Vp/Vs* values were anomalously high, probably due to the presence of water (Audet et al., 2009). Abnormally high *Vp/Vs* ratio was observed beneath the Tibetan Plateau and was explained by both partial melting and fluid content in the crust (Xu et al., 2007). The *Vp/Vs* in volcanic regions is higher than normal due to volcanic lava and magma chambers (Koulakov et al., 2011).

1.1.3 The Stacking Amplitude (R). The stacking amplitude is related to the thickness of the transition zone from crust to mantle (Nair et al., 2006; Liu & Gao, 2010). Thus it provides important clues to the geologic and tectonic processes that have been dominant in the region (Zhu and Kanamori, 2000; Gao et al., 2004; Al-Damegh et al., 2005; Nair et al., 2006; Liu & Gao, 2010). Several additional factors can influence the *R* value, including lateral velocity variations in the crust and Moho topography (Liu & Gao,

2010). Incoherent stacking caused by lateral velocity variations can reduce these values. A lower *R* value represents either a disturbed Moho or less coherently stacked *PmS* phases from deeper Moho (Andrews et al., 1985; Moidaki et al., 2013). Rapid Moho topography variations can cause the Moho converted phases to become scattered. As a result, the amplitudes are reduced (Liu & Gao, 2010).

1.2. PREVIOUS STUDIES

Numerous active-source seismic refraction/reflection, potential field, and receiver function studies have been conducted in the western US (e.g. Pakiser, 1963; Warren et al., 1973; Prodehl, 1979; Braile et al., 1989; Prodehl & Lipman 1989; Catchings & Mooney, 1991; Snelson et al., 1998; Gorman et al., 2002; Li et al., 2002; Magnani et al., 2004; Keller et al., 2005; Frassetto et al., 2006; Rumpfhuber et al., 2009; Keller, 2010; Bashir et al., 2011; Cox & Eager et al., 2011). These investigations suggested significant variations in crustal characteristics beneath the western US.

1.2.1 Seismic Refraction/Reflection Studies. Seismic crustal refraction studies were conducted within the western US with emphasis on the Basin and Range, Colorado Plateau, middle Rocky Mountains, Yellowstone National Park, and adjacent eastern Snake River Plain.

An average crustal thickness of 29-30 km was found beneath the Coast Range in California (Warren, 1981; Blümling & Prodehl, 1983; Walter & Mooney, 1987). Blümling and Prodehl (1983) used local earthquake data with an existing seismic refraction data recorded in 1967 (Stewart, 1968) for their interpretation. Seismic refraction profiles were carried out along the San Andreas Fault (Catchings & Kohler,

1996). They concluded that the crustal thickness beneath the San Francisco Bay Area is 22 km. Another study combining active-source refraction and earthquake data in the western foothills of the Sierra Nevada (Spieth et al., 1981) concluded that the crustal thickness averages 39 km beneath the study area.

Leaver et al. (1984) interpreted data from seismic refraction investigations performed by the United States Geologic Survey (USGS) and data from regional earthquakes recorded in northern Oregon and Washington. Their interpretation concluded that the crustal thickness beneath the Oregon Cascades is about 45 km. USGS had continued the investigation of the Oregon Cascades, from the eastern High Cascades to the eastern High Lava. Crustal thickness was determined as 37 km and magmatic underplating was inferred (Catchings & Mooney, 1988b) beneath the study area.

Crustal thickness beneath the Willamette Lowland of the Cascadia Range was imaged as 45-50 km by previous seismic surveys using the refracted phase and wide-angle reflections studies (Tre'hu et al., 1994). This crustal thickening occurred along the subduction zone was interpreted as the incorporation of a block of oceanic crust within the accretionary prism. Wide-angle seismic studies across the Columbia Plateau in southern Washington (Parsons et al., 1998, 1999) concluded that alternating thinning and thickening along the Washington coast may result from folding and imbrications of the Siletz terrain. They observed a crustal thickness of 35-45 km beneath the Cascade Range, with thinner crust of 30-35 km east of the volcanic arc beneath the Columbia Plateau flood basalt province. Gerdom et al. (2000) used data recorded by two profiles located near 44.7^{0}N and interpreted that the Moho is at 30 km depth.

The USGS conducted a seismic survey to characterize crustal structure beneath northeastern California including the Cascade Range, Modoc Plateau, and Basin and Range (Zucca et al., 1986; Fuis et al., 1987; Mooney & Weaver, 1989; Schultz & Crosson, 1996). They found that the Moho is about 38 km deep under the Modoc Plateau (Figure 1) and is underlain by a basement of granitic and metamorphic rocks that are the roots of an ancient arc similar to that of the Sierra Nevada. Although southern Oregon and northern California are underlain by a stack of oceanic layers and the Moho beneath the area has not been reliably determined, they interpreted that a complex suture zone between the Modoc Plateau and Kalamath crust occurs beneath the Cascade Range. The crustal thickness estimation beneath it was 38-40 km.

During the Mendocino Triple Junction experiment, offshore multichannel seismic (MCS) reflection data were collected and combined interpretation with gravity data indicated a crustal thickness ranging from 20 km near the coast to 27 km at the east side of the Coast Ranges (Henstock et al., 1997; Leithner et al., 1998; Henstock & Levander, 2000).

The Bay Area Seismic Imaging Experiment (BASIX) comprised three complementary seismic methods including high-resolution reflection profiling, wide-angle reflection/refraction profiling, and multichannel seismic profiling (Hollbrook et al., 1996; Hole et al., 2000). The studies found a 25 km thick crust beneath the Bay Area and lateral variations of the velocity contrasts from upper to lower crust. The contrasts are correlated with surface faults, indicating changes in the depth of the mafic lower crustal layer.

The Southern Sierra Nevada Continental Dynamics (SSCD) project recorded seismic refraction data along lines in central California. The SSCD interpretation imaged crustal root of 40-42 km beneath the area east of the Sierra Nevada crest. The observed crustal thickness decreases to less than 25 km at the coast and to 30-35 km in the Basin and Range Province (Wernike et al., 1996; Ruppert et al., 1998; Fliedner et al., 2000).

In the Basin and Range Province, the USGS conducted seismic refraction studies to investigate regional crustal structure at a possible nuclear waste repository site near the Yucca Mountain (Hoffman & Mooney, 1983; Brocher et al., 1996). The results showed that the average crustal thickness beneath the study area is 35 km and excluded the existence of a lower-crustal magma chamber. A 340 km seismic refraction profile that crossed the Basin and Range-Middle Rocky Mountains in northern Utah (Braile et al., 1974) indicated that crustal thickness beneath the eastern Basin and Range averages 28 km and it thickens to 40 km beneath the Middle Rocky Mountains. An average crustal thickness of 43 km was observed beneath the neighboring Yellowstone Plateau (Smith et al., 1982).

In the Rio Grande Rift, numerous studies (Keller et al., 1979; Olsen et al., 1979; Olsen, 1983; Sinno et al., 1986; Prodehl & Lipman, 1989) revealed that the crust beneath the rift axis is 34 km, which is 10-15 km thinner than the crust beneath the adjacent Great Plains and Colorado Plateau. An upward warping of the Moho beneath the Rio Grande Rift was observed (Keller et al., 1979; Gish et al., 1981; Sinno et al., 1981) and the crust thins rapidly from near 37 km to less than 25 km toward the south.

Seismic refractions profiles were recorded in the Colorado Plateau Hanksville-Chinle (Roller, 1965), Gila Bend-Surprise, and Blue Mountain-Bylass (Warren, 1969).

Thei results suggested that the crustal thickness averages 40-43 km beneath the Colorado Plateau. Hauser and Lundy (1989) combined their seismic reflection data with the previous refraction data and interpreted that the Moho is at least 50 km deep beneath the Colorado Plateau. The Pacific to Arizona Crustal Experiment (PACE) also carried out along profiles in the Colorado Plateau and Grand Canyon (Wilson & Fuis, 1987; McCarthy et al., 1991; Wilson et al., 1991; Wolf & Cipar, 1993) and concluded that the average crustal thickness is 45±3 km.

The Deep Probe experiment (Henstock et al., 1998; Snelson et al., 1998; Gorman et al., 2002) and Continental Dynamics-Rocky Mountain (CD-ROM) study (Keller et al., 1999; Karlstrom & CD-ROM Working Group, 2002; Karlstrom et al., 2005; Snelson et al., 2005) aimed to conduct a detailed crustal and upper mantle study beneath the Wyoming Province, Southern Rocky Mountains and the Colorado Plateau. Their result showed that the crustal thickness beneath the Wyoming Province ranges between 49 and 60 km, includes a 10-30 km thick high velocity lower crustal layer. Beneath the southern Rocky Mountains, it varies between 40 and 50 km with a 10-15 km high velocity lower crustal layer. Crustal thickness increases from ~45 km under New Mexico to 55 km in Central Colorado and thins 40-45 km under southern Wyoming. The southern transect of the CD-ROM profiling under the Jemez Lineament observed crustal thickness of 40-43 km south of Las Vegas and 33-35 km to the north (Magnani et al., 2005).

In the Great Plains province, several seismic-refraction surveys were conducted (Jackson et al., 1963; McCamy & Meyer, 1964; Mithchell & Landisman, 1970). An average crustal thickness of 48 km was observed along a line trending north from Lamar, Colorado to Sidney, Nebraska, and 46 km near Tulsa, Oklahoma (Ramesh et al., 2002;

Gilbert & Sheehan, 2004; Wilson et al., 2005; Frassetto et al., 2006; Gilbert et al., 2007; Gilbert, 2012).

Recently, Keller (2013) compiled controlled source and passive source investigations for crustal thickness studies of North America and indicated that little or no continental crust may remain under the Salton Trough in California. The western Idaho shear zone was affected by multiple episodes of magmatism since initial accretion was occurred. An unusually thick crust of more than 50 km was observed beneath the Archean Wyoming Province. This thicker than a typical craton thickness is due to the existence of a fast and thick lower crustal layer (the 7.xx layer).

1.2.2 The Consortium for Continental Reflection Profiling (COCORP). The large-scale continental reflection studies (e.g. Oliver & Kaufman, 1976; Brown et al., 1979; Brewer et al., 1980; Brewer et al., 1982; Allmendinger et al., 1983, 1987;) investigated the Earth's crust in great detail by applying vertical-incidence reflection profiling and applied seismic processing and interpretation for imaging the whole crust. Results from two deep seismic reflection profiles recorded by COCORP in the Oregon Coast Range concluded that eastward dipping reflections at depths of 35-40 km may represent the decollement above the subducting Juan de Fuca plate (Keach et al., 1989). The COCORP 40^0 N transect (Allmendinger et al., 1987; Hauser et al., 1987b) detected the Moho at 30 km beneath the Basin and Range and at 48 km underneath the Colorado Plateau. The refraction profiling in the western and northern Mojave Desert of California exposed that the crustal thickness is 33 km in the north and 26-29 km in the south of the survey area (Cheadle et al., 1986). The COCORP study across the Rocky Mountains (Smithson et al., 1979; Brewer et al., 1980, 1982; 1989) concluded that the crust beneath

the Rocky Mountains is 40-50 km and the mountain ranges are apparently underlain by moderately dipping thrust faults. The Death Valley COCORP seismic study determined a crustal thickness of about 30 km. Hauser et al. (1987a) found non-reflective Moho beneath the Colorado Plateau and they interpreted that the development of reflectors at the Moho was clearly influenced by extension and associated igneous processes. COCORP beneath the Rio Grande Rift (Brown et al., 1979; Oliver & Kaufman, 1976) determined a crustal thickness of 35 km and they proposed a magma body in the Socorro area at the depth of about 20 km. The Moho beneath the Williston basin was found at the depth of 39-45 km and is characterized by a strong reflectivity. However, west of the Williston basin the base of the crust is characterized by a relatively abrupt decrease in reflectivity (Latham et al., 1988).

1.2.3 Receiver Function Studies. RF studies (Baker et al., 1996; Ichinose et al., 1996; Jones and Phinney, 1998; Lewis et al., 2000; Zhu and Kanamori, 2000; Yan & Clayton, 2007) using existing dense network in the southern California revealed an average crustal thickness of 29 km, ranging from 21 to 37 km. Deeper Moho was found underneath the eastern Transverse Range, the Peninsular Range (36-41 km) and the Sierra Nevada, where the batholiths is relatively intact. Crust thins (26-32 km) beneath the Mojave Province, where the batholith is highly deformed and disturbed. The thinnest crust was observed beneath the Inner California Borderland (21-22 km) and Salton Trough (22 km). Depth to the Moho is 33±3 km near the Pacific coast of Baja. Ovearll, the lack of correlation between topography and Moho depths suggested lateral density variation in the lower crust or upper mantle (Ichinose et al., 1996).

The analysis of RFs from 206 broadband stations within the High Lava Plains (HLP) and surrounding regions revealed significant variations in crustal thickness and crustal composition beneath the area (Eagar et al., 2011). The results revealed an average crustal thickness of 42.3 ± 1.2 km beneath the Cascade volcanic arc, about 25 km beneath central HLP and about 35 km beneath the western Snake River Plain/southern Idaho Batholith (Eagar et al., 2011). They also suggested the existence of about 2% partial melt beneath HLP corresponding to both abnormally high Poisson's ratios (~0.32) and a low-velocity zone.

The Basin and Range Province and its surroundings were investigated by numerous receiver function studies (Özalaybey et al., 1997; Sheehan et al., 1997; Peng & Humphreys, 1998, 1998). Özalaybey et al. (1997) used an inversion method that takes the advantage of average velocity information in the surface-wave method and differential velocity information contained in the receiver function method, thus minimizing the non-uniqueness problem that results from the velocity-depth trade-off. Their observation found a high velocity crust with a normal thickness of 38 km beneath central and eastern Nevada, in contrast to the thin and slower crust beneath the western Basin and Range. Peng and Humphreys (1998) used RFs recorded at 36 stations along a northwest oriented profile centered on the eastern Snake River Plain. Their results revealed that the Moho depth is 42 km beneath the Snake River Plain, shallows to 37 km to either side, and thickens abruptly to 47 km beneath southwestern Wyoming. A low velocity layer was found beneath the southeast part of the Snake river Plain, probably indicating partial melt of the lowermost crust.

Several receiver function studies in the western Cascadia, Colorado Plateau-Basin and Range, and Rocky Mountain Front were carried out using portable seismic arrays. The Western Cascadia experiment (Rondenay et al., 2002) used the method that developed by Bostock et al. (2002) to image lithospheric structures using teleseismic *P* wave coda recorded on dense arrays of seismometers. They determined that the crustal thickness is 35-40 km beneath the Western Cascades. Crustal structure beneath Corvallis, Oregon was studied by teleseismic *P* and *S* travel times determined from the converted phase. The Moho depth was determined at 45 km beneath the study area (Langston, 1977).

The Colorado Plateau-Great Basin experiment analyzed RFs using frequency domain deconvolution of the vertical component *P*-wave from the radial components *P*-wave (e.g. Owens et al., 1984). Crustal thickness of 35±5 km beneath the Great Basin (with a strong Moho conversion) and 42±5 km beneath the Colorado Plateau (with a weaker Moho conversion) were observed.

The Rocky Mountain Front experiment was carried out from the Great Plains of Kansas, across the Colorado Rocky Mountains, and into the eastern Colorado Plateau. The RFs were calculated using a time domain deconvolution approach and the crustal thickness was determined by a grid-search comparison of observed receiver functions with synthetics. The grid-search technique allows visualization of the trade-offs inherent in receiver functions in order to select the best model (Sheehan et al., 1995). They determined an average crustal thickness of 43.8±0.4 km, 49.9±1.2 km, 50.1±1.3 km and 43.1±0.9 km beneath the Kansas Great Plains, Colorado Great Plains, Colorado Rocky Mountains, and northeast Colorado Plateau, respectively.

The receiver function study by Rumpfhuber et al. (2009) tied the Continental Dynamics of the Rocky Mountains and Deep Probe seismic experiment. The RF study includes 24 broadband seismic stations, located along the northern transect of the CD-ROM experiment, with a spacing of about 10 km and recorded for 1 year. To compute RFs they used an iterative deconvolution technique of Ligorria and Ammon (1999), which represents an extended version of the frequency domain division into the time domain. They concluded that the average crustal thickness along the CD-ROM northern transect is about 51 km and the Vp/Vs ratio is 1.762.

Several RF studies using broadband seismic data (Zandt et al., 1995; Gilbert & Sheehan, 2004; Wilson et al., 2005; Frassetto et al., 2006; Gilbert et al., 2007; Wilson et al., 2010; Bashir et al., 2011; Gilbert, 2012) were conducted in the Colorado Plateau and the Basin and Range Province. The thickest crust of 45-50 km was observed beneath the Rocky Mountains and High Plains in Colorado. The RF study of Bashir et al. (2011) suggested crustal thinning beneath the Basin and Range. Similar to previous studies, the study of Bashir et al. (2011) suggested that a thin crust of about 30 km is inadequate to support the high elevations of some metamorphic core complexes. The thick crust of 42.3 ± 0.8 km beneath the Colorado Plateau was corresponding to a high velocity lower crustal layer (Bashir et al., 2011). The *Vp/Vs*, reliably determined from RFs stacking (Bashir et al., 2011) shows a mean of 1.761 ± 0.014 for the Basin and Range and 1.825 ± 0.009 for the Colorado Plateau.

RFs analyses were conducted at evenly sampled stations of the Transportable Array component of the Earthscope USArray, within the western United States (Gilbert, 2012). In this study, the iterative deconvolution method (Ligorria & Ammon, 1999) was

used to isolate *P*-to-*S* conversion on the radial component. A constant *Vs* of 3.8 km/s and a fixed *Vp/Vs* of 1.74 was utilized for stacking the RFs to generate the map of crustal thickness. The RF results revealed a crustal thickness of ~40 km along the Snake River, which is distinct from the High Lava Plains and surrounding Rocky Mountains and Basin and Range (35km). The crust thickens to >35 km in southern Nevada and thins to nearly 30 km beneath the northern Basin and Range. Large crustal thickness beneath the Colorado Plateau (40-50 km) and the Bouguer gravity anomaly suggested that the source of buoyancy comes from the mantle (Gilbert, 2012).

The Earth Scope Receiver Survey (EARS) uses the H-k stacking technique of Zhu and Kanamori (2000) to automatically measure the crustal thickness and Vp/Vs across the continental US, using the Incorporated Research Institute for Seismology (IRIS) Data Management Center (DMC) waveform archive. Their estimation of crustal thickness ranges from 18 to 66 km and Vp/Vs varies between 1.60 and 2.10 (http://www.iris.edu/dms/products/ears/) beneath the western US.

Most of the previous receiver function studies interpreted the crustal structure and evolution based primarily on crustal thickness measurements, while several other studies (e. g. Sheehan et al., 1995; Gilbert & Sheehan, 2004; Gilbert et al., 2007; Rumpfhuber et al., 2009; Bashir et al., 2011; EARS) also utilized Vp/Vs. Most of the previous studies were performed with limited data.

1.3. TECTONIC SETTING AND HISTORY OF THE STUDY AREA

Assembly of the Laurentian Shield, the core of the North American continent, occurred in 2.4-2.0 Ga (Hoffman, 1988; Whitmeyer & Karlstrom, 2007). Since then, a series of tectonic events ranging from Proterozoic orogenesis (Whitmeyer & Karlstrom,

2007), Jurassic Farallon plate subduction and its flattening in the late Cretaceous to early Tertiary (Saleeby, 2003), Cretaceous Sevier Orogeny (DeCelles, 2004), Late Cretaceous Laramide Orogeny (Bird, 1988) to Cenozoic uplift of the Colorado Plateau (Liu &Gurnis, 2010), and Late Cenozoic Basin and Range extension (Menges & Peartree, 1989), have played a significant role in the development of the western North American continent. These tectonic events could have influenced crustal structure and composition.

Tectonically, the study area includes the subduction zones in the Pacific Northwest, a major strike-slip plate boundary in California (the San Andreas Fault), wide continental extension in the Basin and Range Province, Rocky Mountains, and Great Plains, which is a wide area of flat land (Figure 1.2). Those provinces are distinguished by their surface elevation, crustal thickness, crustal composition, tectonic deformation, heat flow, Poisson's ratio, and Bouguer gravity anomalies (Lachenbruch & Sass, 1977; Christensen, 1996; Frassetto et al., 2006).

1.3.1 Precambrian. During the Proterozoic Eon (2.4-2.0 Ga), the Canadian Shield was assembled by collisions of Archean continents and terranes (Whitmeyer & Karlstrom, 2007). Later (2.0-1.8 Ga), it grew as island arcs such as Thelon, La Ronge, Torngat, Little Belt, and Great Bear arcs which were accreted to the Wyoming Province (Bowring & Karlstrom, 1990; Whitmeyer & Karlstrom, 2007). Proterozoic lithosphere accreted to this passive margin from about 1.8 - 1.0 Ga, which continued the formation of the North American craton (e.g., Hoffman, 1988). This accretionary event collapsed the passive margin at the southwestern edge of the Wyoming craton and created the Cheyenne belt suture (e.g., Karlstrom & Houston, 1984; Chamberlain et al., 1993) near the present Colorado-Wyoming border (Figure 1.2).

The Mojave Province, deformed plutons with ages of 2.1-1.2 Ga intruded supracrustal rocks, is underlain mainly by Mesozoic granitoids and metamorphic rocks (Bennett & DePaolo, 1987; Wooden et al., 1988; Chamberlain & Bowring, 1990; Wooden & Miller, 1990; Anderson et al., 1991). The Mojave Province is clearly defined by the San Andreas and Garlock faults (Burchfiel & Davis, 1981). Since mid-Miocene, a combined effect of lateral displacement along both faults has resulted in a north-south compressive regime (Bohannon & Howell, 1982).

The northeast trending Yavapai and Mazatzal terranes (Figure 1.2), which were created by Middle Proterozoic (1.8-1.6 Ga) tectonic events, involved numerous tectonic pulses including accretion, back-arc spreading, and continental margin volcanic arcs (Bickford et al., 1986; Karlstrom & Bowring, 1993; Whitmeyer & Karlstrom, 2007). Both the Yavapai and Mazatzal provinces are divided by major shear zones that are indicative of continuous deformation during Precambrian time. The majority of the Yavapai province consists of Juvenile crustal materials while the majority of the Mazatzal province consists of supracrustal rocks (e.g., Karlstrom & Bowring, 1988, 1993).

The Grenville orogen associated with continent-continent collision of Laurentia with African and South American cratons took place at 1.3-1.0 Ga (Wynne-Edwards, 1972). The western North America has undergone periodic rifting events that terminated in separation of North America from the western (Rodinian) continent between 1.0 and 0.6 Ga. It is preserved as part of the Great Unconformity (Karlstrom & Humphreys, 1998). During this time the extension created a passive margin along the western margin of North America, opening a proto-Pacific basin (e.g., Parsons, 1995).

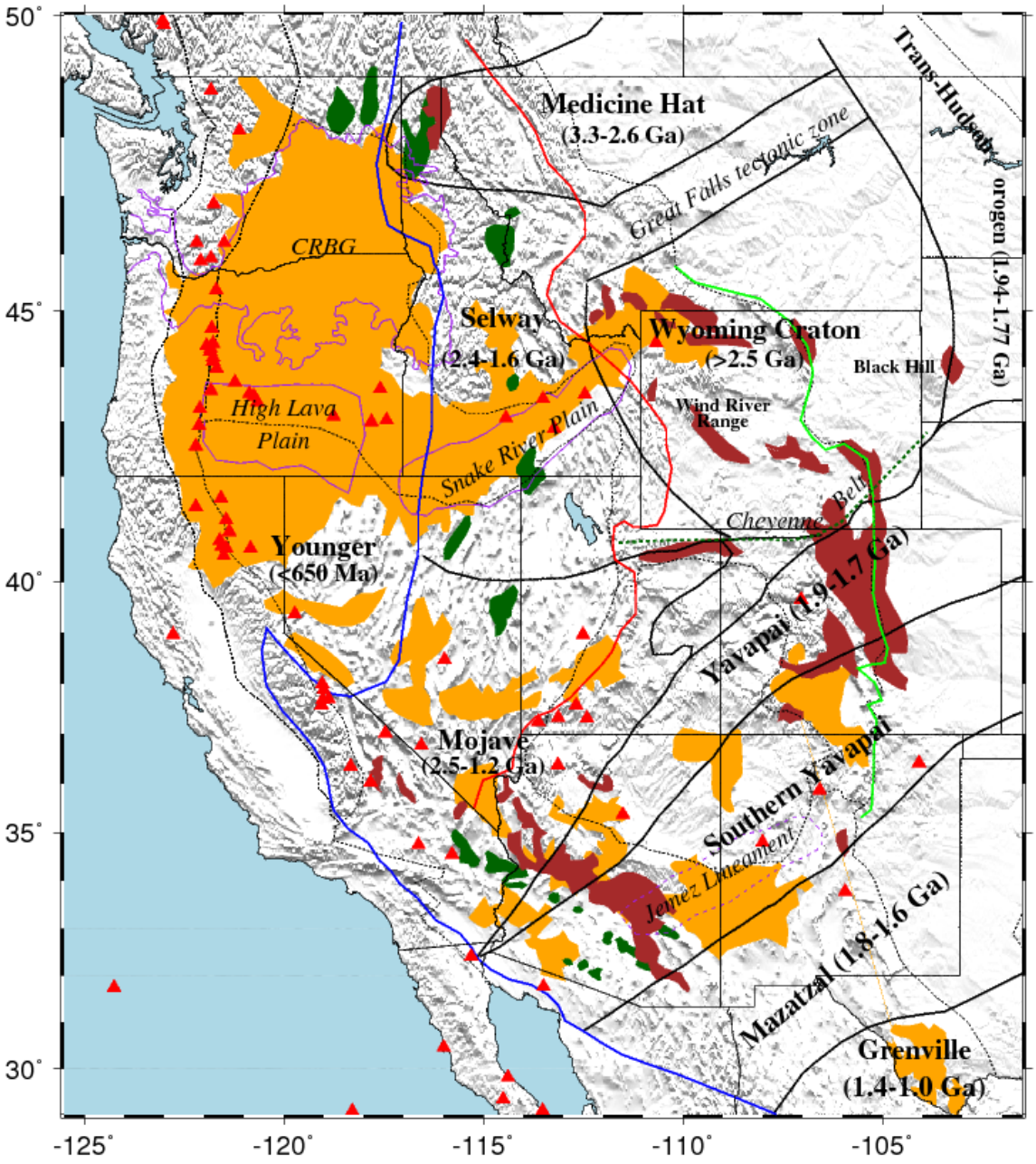

Figure 1.2. Major ancient terranes and their ages. Bold black lines show boundary of ancient terranes. Dashed lines represent present tectonic provinces. Orange areas denote volcanic fields. Green areas show metamorphic core complexes (MCC). Brown areas are Precambrain outcrops. The bold blue line indicates the western Margin of North America that rifted away from Precambrian supercontinent at about 650 Ma. The bold red line is the Sevier belt. The bold green line is Laramide orogeny, and red triangles show volcanoes. CRBG-Columbia River Basalt Group (Faulds & Vagra, 1998; Karlstrom and Humphreys, 1998; Gilbert, 2012).

1.3.2 Paleozoic-Mesozoic. During the Cambrian-Devonian time, the Rocky Mountain region was primarily under shallow marine environment with some uplifts and deep basins (Kluth & Coney, 1981). During middle Devonian-Mississippian, the Antler orogeny caused compressional deformation in western North America (Parsons, 1995). Precambrian rocks were uplifted to form Ancestral Rocky Mountains in Colorado and New Mexico during the Pennsylvanian time (Kluth & Coney, 1981).

During the Permian time, linear basins were formed west of the Antler orogenic belt, due to back-arc extension (Parsons, 1995). Major tectonic events during this time were concentrated along the cratonic boundaries (Sloss, 1988). Lack of major tectonic events and magmatism east of the Sevier belt possibly suggests that cratonic development was dominated by crustal deformation but not major mantle modification. Paleozoic platforms remained nearly flat until the late Cretaceous Laramide orogeny initiated (Karlstrom & Humphreys, 1998).

From late Triassic (~210 Ma) to Cretaceaous (~85 Ma), an increase in plutonic and volcanic activities created batholiths such as the Sierra Nevada (Bateman, 1988). The large volume of Cretaceous intrusions migrated eastward from western Sierra Nevada at a rate of 2.7 mm/yr. This slow and constant migration of the intrusions terminated abruptly, which may indicate an increase in the rate of convergence between the North American and eastern Pacific Plates and dramatic flattening of the subduction (Chen & Tilton, 1982).

The Laramide orogeny (75-45 Ma) overlapped with the Sevier orogeny (90-60 Ma) in time and regions. It affected the western US due to flattening of the Farallon plate subduction. The western United States orogenic plateau initially elevated during

Laramide (Bird, 1979). The Sevier orogeny is considered as a thin-skinned deformation where only the upper crust consisting of Proterozoic to Mesosoic sequences was deformed to create the Cordilleran thrust system (Allmendinger, 1992). In contrast, the Laramide (Late Cretaceous to Miocene) is a thick-skinned deformation which thickened not only the upper crust but also lower crustal (Bird, 1988; Erslev, 1993) and initiated the Rocky Mountain Foreland Uplift. The Sevier-Laramide tectonic events initiated broad uplift in the entire western US, but the increasing in crustal thickness is not sufficient to explain this uplift. Therefore, the Sevier-Laramide orogeny maybe also responsible for increasing the buoyancy of the upper mantle (Karlstrom & Humphreys, 1998). During the Laramide orogeny, a significant crustal thickening event took place beneath the Rocky Mountain Foreland and the Great Plains. Before the Sevier-Laramide orogeny, the crust beneath the Great Plains was likely as thick as normal continental crust. The low-angle subduction of the Farallon slab beneath the western US might provide basal shear stress leading to thickened crust beneath the Great Plains (Bird, 1984). Normal arc magmatism continued from the north Cascades across eastern Washington, Idaho, western Montana, and northeastern Wyoming during the Laramide orogeny (Christiansen & Yeats, 1992). At the same time, the Colorado Plateau was compressed against North America (Hamilton, 1989; Saleeby, 2003) and northeast directed shortening occurred beneath it (Varga, 1993; Erslev, 2005).

1.3.3 Cenozoic. During the Cenozoic collapse of the orogenic event, the lithosphere in the current Basin and Range area experienced extension. This widespread extension was driven by gravitational collapse, possible contraction of the initiation of the Farallon plate foundering, upwelling of the asthenosphere, and resulting magmatic

heating (Coney & Harms, 1984; Hodges & Walker, 1995; Humphreys, 1995). The width of the Basin and Range Province extension was doubled (Wernicke et al., 1988). The extension led to the formation of the metamorphic core complexes (MCCs) which are exhumed metamorphic and igneous rocks in the previously over thickened crust (Coney & Harms, 1984). Numerous studies (Lachhenbruch & Sass, 1978; Zandt et al., 1995; Frassetto et al., 2006; Gilbert et al., 2007; Bensen et al., 2009; Buehler & Shearer, 2010) indicated that the BRP is characterized by high heat flow, low elevation, low upper mantle seismic velocities, and thin crust. The gravitational collapse affected not only the BRP but also the Rio Grande Rift (Wernicke et al., 1988). The rift was localized along a zone of extension and the Laramide strike-slip faulting. At the same time, the Colorado Plateau may have initiated. Most of the studies proposed that 2 km (above sea level) uplift of the Colorado Plateau initiated at the same time period as the BRP extension occurred (Spencer, 1996; Sonder & Jones, 1999; Roy et al., 2009; Liu & Gurnis, 2010). However, the timing of the uplift of the Colorado Plateau is still in debate.

During the early Oligocene (~30 Ma), when the western edge of North America gradually encountered and overrode the divergent boundary separating the Farallon and Pacific plates, the Pacific and North American Plates began to interact (Severinghaus & Atwater, 1990). The Juan de Fuca plate, a remnant of the Farallon plate, has been subducting beneath the northwestern US since 10 Ma (Severinghaus & Atwater, 1990).

1.4. RATIONALE OF THE STUDY

This study is motivated by several aspects, such as the large number of seismic stations within the study area, the high quality data recorded at these stations, the need for

a uniform dataset of crustal thickness and *Vp/Vs* measurements, and in-depth investigations of both stacking amplitude (*R)* of *P-to-S* converted phases and their multiples. In fact, none of the previous studies within the western US determined *R* values, which are efficient in providing additional information about the structure and evolution of the crust, particularly in areas with potentially magmatic underplating and other forms of magmatic modification of the original crust (Nair et al., 2006; Liu & Gao, 2010).

In spite of numerous studies, the formation and evolution of the continental crust is still poorly understood. This study uses a high quality data set recorded at the EarthScope Transportable Array and other broadband seismic stations to investigate the spatial distribution of crustal thickness *(H), Vp/Vs*, and *R* values and to address several important issues such as the relationships between crustal thickness, Vp/Vs and the age of the tectonic provinces. The western United States is an ideal locale to provide constraints for the important issues. The existence of several crustal terrains and provinces with different ages (Figure 1.2) in the study area may give us a better understanding about not only structure of the continental crust but also its evolution over time.

2. DATA AND METHODS

2.1. DATA

The three-component broadband teleseismic data set used for this study was requested from the IRIS DMC. Within the study area (29.00^0N to 50.00^0N and -124.00^0E to -102.00^0E), a total of 1007 stations (Figure1) have available data at the time when the data were requested. Most of the stations belong to TA (EarthScope Transportable Array) and the others belong to AR(Northern Arizona Network), BK (Berkeley Digital Seismograph Network), CI (Caltech Regional Seismic Network), EP (UTEP Seismic Network), G (GEOSCOPE), GS (US Geol. Sur.Networks), II (Global Seismograph Network), IM (International Miscellaneous Stations), IU (IRIS/USGS Network), IW (Intermountain West), SC (New Mexico Tech Seismic Network), TS (TERRAscope), US (United States National Seismic Network), XC (Yellowstone Intermountain Seismic Array), XE (Sierra Nevada EarthScope Project- EarthScope Flex Array), XF (Laramie Telemetered Broad-band Array), XG (Rocky Mountain Front), XK (CD-ROM), XL (Consortium for Arizona Reconnaissance Seismic Experiment), XM (Rio Grande Seismic Transect-LA RISTRA), XR (Florida to Edmonton Seismic Experiment), XS (Montana BB Array), XT (Colorado BB Array – Lodore), and XV (Bighorn Arch Seismic Experiment), and Z2 (NOISY). There are 636 TA stations which have a nominal spacing of 70 km. Data from earthquakes with epicentral distances from 30^0 to 180^0 were requested from the IRIS DMC for the study. The cut-off magnitude (Mc) was calculated using (Liu & Gao, 2010):

$$Mc=5.2+(D_e-30.0)/(180.0-30.0)-H_f/700.0 \quad (1)$$

where D_e is the epicentral distance in degree and H_f is the focal depth in km. The resulting M_c ranges from 4.2 (for events with D_e = 30° and H_f = 700 km) to 6.2 (for events with De = 180° and H_f = 0 km). The parameters used in this equation are determined from numerous tests and aimed at balancing the quantity and quality of the seismic data to be requested (Liu & Gao, 2010). The broadband, high-gain data of all the events that satisfy the above criteria for M_c from different epicentral distances and focal depths were requested. The seismograms were windowed to start at 20 s before and 360 s after the first P-wave arrival, calculated using the IASP91 earth model. The seismograms were band-pass filtered in the frequency band of 0.08 - 0.8 Hz to enhance the signal. The events having a signal to noise ratio (S/N) of 4.0 or greater on the radial component were selected. The selected seismograms were converted into radial receiver functions using the procedure of Ammon et al. (1991). A total of 151,487 high quality RFs were used for the study.

2.2. STACKING OF THE RECEIVER FUNCTIONS

Teleseismic *P*-wave receiver function analysis is a widely used tool for detecting velocity discontinuities beneath isolated receivers or under receiver arrays (Langston, 1977). RFs have been used to study the Moho depth and the ratio of crustal *P* and *S* wave velocities (Zhu & Kanamori, 2000; Gao et al., 2004; Nair et al., 2006) and other upper mantle and mantle transition zone seismic discontinuities (Vinnik & Montagner, 1996; Zorin et al., 2002; Liu et al., 2003; Liu & Gao, 2006; Gao & Liu, 2014).

A receiver function can be calculated by deconvolving the vertical component from the radial component for a given event (Phinney, 1964; Langston, 1977; Ammon et al., 1990; Sheehan et al., 1995; Dueker & Sheehan, 1998; Ramesh et al., 2002; Gilbert et al., 2003). Primary conversion (*PmS* or *Ps*) and multiple phases (*PPmS* which is also called *PpPs* and *PSmS* which is also known as *PpSs*) can frequently be observed (Figure 2.1). Multiples are weaker than the *Ps* wave and therefore they are occasionally hard to be recognized (Yuan et al., 2002). Crustal thickness and the average crustal V_p/V_s ratio can be estimated by utilizing both the *Ps* and crustal multiples (Zhu & Kanamori, 2000).

A grid search using a stacking method developed by Zhu and Kanamori (2000) is used to determine crustal structure from observed receiver functions. This method stacks receiver functions by varying the crustal thickness *H* and *Vp/Vs*. For a given candidate pair of *H* and *Vp/Vs*, the arrival times of the *PmS, PPmS,* and *PSmS* phases are calculated for each receiver function, using the ray parameter of the event. The stack is produced by summing the amplitudes of each receiver function at each of these travel times.

The stacking was done using the equation:

$$A(H_i, \phi_j) = \sum_{k=1}^{n} w_1 S_{k\left(t_1^{(j,j)}\right)} + w_2 S_{k\left(t_2^{(i,j)}\right)} - w_3 S_{k\left(t_3^{(i,j)}\right)} \qquad (2)$$

where the weighting factors w_1, w_2, and w_3 are related to *PmS, PPmS,* and *PSmS* respectively and the sum of the factors equals to 1. t_1, t_2 and t_3, are predicted arrival times of *PmS, PPmS,* and *PSmS* phases, respectively, which can be calculated using (Nair et al., 2006).

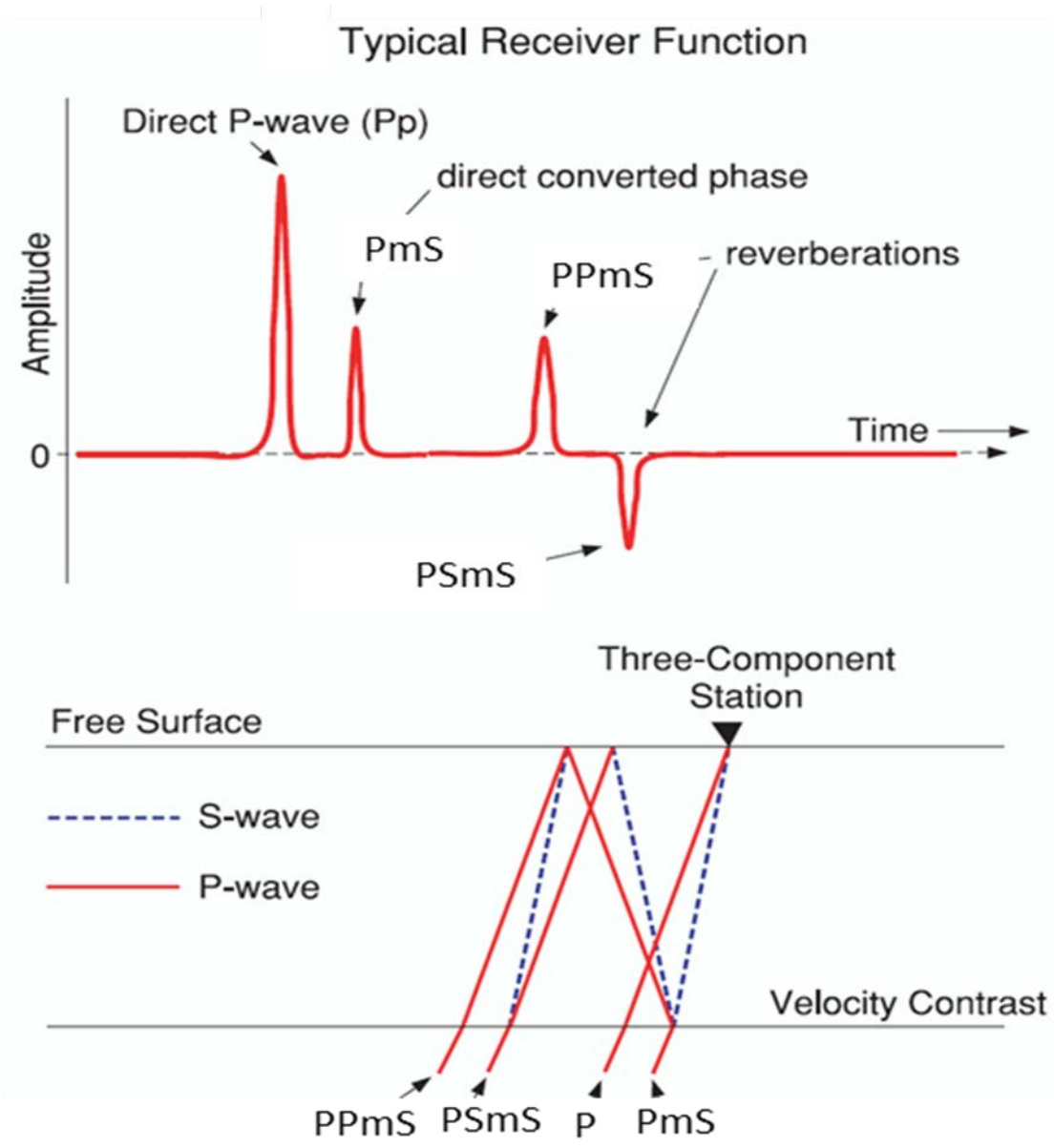

Figure 2.1. The amplitudes and ray paths of the major converted *PmS* wave and multiples. http://eqseis.geosc.psu.edu/~cammon/HTML/RftnDocs/rftn01.html.

$$t_1^{(i,j)} = \int_{-H_i}^{0} [\sqrt{(V_p(z)/\phi_j)^{-2} - p^2} - \sqrt{V_p(z)^{-2} - p^2}]dz \quad (3)$$

$$t_2^{(i,j)} = \int_{-H_i}^{0} [\sqrt{(V_p(z)/\phi_j)^{-2} - p^2} + \sqrt{V_p(z)^{-2} - p^2}]dz \quad (4)$$

$$t_3^{(i,j)} = \int_{-H_i}^{0} 2\sqrt{(V_p(z)/\phi_j)^{-2} - p^2}\,dz \quad (5)$$

where p is the P wave ray parameter, H_i is the depth of the candidate discontinuity, ϕ_j is the candidate V_p/V_s (which ranges from 1.65 to 1.95 with an interval of 0.0025) and $V_p(z)$ is the *P* wave velocity at depth *z* (which is between 15 and 55 km with a step of 0.1 km).

The sharpness of the Moho was quantified by the stacking amplitude (relative to that of the direct *P*- wave) corresponding to the optimal H_i and $(Vp/Vs)_j$.

We divide all the stations into 3 categories including A, B and C. For stations in category A, we observed an unambiguous *PmS* arrival and either a *PPmS* or *PSmS* or both arrivals, resulting in a well-defined single peak on the *H-k* plot (Figure 2.2). A clear *PmS* arrival was observed at stations in category B, however neither *PPmS* nor *PSmS* was observed, leading to a poorly defined peak on the *H-k* plot. None of the Moho phases at stations in category C is observed and results from category C stations are not included in our final results. Figure 2.2 shows the *H-k* plot and associated RFs of station 119A which is a category A station.

In addition, at some stations a clear arrival before *PmS* was observed and it is named as *PuS*. This secondary arrival and associated multiples are noticeably clear on the *H-k* plot (Figure 2.3).

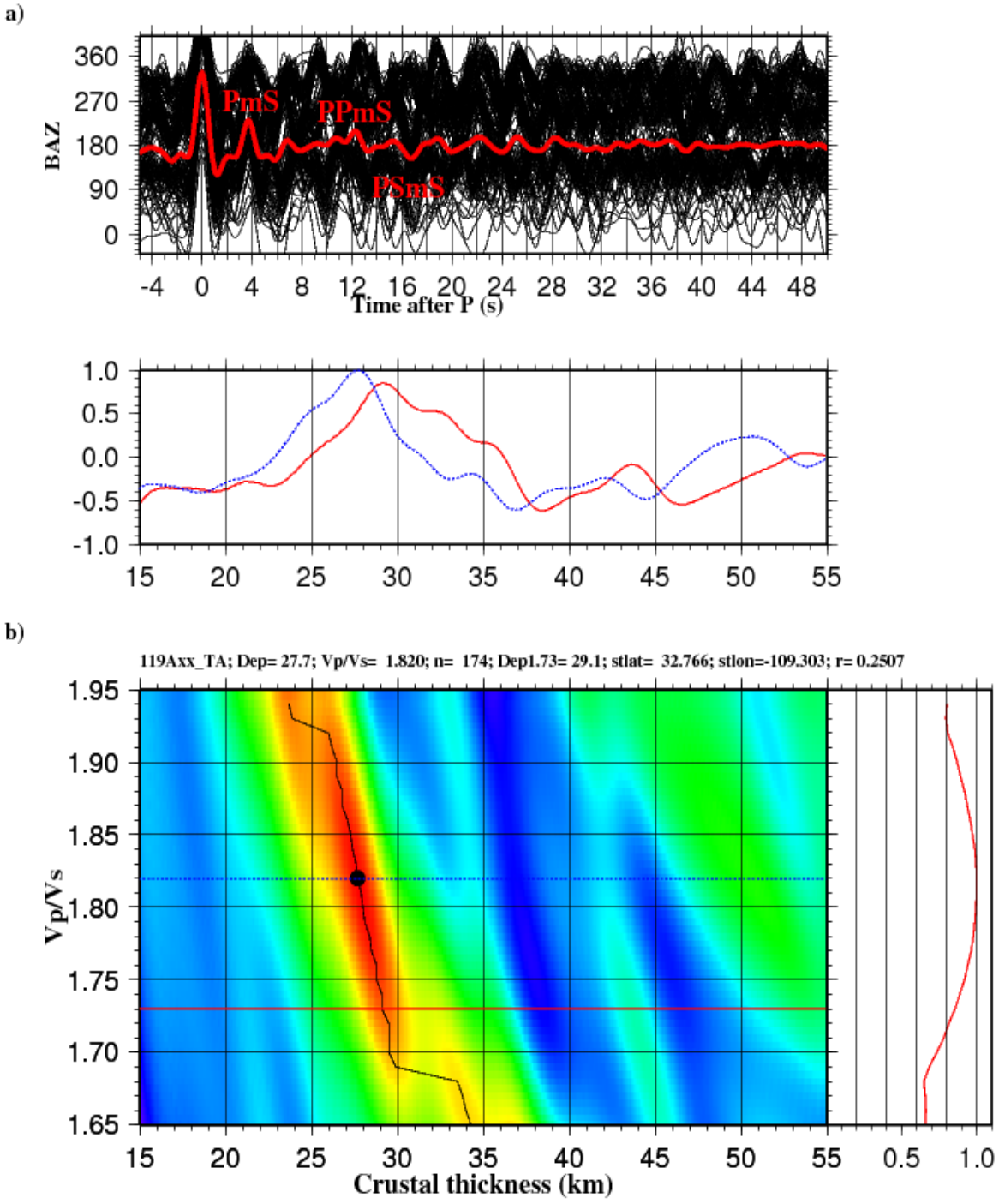

Figure 2.2. Analysis of data from station 119A which is a quality A station located in southern Kansas. (a) Radial receiver functions plotted against the back azimuth. The red line is the result of simple time domain stacking of all the RFs. *PmS* indicates P-to-S converted phases from the Moho. *PPmS* and *PSmS* are multiples. (b) *H-k* plot. The black dot indicates the maximum stacking amplitude.

The calculation of the moveout time requires a mean crustal *P* wave velocity. Previous active and passive source seismic suggested an average *P* wave velocity of 6.2 km/s in the Basin and Range (Christensen & Mooney, 1995), 6.1-6.3 km/s in the Colorado Plateau (Pakiser, 1989), 6.1-6.3 km/s within the Rocky Mountains (Prodehl & Lipman, 1989), 6.1 km/s in the Great Plains (Borcherdt & Roller, 1976), 6.3-6.5 km/s in the Snake River Plain (Braile et al., 1982; Hill & Pakiser, 1966), and 6.3 km/s in the Columbia Plateau (Catchings & Mooney, 1988a). As demonstrated by Nair et al. (2006), a 5% difference between the real and used crustal velocities for the stacking would lead to an error of about 2.5 km in the resulting *H* value and about 0.012 in the resulting *Vp/Vs*. Therefore an average crustal velocity of 6.1 km/s, which is used for the study, only leads to minimal error. This is because the difference between previously determined crustal velocity and the velocity that we used for this study is 1.6% in the Basin and Range and the Great Pains, 1.6-3.2% in the Rocky Mountains and Colorado Plateau, 3.2-6% in the Snake River Plain, and 3.2% in the Colombia Plateau.

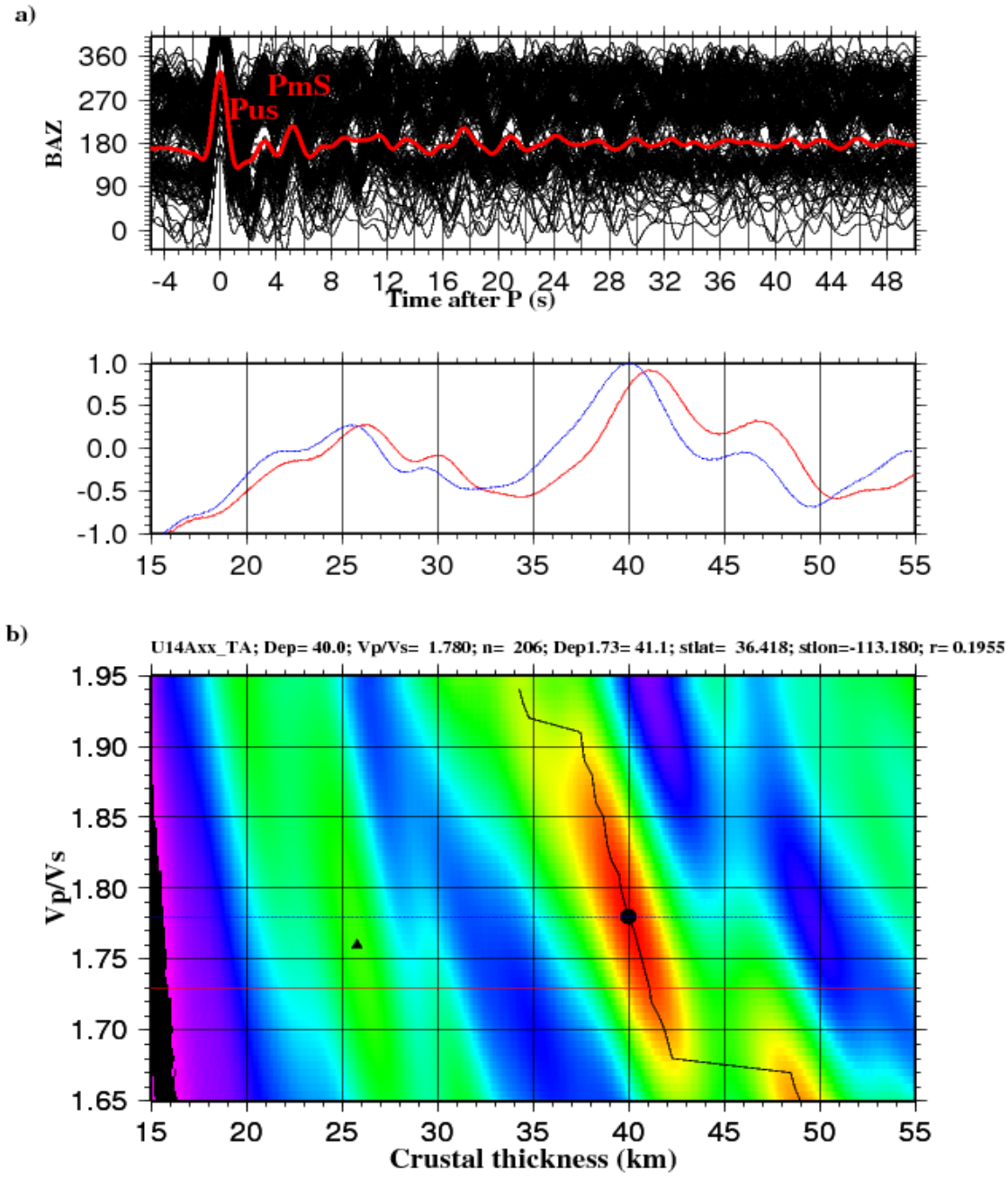

Figure 2.3. Stacked receiver functions for a station with the *PuS* arrival. a) Individual (thin black lines) and stacked (thick red line) receiver functions for station U14A, showing the *PuS* arrival at about 3 s after the direct P wave. b) Corresponding $H - k$ plot. Black dot corresponds to the optimal H and Vp/Vs associated with the Moho, and the triangle represents the optimal values for the boundary at the top of the lower crustal layer.

3. RESULTS AND COMPARISON WITH PREVIOUS STUDIES

A total of 151,487 high-quality receiver functions with well-defined primary *P* arrivals were used for this study. The results include 389 category A stations and 223 category B stations. The *H, Vp/Vs,* and *R* are determined with a high confidence at the category A stations, however not at the category B stations. Thus, we use all three parameters (*H, Vp/Vs,* and *R*) from the "A" stations and only *R* and *Hn* (crustal thickness corresponding to a nominal Vp/Vs of 1.732) values from "B" stations for our database (Appendix).

Our observations of the crustal parameters, including *H, Vp/Vs,* and *R,* correspond well with various physiographic provinces. The receiver function results presented here show systematic spatial variations of crustal structure throughout of the western US.

3.1. CRUSTAL THICKNESS

The western US is characterized by a significant crustal thickness variability, from 21 km to 57 km with a mean value of 38.5±0.8 km (Figure 3.1). The Pacific Boarder along the coast has thinner crust (26.5±2.1 km) comparing to the bordering Cascade volcanic arc (36.3±2.7 km) and the Sierra Nevada batholiths (39.4±2.8 km). Crustal thickness beneath the Basin and Range (32.9±1.5 km) is thinner than the surrounding regions. Crust beneath the northern part of the Columbia Plateau is thicker than the other part of the plateau. The crust thickens eastward beneath the Colorado Plateau (43.6±1.8 km), Rocky Mountains (42.6±1.9 km) and mountains in western Montana and northern

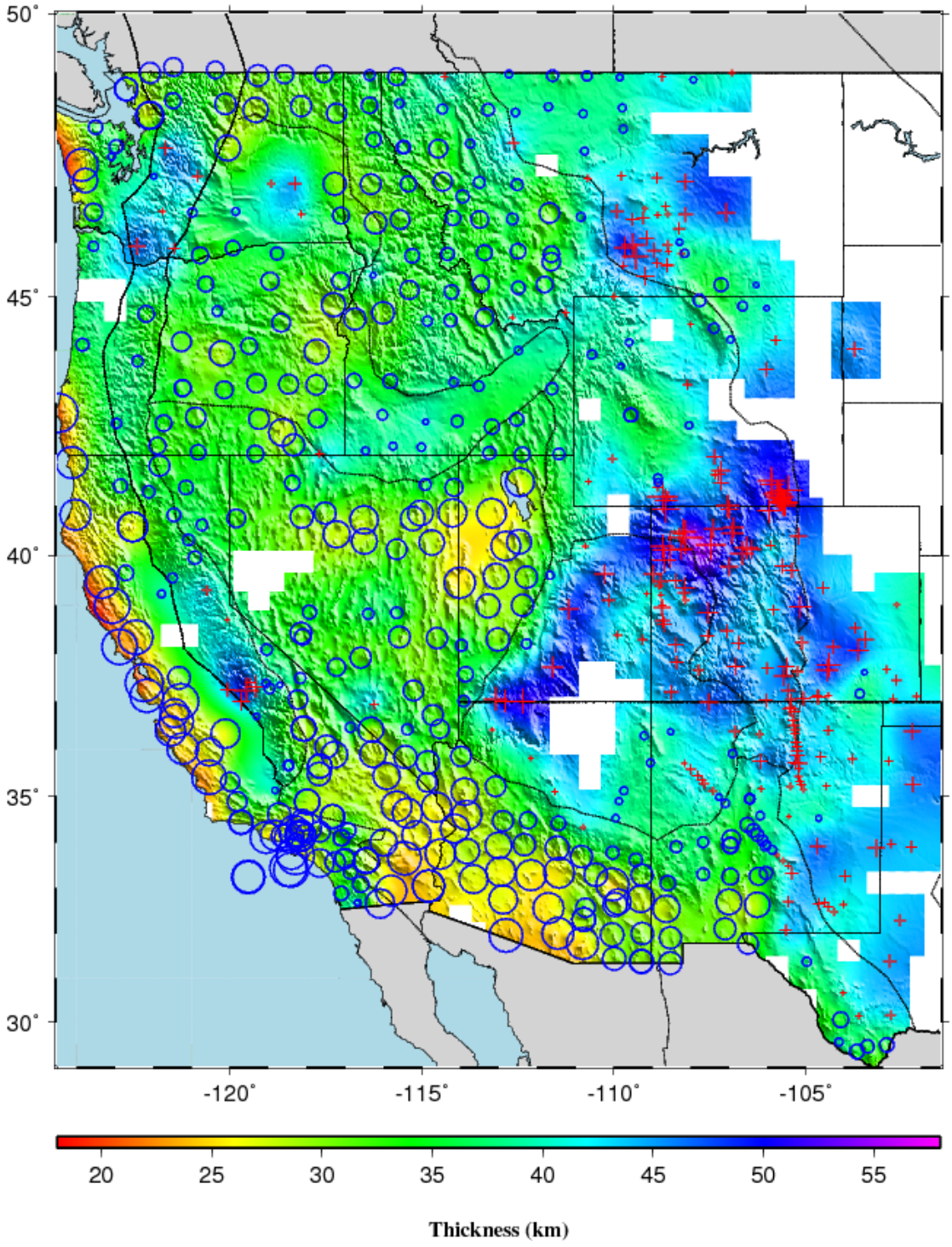

Figure 3.1. Resulting crustal thickness from category A and B stations. The mean crustal thickness corresponds well with major tectonic provinces. The white areas have no good data coverage.

Idaho relative to the central and southern Great Plains (42.7±1.1 km). However, the crust thins (<40 km) beneath the northern part of the Rocky Mountains. The thickest (>55 km) crust that we observed is beneath the Cheyenne Belt (Figure 1.2). The San Francisco Bay Area is characterized by the thinnest (22 km) crust. There are some abrupt changes in crustal thickness underneath the Wasatch Front between the Rocky Mountains and Basin and Range, the Cascade Range and Columbia Plateau in Washington, beneath the Owyhee Plateau, Big Horn Basin, Cheyenne Belt between Basin and Range, Colorado Plateau, and the southern Sierra Nevada and Pajarito Mountain at the boundary between the Basin and Range and the Great Plains.

3.2. Vp/Vs

In order to obtain the depth to the Moho from the *P-to-S* conversion, we calculate the *Vp/Vs* using the Zhu and Kanamori (2000) method. Resulting V_p/V_s values range between 1.68 and 1.94 with an average of 1.77±0.06 in the entire study area (Figure 3.2). This result is consistent with the global average crustal *Vp/Vs* of 1.78 (Braile et al., 1989; Clarke and Silver, 1993; Christensen, 1996; Zhu and Kanamori, 2000). Several areas of high *Vp/Vs* ratios, reaching values >1.85, are observed in the Columbia River Basalt, High Lava Plain, southern Sierra Nevada, Southern Basin and Range near boundary to the Great Plains. We find lower *Vp/Vs* (<1.72) beneath northern California Coast Range, northern Sierra Nevada, northern Basin and Range, and the Grand Mesa in Colorado. The *Vp/Vs* ratio of 1.73-1.80 across the Rocky Mountains shows felsic to intermediate

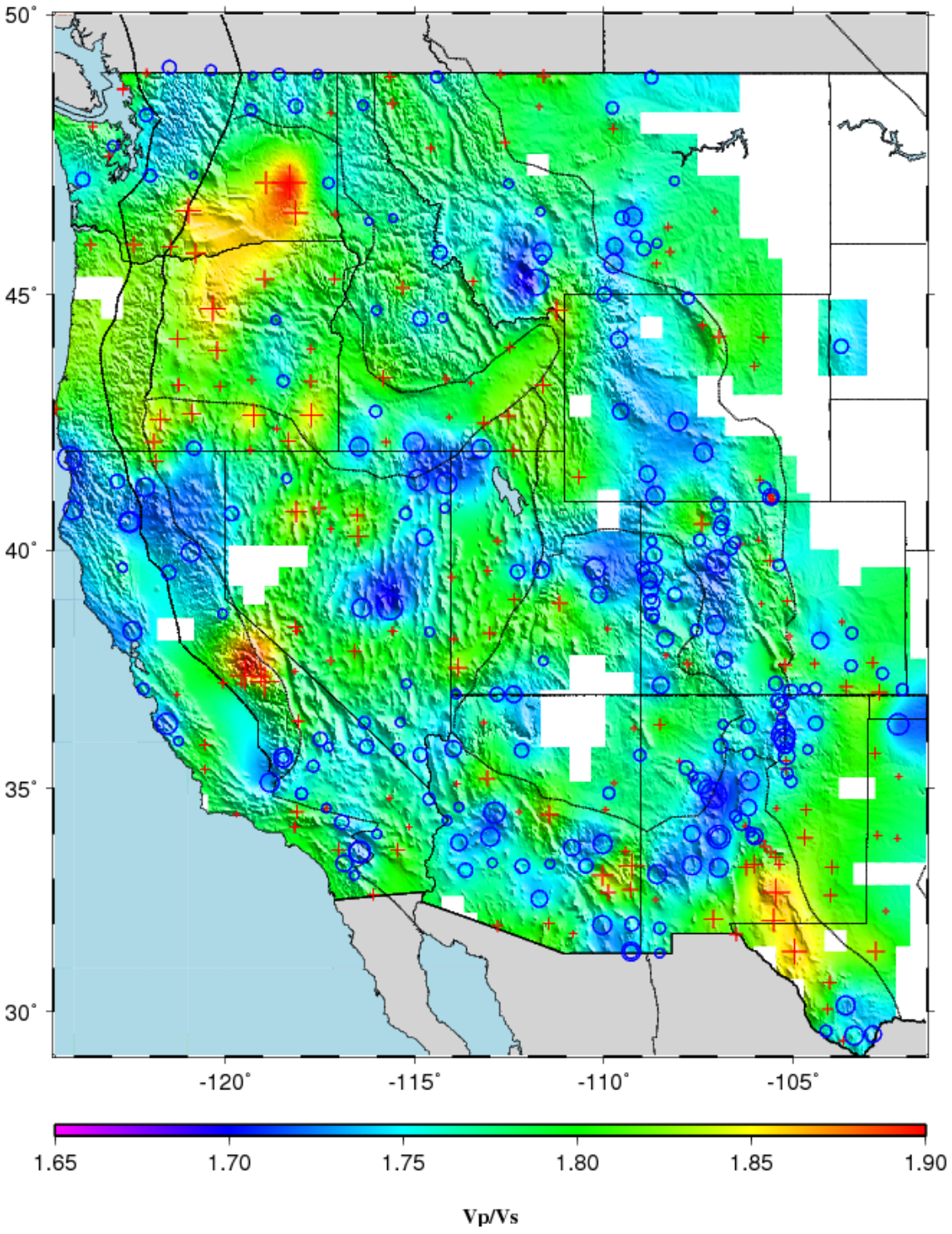

Figure 3.2. Resulting *Vp/Vs* derived from category A stations.

composition. The Colorado Plateau is characterized by *Vp/Vs* of 1.75-1.80 except along the boundary of the Basin and Range (1.81-1.85). The Basin and Range has *Vp/Vs* of 1.80 which is higher than the average. The Great Plains is characterized by the global average *Vp/Vs* except the southern part.

3.3. STACKING AMPLITUDE (*R)*

To determine the apparent sharpness of the Moho beneath a station, we measure *R*, which is the ratio between the stacking amplitude corresponding to the optimal pair of (*H, Vp/Vs*) and the mean amplitude of the direct *P* wave on the radial components. A clear observation of *PmS* and its multiples reflect a sharp Moho. As a function of the angle of incidence, *R* value is affected by variation of the incident angle. Indeed, most of the events with an epicentral distance of $\geq 70^0$, implying that the majority of the rays arrive at the station at a nearly vertical angle. Thus the incident angle effect is weak.

Overall, the *R* values vary from 0.01 to 0.51 with a mean of 0.17±0.08 (Figure 3.3). Extremely small *R* values of <0.1 are observed in the Columbia River Basalt Group within the Columbia Plateau, High Cascade Range, western Sierra Nevada and Great Valley, Idaho Batholith, , Colorado Plateau, along the Laramide orogeny, Wasatch Front, along the boundary between the Rio Grande Rift, and the Great Plains. We find higher *R* values of >0.35 across the Williston Basin, Basin and Range, and northern California Coast Range near the Mendocino Triple Junction.

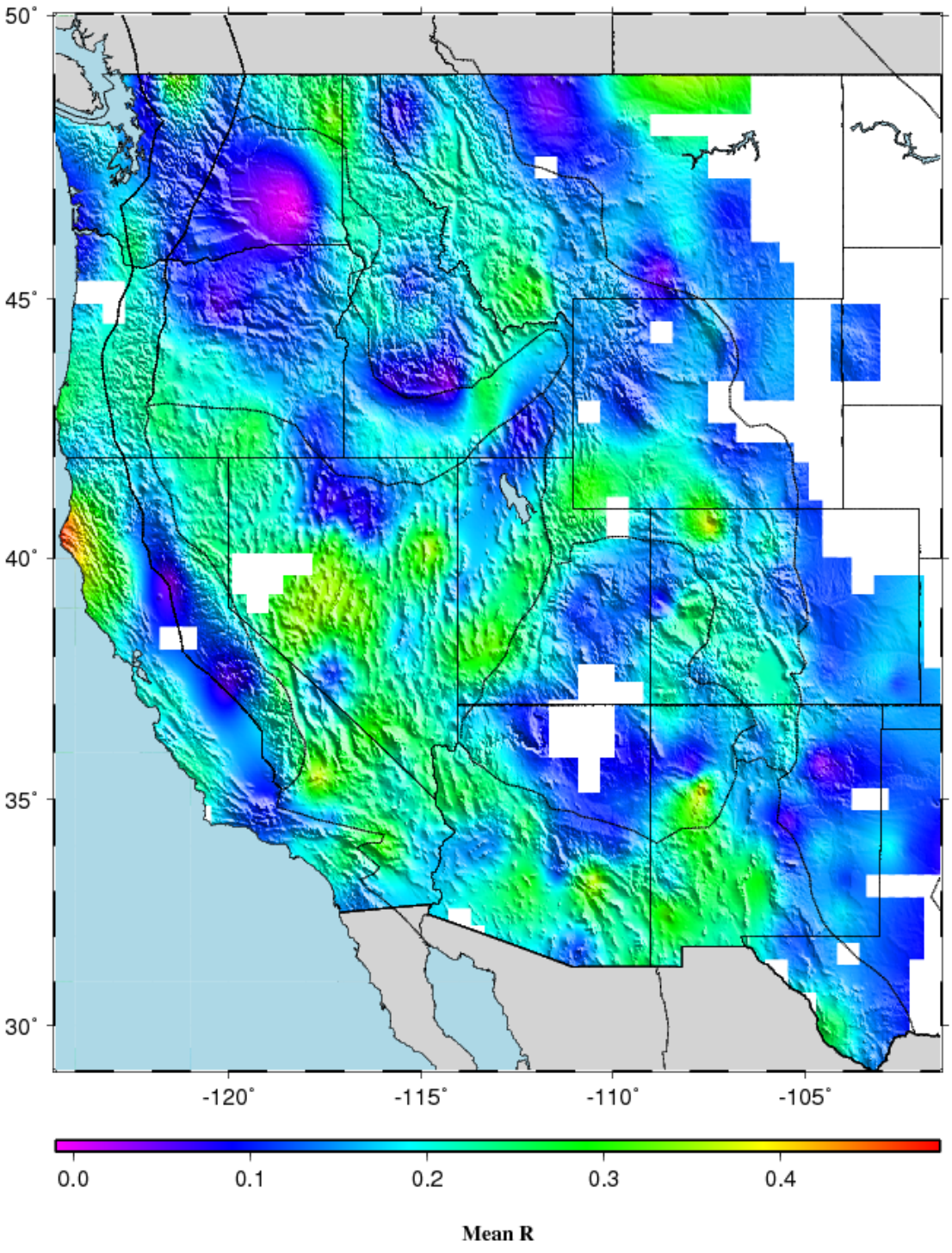

Figure 3.3. Resulting stacking amplitude from all the stations.

3.4. RELATIOHSHIPS BETWEEN CRUSTAL PARAMETERS

We observed a complex relationship between calculated crustal thickness and surface elevations within the study area. Calculated cross correlation coefficient (xcc=0.37) shows no strong, linear relation between crustal thickness and elevation data (Figure 3.4). Our cross correlation result between crustal thickness and *Vp/Vs* value reveals that there is no clear relationship between them. Some of the previous receiver function studies show that geological provinces of different age and tectonic history can be distinguished by the relationship between *Vp/Vs* and the crustal thickness (Egorkin, 1998; Zandt & Ammon, 1995). Egorkin (1998) concluded that *Vp/Vs* is directly proportional to the crustal thickness in the Precambrian Cratons and it is inversely proportional to the *H* in the Cenozoic Basin and Paleozoic fold belts. However, there is no observed noticeable relationship between crustal thickness and *Vp/Vs* in the Precambrian Cratons. According to Zandt and Ammon (1995), *Vp/Vs* increases with age. In contrary, our results are not consistent with this suggestion and no clear connection was detected between *Vp/Vs* and crustal age. Correlation coefficient of -0.23 indicates poor negative correlation between crustal thickness and sharpness of the Moho, which is consistent with the conclusion that a deeper Moho are stacked less coherently (Andrews et al., 1985).

Overall, thicker crust is associated with large negative Bouguer gravity anomaly (Figure 3.5). However, this relation is not valid for some regions including northern Pacific Boarder, Washington and Oregon, northern Columbia Plateau and adjacent Cascade Range, southeastern Washington, northern Rocky Mountains, and northern Basin and Range Province. Bouguer gravity anomaly depends on not only crustal

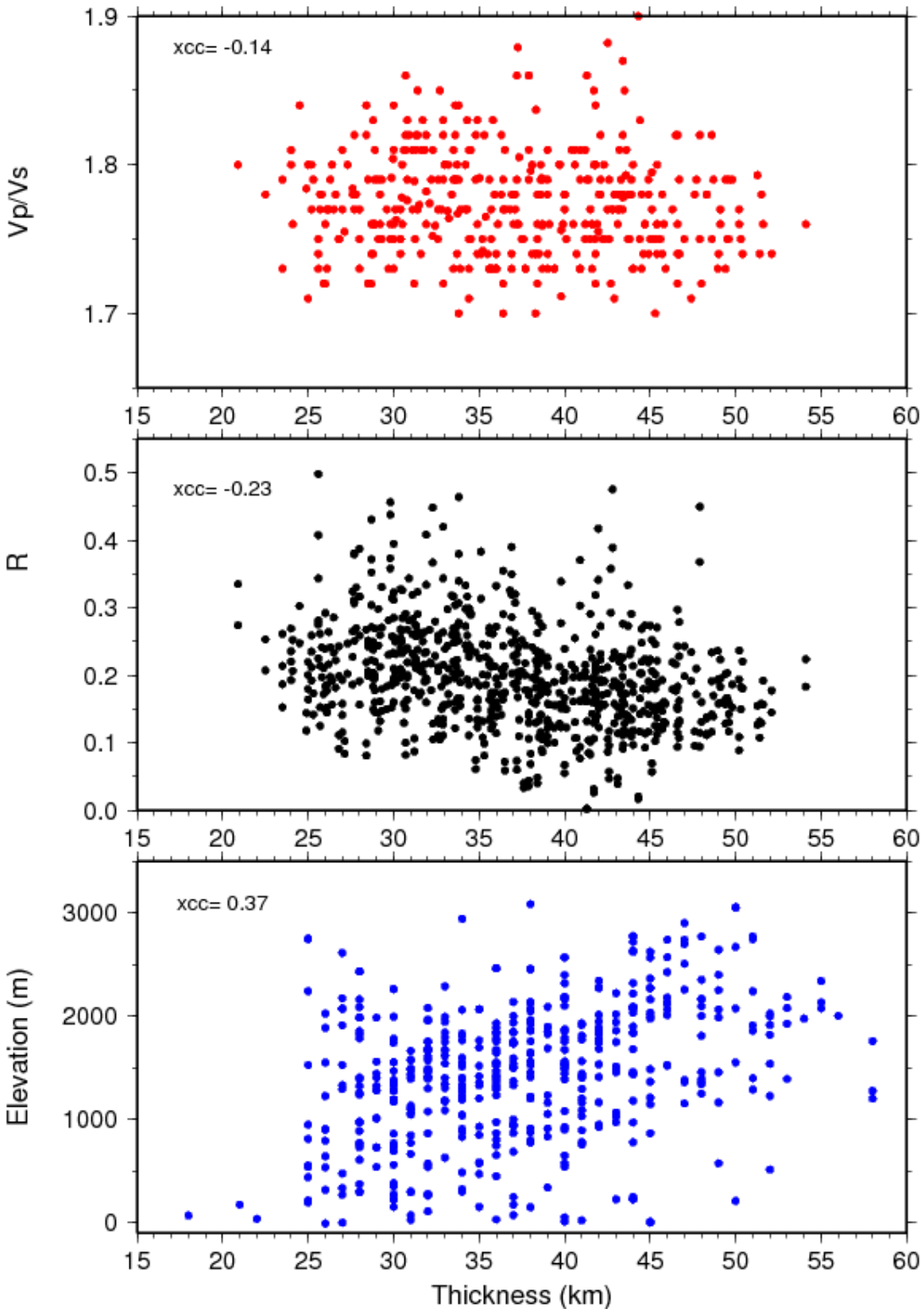

Figure 3.4. Comparison of crustal thickness measurements with Vp/Vs results with stacking amplitude and surface elevation of the stations. XCC means cross correlation coefficient.

thickness but also density structure of the crust and upper mantle.

We selected 4 profiles along the latitude 35^0, 39^0, 43^0, and 47^0N to show lateral variations of the elevation, Bouguer gravity anomaly, crustal thickness, Vp/Vs, and sharpness of the Moho along the major geologic provinces (Figure 3.5).

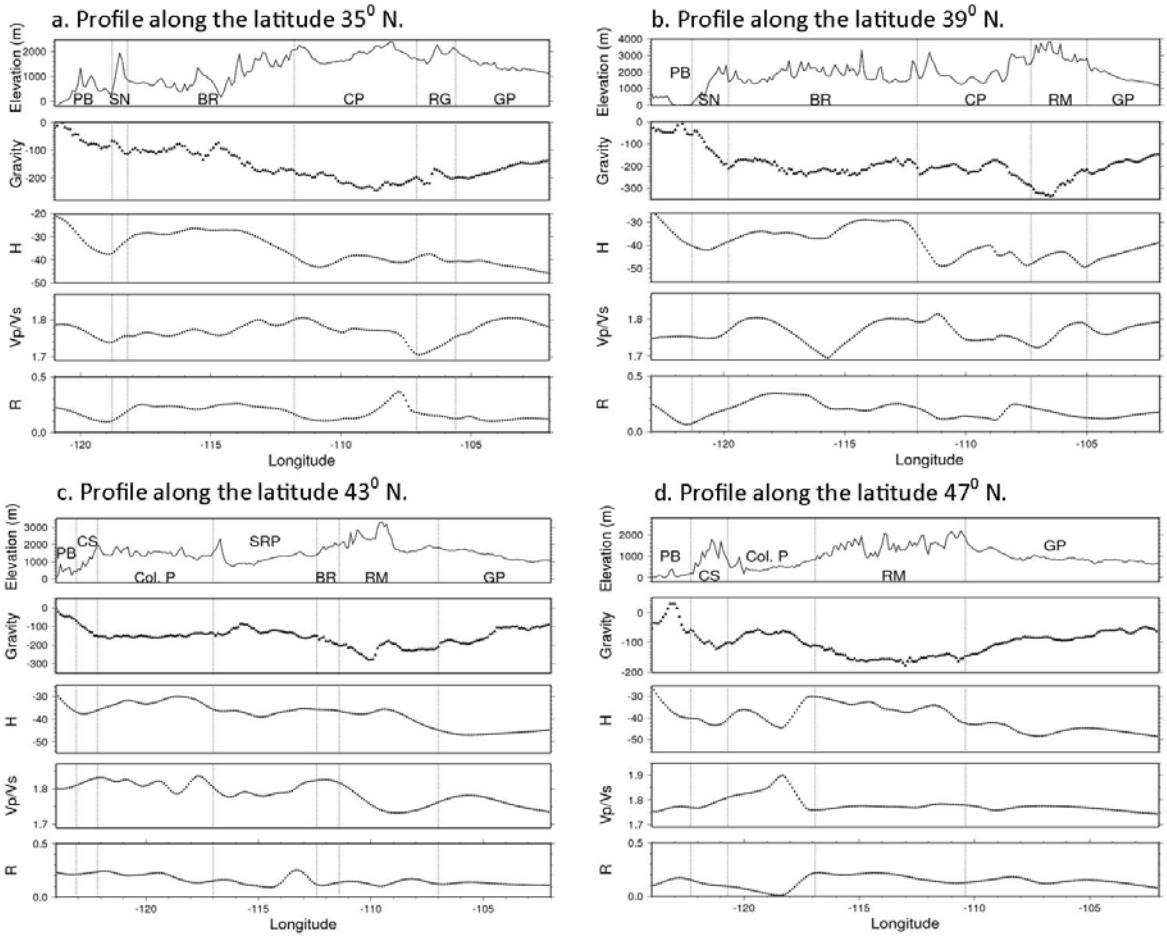

Figure 3.5. Elevation, Bouguer gravity anomaly and crustal parameters (crustal thickness *H, Vp/Vs* and stacking amplitude along the selected latitude profiles). PB-Pacific Border, SN-Sierra Nevada, BR-Basin and Range Province, CP-Colorado Plateau, RGR-Rio Grande Rift, RM-Rocky Mountains, GP-Great Plains, SRP-Snake River Plain, and Col.P-Columbia Plateau.

3.5. COMPARISON WITH PREVIOUS STUDIES

In general, our crustal thickness results are consistent with results from previous seismic refraction and deep reflection surveys including COCORP (Keller et al., 1975; Brown et al., 1979; Pakiser & Brune, 1980; Braile et al., 1982; Allmendinger et al., 1983; Pakiser, 1985; Holbrook & Mooney, 1987; Catchings & Mooney, 1988; Snelson et al.,1998; Gorman et al., 2002; Frassetto et al., 2006; Rumpfhuber & Keller, 2009; Cox & Keller, 2010) and receiver function studies (Sheehan, 1995; Gilbert & Sheehan, 2004; Hansen & Dueker, 2009; Rumpfhuber et al., 2009; Eagar et al., 2011; Frassetto et al., 2011; Gilbert, 2012; Hansen et al., 2011).

We next compared our crustal thickness results with the EarthScope Automated Receiver Survey (EARS) at the IRIS DMC and receiver function result by Gilbert (2012) (Figure 3.6). The EARS is a fully automated data product developed by the University of South Carolina. It calculates bulk crustal properties of stations using receiver function stacking. The procedure of the receiver function processing is the same as the method we use. The events above magnitude 5.5 were used by EARS. They selected the seismograms with no gaps, and a signal and noise ratio of >2. In addition, they used only event-station pairs for which the iterative deconvolution has a greater than 80% match for stacking. A cross correlation coefficient of 0.53 shows that there are positive relations between EARS and our crustal thickness results. The *Vp/Vs* results also show poor relationship with the EARS (xcc=0.25). The EARS results were produced without any manual checking to control data quality. The difference between fully automated processing and seismologists' insight to differentiate reliable results is inevitable.

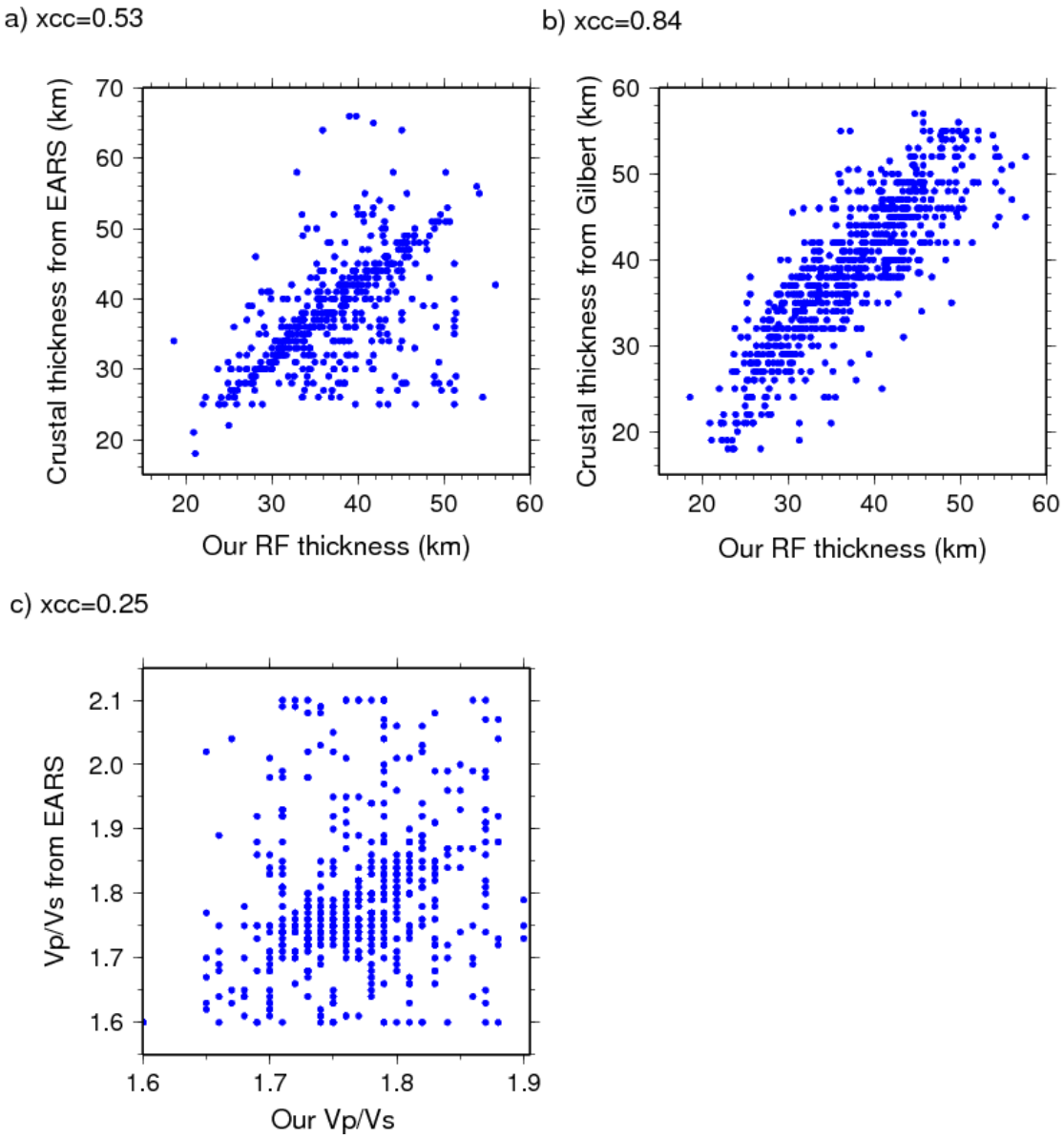

Figure 3.6. Comparison of crustal thickness and *Vp/Vs* result comparison data from the EarthScope Automated Receiver Survey (EARS) at the IRIS DMC and by Gilbert (2012).

In general, crustal thickness results were consistent with Gilbert's RF results (xcc=0.84). However some discrepancies are found in some of the regions. The main reason for the observed discrepancies is that Gilbert (2012) used constant a *Vp/Vs* of 1.74 for the entire study area to determine crustal thickness, while we used a more realistic varying *Vp/Vs* for the stations. Another reason is the dissimilar methodology of the receiver function stacking. Gilbert (2012) used stacking approach with bins whose radii depended on the density of station coverage in an area. The grid used in his study has a bin every 45 km in the north-south and east-west directions and 1 km vertically.

4. SPATIAL DISTRIBUTION OF THE CRUSTAL CHARACTERISTICS AND THEIR TECTONIC SIGNIFICANCE

4.1. PACIFIC BORDER

The crust beneath the northern (north from about 40.5^0N) part of the Pacific Border thickens gradually from 21 km along the coastline to 40 km into the interior. Our crustal thickness result is consistent with the previous COCORP refraction (Keach et al., 1989), reflection (Tre'hu et al., 1994; Miller et al., 1997; Parsons et al., 1998, 1999; Gerdom et al., 2000), and receiver function (Eagar et al., 2011) studies. The thickest (46.1 km) crust is observed in the lowland near the border between Washington and Oregon (Figure 3.1). The Vp/Vs ranges between 1.75 and 1.83 (Figure 3.2). Resulting R values are relatively low (0.09-0.21) (Figure 3.3). Bouguer gravity anomaly changes significantly in this region, from -120 to +50 mGal from south to north (Figure 4.1).

The northern part of the Pacific Border is located in a convergent tectonic regime. The northeast trending Juan de Fuca and Gorda Plates are subducting beneath the continental slope. There are several category B stations in this area indicating that *P-to-S* converted phase is weak. The weak Moho converted phase or even lack of the Moho arrivals were observed previously (Bostock et al., 2002; Gilbert, 2012) and were interpreted as the serpentinization of the mantle wedge due to water released from the subducting Juan de Fuca slab. The resulting *Vp/Vs* values indicate felsic to intermediate crustal composition, which is reasonable for the crust composion of the Siletz terrane, an accreted block of late Paleocene-early Eocene, and the Coast Range terrane (Catchings & Mooney, 1988a; Leaver et al., 1984). Another possibility is that crust consists of metasedimentary rocks of the continental rifting (Wells et al., 1984). Once rifting occurs,

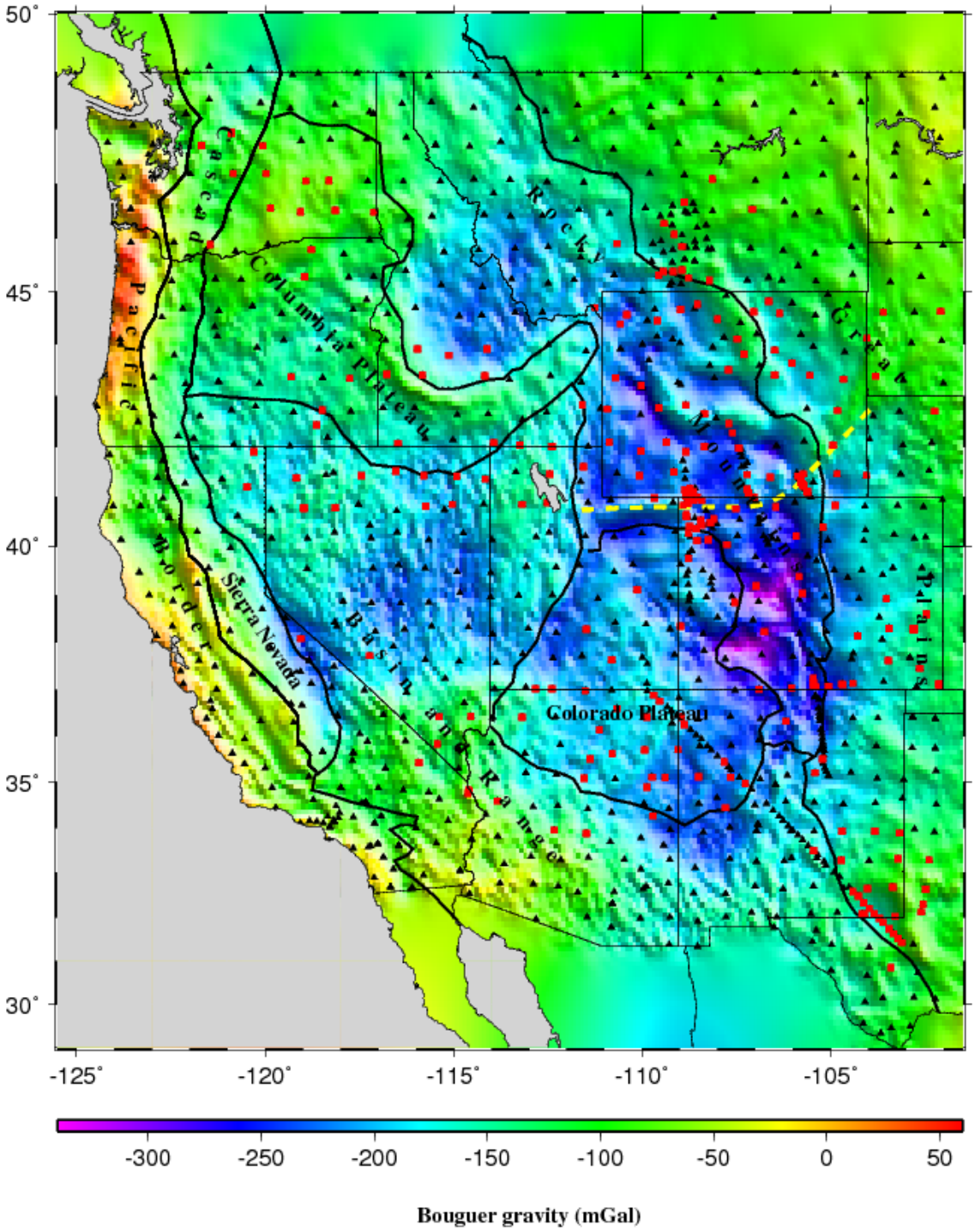

Figure 4.1. Bouguer gravity anomaly map. Black triangles represent seismic stations, red squares are stations that have both Moho arrival (PmS) and secondary arrival (PuS), bold black lines denote boundaries of major tectonic provinces, the dashed yellow line represents the Cheyenne Belt and the red line shows the San Andreas Fault.

large volumes of sediments fill the rift basin and sediments are subsequently metamorphosed by the heat flux from the underlying mantle. As a result, the metasedimentary crust is underlain by an anomalous serpentinized upper mantle (Nicolas, 1985). The resulting low *R* values of <0.2 indicate disturbed Moho, which is consistent with the previous serpentinizied upper mantle model. This region is associated with significant Bouguer gravity anomaly (+50 mGal) (Figure 4.1). The Bouguer gravity anomaly high may indicate a mass excess in either/both the crustal and upper mantle (Thiruvathukal et al., 1970).

The southern part of the Pacific Border, where transform fault regime is dominated, consists of the Coastal Range, Transverse Range, and Peninsular Range. Resulting crustal thickness ranges from 22 km along the coastline to 40 km in the eastern border of the Great Valley where it meets the Sierra Nevada (Figure 3.1). Observed Vp/Vs values vary from 1.73 to 1.80 (Figure 3.2) and R values range from 0.02 to 0.4 (Figure 3.3). Variation in Bouguer gravity anomaly is relatively low (from -75 to +20 mGal) comparing to the northern Pacific Border.

The region is characterized by tectono-stratigraphic terranes that have been accreted to the continental margin by imbricating underthrusting during subduction, obduction, and translation associated with lateral plate motions (Coney et al., 1980; Howel & Vedder, 1981). The Moho is almost flat at about 22-25 km beneath the western Coastal Range then it deepens up to 37-40 km beneath the Great Valley (Figure 6). This crustal thickening is associated with the Franciscan complex, which consists of blueschists and eclogite (Chang-Whan & Liou, 1990). Our *Vp/Vs* observations of 1.73-1.78 support the eclogitic composition (Figure 3.1). Very low *R* value of 0.05-0.12

(Figure 3.3) is determined in the San Francisco Bay area, most of the Great Valley, and the western Sierra Nevada, where a possible slab-free window was depicted (Severinghaus & Atwater, 1990; McCrory et al., 2009). This slab-free window area was confirmed in various studies through geochemical analysis (Benoit et al., 2002; Breitsprecher et al., 2003), radiometric and magmatic activity dating (Cole & Basu, 1995; Cole et al., 2006), and plate kinematic reconstructions (Johnston & Thorkelson, 1997; Wilson et al., 2005). In this region, partially molten basalt sill (Levander et al., 1998) was revealed and we can conclude that low *R* values are associated with it.

4.2 CASCADE RANGE

The Cascade Range is a region of arc magmatism related to subduction of the oceanic lithosphere. It includes middle Tertiary volcanic centers (McBirney, 1978) known as Western Cascades, and Quarternary volcanoes, known as the High Cascades (Heller et al., 1987). We observe a thick crust of 33-45 km (Figure 3.1); similar to the previous refraction study (Leaver et al., 1984) beneath the Cascade Range. The crust beneath the northern part is thicker (40-45 km) than in the southern part (33-40 km) (Zucca et al., 1986; Fuis et al., 1987; Mooney & Weaver, 1989; Schultz & Crosson, 1996). Vp/Vs values range between 1.75 and 1.82 (Figure 3.2). Overall, R values are low (0.1-0.18) within the entire Cascade Range (Figure 3.3). Bouguer gravity anomaly ranges from -150 mGal in the north and south part of the Cascade Range to -50 mGal in the middle part (Figure 4.1), which is located at the boundary between Washington and Oregon.

The thickest crust (46.6 km) (Figure 3.1) is determined across the Mount St. Helen seismic zone, where transition from the Siletz terrane into Cascade arc crust was occurred (Parsons et al., 2005). The *Vp/Vs* determination indicates felsic to intermediate crust beneath the region and it is related to silicic intrusive rocks of Cascadia arc (Paine, 1982). The southern edge of the Cascade Range in northern California is characterized by low *Vp/Vs* and it is related to felsic calc-alkaline magmas from Lassen, Maidu, and Dittmar volcanic centers and Magee Volcano (Borg, 1989; Clynne, 1990, 1993). Borg and Clynne (1998) found that felsic magmas are produced by partial melting of lower crust under variable water content and temperature conditions. Observed low *R* values are consistent with the partial melting produced by subducting slab rise into the overlying upper mantle (Peacock, 1990). Previous seismic and magnetotelluric study (Stanley et al., 1990) indicated that there is a deep crustal conductor (DCC) beneath Oregon and northern California Cascades. The DCC is related to metamorphic fluids and partial melt. Additionally, the oldest arc magmas were transitional tholeiitic to calc-alkaline in composition, while the younger arcs are calc-alkaline (du Bray & John, 2011). Calk-alkaline composition is dominant in the more mature and thicker crust and partial melts were generated beneath thickened crust.

4.3. SIERRA NEVADA

Resulting crustal thickness beneath the Sierra Nevada shows 33-42 km (Figure 3.1) that agrees with the hypothesis of no crustal root or a thin root exists beneath the Sierra Nevada (Carder et al., 1970; Jones et al., 1994; Wernicke et al., 1996; Jones & Phinney, 1998; Frassetto et al., 2011). From the many processes that have affected the evolution of

the crust in the Sierra Nevada region, perhaps the most prominent process has been the removal of the continental lithosphere. Previous seismic studies such as the Southern Sierra Nevada Continental Dynamics (CD) Project (Fliedner & Ruppert, 1996; Jones & Phinney, 1998; Ruppert et al., 1998) and the Sierra Nevada EarthScope Project (Frassetto et al., 2011) suggest that the Sierra Nevada lost mantle lithosphere under its southern part at about 3 Ma.

Most of the Sierra Nevada is characterized by a 32-37 km crust, besides a 50 km thick crust is observed near the Yosemite National Park (Figure 3.1). Overall, observed *Vp/Vs* ranges from 1.73 to 1.81 (Figure 3.2) which indicate felsic to intermediate in composition beneath most of the Sierra Nevada. The R values are really low (0.02-0.18) beneath most of the Sierra Nevada (Figure 3.3). Bouguer gravity anomaly varies from -50 mGal in the western foot hill to -225 mGal in the east along the boundary between the Sierra Nevada and Basin and Range Province (Figure 4.1). The highest *Vp/Vs* are 1.83-1.86, indicating intermediate to mafic crustal composition. When delamination occurs, crust lost the lower part, which leads to an overall felsic crust. Decreasing *R* values are indicator of partial melting beneath most of the Sierra Nevada. Our combined results (deeper Moho, high *Vp/Vs*, and lower R) indicate a mafic residue is still intact beneath the western foothill of the southern Sierra Nevada. Previous gravity modeling along the two profiles across the Sierra Nevada and surrounding areas (Purevsuren, 2010) proposed delamination of the crust at the same location. This foundering may initiated by the slab free window edge arrival beneath the Sierra Nevada (Atwater & Stock, 1998).

4.4. COLUMBIA PLATEAU

The Columbia Plateau area is covered by a thick layer of Columbia River flood basalt that was extruded 17.5-6 Ma and filled pre-existing basins in eastern Washington and northern Oregon (Hooper & Hawkesworth, 1993). It includes the Snake River Plain tectonomagmatic province associated with the Yellowstone hotspot (Pierce & Morgan, 1992) and the High Lava Plain. We observe thicker than normal crust (34-44 km) beneath the northern part of the plateau, where the Columbia River Basalt Group (CRBG) is located. Relatively thin crust (28-35 km) (Figure 3.1) is found beneath the southern part (eastern Oregon). Higher Vp/Vs of 1.80-1.87 is observed in the northern part and it decreases to 1.76 south of the CRBG. The Vp/Vs increases to 1.79-1.84 in the High Lava Plain (Figure 3.2). *R* values are very low (0.01-0.1) beneath most of the northern part and increase to as large as 0.2 southward (Figure 3.3). Bouguer gravity anomaly ranges from -100 to -55 mGal beneath the northern part of the plateau and from -200 to -100 mGal in the southern part (Figure 4.1).

The crust beneath the northern Columbia Plateau is characterized by higher *Vp/Vs* which indicates mafic in composition. Moreover, secondary arrivals before the Moho conversion are observed within the area where thicker crust was observed. These arrivals indicate the existence of a high velocity layer beneath this area. The thickest part is centered at nearly the center of CRBG. Bouguer gravity anomaly is also high (-55 mGal) at the center of CRBG and decreases (up to -80 mGal) toward the edge of the exposed CRBG (Figure 4.1). In addition, the *R* values are significantly low beneath this area. Thicker crust relative to surrounding regions, strong secondary arrivals, increasing *Vp/Vs*, decreasing *R* values, and gravity high are good indications of the presence of pillow

basalts (Christensen, 1996; Liu & Gao, 2010; Moidaki et al., 2013). The results agree with continental rifting model proposed by previous gravity and seismic refraction studies (Catchings & Mooney, 1988a).

The High Lava Plain (HLP) is characterized by thin crust (26-30 km) (Figure 3.1) with high *Vp/Vs* (1.83-1.85) (Figure 3.2), as expected in this area which is composed of accreted oceanic terranes. An abrupt change in crustal thickness and *Vp/Vs* between HLP and the Owyhee Plateau is observed. This change may imply crustal transition from accreted oceanic to stable cratonic areas. The *Vp/Vs* values show felsic crust beneath the Owyhee Plateau. It can be explained by silicic welded rhyolite and ash-flow tuff associated with the Owyhee-Humboldt volcanic field (Brueseke et al., 2004).

Resulting *H* ranges from 35 to 42 km beneath the Snake River Plain (SRP) where it is believed that the depressions were resulted from the passageway of the North American Plate above a stationary mantle plume that is currently situated beneath the Yellowstone National Park (Pierce & Morgan, 1982). Crustal thickness determinations from our RF are similar to those from previous gravity (Mabey, 1976, 1978) and seismic refraction (Sparlin et al., 1982) studies. The *Vp/Vs* values are slightly different in the eastern and western SRP. They range from 1.78 to 1.83 beneath the eastern part and 1.73-1.79 beneath the western part (Figure 3.2). The western SRP is located in a north-northwest trending fault-bounded graben while the eastern SRP is a large northeast trending structural downwarp that formed due to the weight of the overlying volcanic rocks (Pierce & Morgan, 1982). Our result is consistent with the results from previous RF studies using a denser PASSCAL experiment, transportable arrays, and University of Utah/Teton/National Seismic network stations (Yuan et al., 2010) and a seismic

refraction survey (Braile et al., 1982). Higher *Vp/Vs* and lack of well-marked graben along the eastern SRP indicate partial melt beneath it, while, decreasing *Vp/Vs* beneath the western SRP may show that plume related material is already cooled.

4.5. BASIN AND RANGE

The Basin and Range Province (BRP) is an unusually wide continental rift zone. Previous studies show that it has a 28-35 km thick crust with *Vp/Vs* of 1.78 (Prodehl, 1979; Gish et al., 1981; Frassetto et al., 2006; Bashir et al., 2011). Our receiver function results show that the crustal thickness varies from 25 to 38 km (Figure 3.1), Vp/Vs values range between 1.73 and 1.83 (Figure 3.2), and R values vary between 0.1 and 0.3 beneath the area (Figure 3.3). The region is characterized by relatively large and spatially varying negative Bouguer gravity anomalies of -240 to -30 mGal (Figure 4.1).

In the northern BRP, the crustal thickness is small (24-30 km) beneath the Lahonton and Bonneville depressions, where present day extension is more acute (Thompson & Burke, 1974; Smith, 1978; Vetter & Ryall, 1983) and it thickens southward (southern Nevada). Observed high *Vp/Vs* values (1.81-1.84) may relate to the volcanic fields of the region. The average *Vp/Vs* value is 1.81 which is higher than the global average. These higher values maybe related to upwelling mantle beneath the Great Basin. Extensive stretching causes significant effects on the lithosphere and relieves pressure on the underlying upper mantle. Melting point in this area decreases and partial melting begins to occur (Thatcher et al., 1999). Hot rock buoyancy creates regional upwelling of the mantle, leading to uplift. Regional uplift is active in the region as indicated by a recent GPS survey (Hammond, 2004) which estimated ~1.5 mm/yr of

vertical motion across the Basin and Range. In addition, lower *R* values beneath the Great Basin and Wasatch Front are associated with the mantle upwelling as well.

The southern BRP is characterized by a 24-35 km crust (Figure 3.1) which is consistent with the results from previous refraction studies (Gish, et al., 1981) and RF results (Bashir et al., 2011). To the east of the Peninsular Range, the crust rapidly thins beneath the Salton Trough to 24 km where the crust completely rifted (Elders et al., 1972) apart and a new crustal section has been formed. Sedimentary rocks, metasedimentary rocks, and intrusions are observed in the section (Fuis et al., 1984). Small *R* values in the Salton Trough are observed, which indicates that the sharpness of the Moho is low due to hot mantle melting beneath the rift axis.

The Rio Grande Rift (RGR), which is located in the southeastern part of the BRP, separates the Great Plains and Colorado Plateau and the BRP in the south by its major continental rift structure. The RGR was stimulated by regional extension, which is in turn related to “ignimbrite flare-up” (Humphreys, 1995). Crustal thinning may have been caused by upper-mantle asthenospheric upwelling beneath it. The present RF result shows that the crust thickens from south to the north from less than 30 km to more than 40 km beneath the rift. Previous seismic refraction studies (Olsen et al., 1979; Sinno et al., 1986) conducted at the southern Rio Grande Rift indicated that the crustal thickness is 32 km and the crust thins 4-6 km toward the south. Receiver function studies along the RISTRA (Wilson et al., 1986) transect observed the thinnest crust of 35 km right beneath the rift axis, which is consistent with our observation of 36.2 km along the transect (Figure 3.1). The *Vp/Vs* ranges from 1.73 in the northern rift area to 1.86 beneath the southeastern part (Figure 3.2). Decreasing *R* value toward the southeastward where *Vp/Vs*

reaches the maximum value may indicate partial melting. We have observed a crustal thickness of 46 km beneath the Proterozoic igneous Pajarito Mountain in the southern edge of Pedernal uplift, which was formed during the Laramide. Resulting *Vp/Vs* of 1.85 agrees with the conclusion about the presence of a large, dense, mafic intrusion which may have been emplaced during the Proterozoic rifting (Bowsher, 1991; Roberts et al., 1991).

4.6. COLORADO PLATEAU

The resulting crustal thickness from our RF study ranges from 38 to 50 km (Figure 3.1) and the *Vp/Vs* measurement ranges from 1.74 to 1.83 (Figure 3.2), which is consistent with previous studies (Roller, 1965; Prodehl, 1979; Wolf & Cipar, 1993; Sheehan et al., 1995; Wilson et al., 2005; Bashir et al., 2011) that concluded crustal thickness beneath the Colorado Plateau (CP) is 40-45 km and *Vp/Vs* ranges from 1.65 to 1.89. We observed relatively low *R* value of 0.05-0.20 for the entire plateau area (Figure 3.3). The crustal thickness ranges from 32-35 km along the boundary with BRP to 40-51 km in the interior of the plateau high *Vp/Vs* from 1.72 to 1.83 and low Moho sharpness between 0.05 and 0.19 beneath the CP are observed. Bouguer gravity anomaly gradually varies from -150 mGal in the west to -300 mGal in the east (Figure 4.1).

The Colorado Plateau may have a stronger lithosphere than the surrounding areas (Blackwell et al., 1991; Lee et al., 2001, West et al., 2004; Bashir et al., 2011), and it has thicker crust similar to the crust beneath the Laramide Orogen and the Great Plains (Prodehl & Lipman, 1989; Wilson et al., 2005). The cause of the uplift of the CP and its tectonic stability is debatable. Delamination of the mantle lithosphere (Bird, 1979;

Beghoul & Barazangi, 1989; Zandt et al., 1995), warming of a heterogeneous lithosphere (Roy et al., 2009), and mantle convection (Liu & Gurnis, 2010) mechanisms were proposed to explain the present day high elevation. The most trivial explanation about the stability of the crust is a mechanically strong lithosphere (Blackwell et al., 1991; Lee et al., 2001), while a mafic, dense, and mechanically strong lower crust (Bashir et al., 2011) may be responsible for the tectonic stability of the plateau. We also observed secondary peak before the Moho arrivals at stations located at the northeastern part of the CP and the transition zone between CP and BRP (Figure 4.1). Existence of this lower layer (7.xx layer) may make *R* values smaller due to a reduced velocity contrast between the crust and mantle. Our result from RF supports felsic upper crust with mafic lower crust model proposed by Bashir et al. (2011).

4.7. ROCKY MOUNTAINS

The eastern extent of the Laramide deformation is the Rocky Mountains (Dickinson & Snyder, 1978). The resulting crustal thickness of the Rocky Mountains shows the thickest crust of >50 km beneath the southern part (western Colorado and southeastern Wyoming) and it becomes thinner toward north to <40 km (Figure 3.1). Previous reflection studies (Allmendinger et al., 1982; Brewer et al., 1982; Prodehl & Lipman, 1989) concluded that the crustal thickness beneath the Rocky Mountains ranges from less than 40 km to more than 50 km. The thickest is in southern Montana and Colorado, which is similar to our results. Receiver function studies (Sheehan et al., 1995; Gilbert, 2012) observed the thickest crust (>50 km) beneath the Rocky Mountains along the border between Colorado and Wyoming and ~40 km elsewhere in Wyoming, Montana,

and New Mexico. The *Vp/Vs* (1.73-1.79) is similar to the global average (Figure 3.2). The *R* values range from 0.1 to 0.2 (Figure 3.3). Overall,the Bouguer gravity anomaly gradually decreases toward south from -150 to -350 mGal (Figure 4.1).

No crustal root was observed in the northern part of the Rocky Mountains (western Montana and northern Idaho), which is characterized by crustal thickness of 33-42 km (Figure 3.1). The Yellowstone Plateau, consisting of Pleistocene silicic lavas and ash flow tuffs, lies between northern and middle Rocky Mountains. This region is believed to be a mantle hot spot, which tracks along the SRP (Smith & Christiansen, 1980). Our RF result shows that the crust is 40-43 km thick (Figure 3.1) and it has *Vp/Vs* values of 1.71-1.74 (Figure 3.2). The *R* value in this area is low, which is consistent with the hot spot model.

The middle Rocky Mountains consists of the Idaho-Wyoming overthrust belt that was formed as part of the Laramide deformation. Thicker crust was observed beneath the Beartooth Mountains, Wind River Mountains, and Granite Mountains which are Precambrian outcrops. Crustal thickness of 43 km is observed beneath the Big Horn basin, and crust thins (30 km) beneath the Big Horn Arch. We have observed secondary arrivals before the Moho arrivals beneath the Big Horn Mountains area (Figure 4.1). The western part (along the boundary between Idaho and Wyoming) is characterized by Sevier and Laramide overlapping that underwent reverse faulting by crustal detachment during lithospheric coupling in a low-angle subduction. There is an abrupt crustal thickness change near the Wasatch front. Some studies (Gough, 1984; Schmandt & Humphreys, 2010) proposed mantle upwelling and partial melt beneath the Wasatch

Front. Our result shows that thin crust, high *Vp/Vs*, and low *R* values may support the previous conclusion.

The Wyoming Basins, which subsided during the Laramide orogeny along deep faults, separate middle and southern Rocky Mountains. The Wyoming Basins are characterized by large thrust faults which border the uplifted blocks and thick sedimentary fills (Greis, 1983). COCORP revealed crustal thickness of 30-41 km which is consistent with our result. *Vp/Vs* ranges from 1.73 to 1.79 which shows felsic to intermediate composition. R values of 0.06-0.18 are observed in the Wyoming Basins.

The Cheyenne Belt is a tectonic suture zone between the Archean Wyoming craton and Proterozoic arc terrains. The crust thickens beneath the Cheyenne Belt due to tectonic inter-wedging (Morozova, 2005) between old continent and younger arcs. The thickest crust was observed beneath the Laramie Range, Sierra Madre Mountains, and Uinta Mountains. The crust gradually thins southward.

Overall, there was no observed Airy crustal root beneath the Rocky Mountains and the *Vp/Vs* is the same as the global average. In addition, we also observed secondary arrivals before the Moho phase beneath the Precambrian outcrops north from the Cheyenne belt and along the Cheyenne Belt (Figure 4.1). These arrivals are likely related to the high velocity lower crustal layer (7.xx layer).

4.8. GREAT PLAINS

The Great Plains is characterized by thick crust of 38-52 km (Figure 3.1), Vp/Vs of 1.75-1.83 (Figure 3.2), and R values of 0.05-0.2 (Figure 3.3). Bouguer gravity anomaly is relatively uniform within the Great Plains. Some lower Bouguer gravity anomalies up to -

250 mGal are associated with the boundary between the southern Rocky Mountains and Great Plains.

We observed a 46 km thick crust beneath the Black Hills which was uplifted during the Laramide Orogeny. This Precambrian outcrop is characterized by a *Vp/Vs* of 1.75 which indicates a felsic composition and an *R* of 0.12. Crustal thickness ranges from 40 to 46 km beneath the Denver Basin and the *Vp/Vs* varies from 1.73 to 1.75.

The southern part of the GP is characterized by a nearly flat Moho. Moreover, we observed strong secondary arrivals before the P-to-S conversion from the Moho beneath the southeastern Colorado and Delaware Basin (southern part of the RISTRA transect). The *Vp/Vs* value increases south toward the RGR and GP boundary and the *R* values are almost uniform, ranging from 0.05 to 0.15 (Figure 3.3).

5. CONCLUSIONS

The receiver function (RF) database, including crustal thickness *(H)*, *Vp/Vs*, and the sharpness of the Moho, beneath the western US is valuable for examining the nature and origin of the crust and investigating crustal structure and evolution. The *H*, *Vp/Vs,* and *R* values can be used to describe different crustal blocks and suture zones, to determine magmatic modifications of the original crust, and to define crustal deformation.

Based on the results from the present RF observation at more than 1000 stations, we conclude the following:

1. Vp/Vs and crustal ages. Some studies (e.g., Zandt & Ammon, 1995) suggested that crust with different ages has different *Vp/Vs* values. They measured the highest *Vp/Vs* value of 1.84±0.06 for Precambrian shields, intermediate 1.78±0.06 for Proterozoic platform, and the lowest 1.73±0.09 for Cenozoic and Mesozoic crust. But this variation was not observed on the Kaapvaal craton (Nair et al., 2006). The study area includes several major crustal blocks, such as the Archean Medicine Hat and Wyoming Craton, Proterozoic Mojave, Yavapai and Mazatzal terraines, and the Granite-Rhyolite province with different ages. No significant differences in *Vp/Vs* values for those provinces are observed in this study.
2. Relationship between crustal thickness and Vp/Vs**.** Some studies (e.g., Egorkin, 1998) showed that *Vp/Vs* values are likely to be positively correlated with crustal thickness in Precambrian Cratons and inversely proportional to each other in the Cenozoic basin and Paleozoic fold belt. This relationship was not observed in the present study.

3. The influence of the passage of a mantle plume on crustal evolution. Resulting *Vp/Vs* and their variations show that the crust beneath the western and eastern Snake River Plain is slightly different. Higher *Vp/Vs* (1.78-1.83) and lack of well-marked graben along the eastern SRP indicate partial melt, and decreasing *Vp/Vs (*1.73-1.79) to the west may suggest thet plume related material has already cooled.
4. Crustal structure and composition beneath rift. Along the Rio Grande Rift, *Vp/Vs* increases from 1.75 in the north to 1.86 in the southeastern part. Decreasing *R* value toward the southeastward where *Vp/Vs* reach the maximum value may indicate partial melting. The same relation is observed beneath the Columbia Plateau. The result show that the Columbia River Basalt Group has emplaced in a continental rift basin.
5. Lithospheric delamination or foundering. The observed *Vp/Vs* ranges from 1.73 to 1.75, which shows felsic in composition beneath most of the Sierra Nevada. The highest *Vp/Vs* values we observed here are 1.83-1.86, indicating mafic composition of the crust, which is located at where the thickest crust observed. When delamination occurs, the crust lost the lower part and it leads to an overall felsic crust. Resulting *R* value decreases from 0.20 to 0.03 beneath the western Sierra Nevada. Our combined result (deep Moho, high *Vp/Vs*, and lower *R*) indicates that lithospheric foundering is currently located beneath the western foothill of the southern Sierra Nevada.
6. 7.xx layer. Secondary arrivals before the Moho conversion were observed beneath the Wyoming craton, Colorado Plateau, Delaware Basin, the southeastern

Colorado, along the Cheyenne Belt, the boundary between Snake River Plain, and the Basin and Range Province. These arrivals are potentially related to the 7.xx layer determined previously.

APPENDIX

Crustal thickness (H, H_n), V_p/V_s (φ), and stacking amplitude (R). PB- Pacific Border, GP-Great Plains, BR-Basin and Range, SN-Sierra Nevada, CS-Cascade, CP-Colorado Plateau, RM-Rocky Mountains and ColP-Columbia Plateau.

Name	Net-work	Lat.	Lon.	RF	H	Vp/Vs	Hn	R	Cate-gory	Area
109C	TA	32.889	-117.105	554	28.7	1.83	34.9	0.04	B	PB
112A	TA	32.536	-114.580	124	23.6	1.72	23.4	0.22	C	BR
113A	TA	32.768	-113.767	262	27.0	1.71	26.7	0.24	C	BR
114A	TA	32.751	-112.883	110	23.7	1.84	26.8	0.09	B	BR
115A	TA	32.701	-112.228	221	25.7	1.77	26.3	0.20	C	BR
116A	TA	32.562	-111.704	254	25.6	1.74	25.7	0.23	A	BR
117A	TA	32.572	-110.739	164	31.5	1.78	32.1	0.12	B	BR
118A	TA	32.640	-109.970	188	30.0	1.70	29.4	0.17	B	BR
119A	TA	32.766	-109.303	174	27.7	1.82	29.1	0.25	A	BR
120A	TA	32.547	-108.633	97	27.7	1.78	29.1	0.31	A	BR
121A	TA	32.532	-107.785	394	29.4	1.81	30.4	0.17	C	BR
122A	TA	32.700	-107.001	13	27.1	1.81	28.4	0.41	B	BR
123A	TA	32.635	-106.262	18	28.5	1.76	28.8	0.25	B	BR
124A	TA	32.700	-105.454	129	43.4	1.87	46.4	0.16	A	BR
125A	TA	32.659	-104.657	117	43.4	1.74	43.6	0.11	B	GP
126A	TA	32.646	-104.020	136	41.2	1.81	43.9	0.18	A	GP
127A	TA	32.676	-103.357	188	46.6	1.81	51.5	0.15	C	GP
128A	TA	32.621	-102.485	166	48.3	1.82	40.2	0.12	C	GP
214A	TA	31.956	-112.812	552	24.0	1.80	25.1	0.19	A	BR
216A	TA	32.002	-111.457	168	25.0	1.80	26.3	0.18	A	BR
217A	TA	31.775	-110.816	194	24.9	1.78	25.8	0.12	A	BR
218A	TA	31.974	-110.046	214	29.7	1.73	29.7	0.23	A	BR
219A	TA	31.999	-109.259	167	30.4	1.75	30.7	0.21	A	BR
220A	TA	31.904	-108.527	173	30.5	1.76	31.2	0.27	A	BR
222A	TA	32.105	-107.101	106	30.8	1.83	32.5	0.22	A	BR
224A	TA	32.076	-105.523	166	43.5	1.85	50.6	0.13	A	BR
226A	TA	32.062	-104.101	60	39.9	1.87	42.4	0.10	C	GP
226B	TA	32.078	-104.165	56	39.1	1.84	41.2	0.08	C	GP
228A	TA	32.118	-102.592	185	39.3	1.84	44.6	0.11	C	GP
318A	TA	31.439	-109.991	181	30.4	1.70	29.9	0.16	B	BR
319A	AR	31.376	-109.281	179	29.3	1.75	29.7	0.27	A	BR
319A	TA	31.376	-109.281	337	30.0	1.73	30.0	0.26	A	BR
320A	TA	31.337	-108.528	112	30.1	1.77	30.8	0.20	A	BR
325A	TA	31.371	-104.971	144	37.9	1.86	40.6	0.14	A	BR

328A	TA	31.382	-102.810	163	44.4	1.83	50.8	0.12	A	GP
425A	TA	30.786	-104.986	135	31.9	1.83	33.4	0.07	C	BR
426A	TA	30.669	-104.029	124	40.4	1.81	42.0	0.18	A	BR
428A	TA	30.726	-102.685	60	34.8	1.83	39.8	0.10	C	BR
438A	TA	30.750	-95.474	36	26.8	1.75	27.5	0.09	A	BR
526A	TA	30.061	-104.090	95	34.2	1.80	38.8	0.24	A	BR
527A	TA	30.146	-103.612	136	40.9	1.73	40.9	0.16	A	BR
528A	TA	30.162	-102.788	116	43.4	1.70	42.5	0.18	B	BR
529A	TA	30.125	-102.220	137	41.2	1.74	41.7	0.12	C	BR
626A	TA	29.554	-104.133	98	38.4	1.76	39.1	0.24	A	BR
627A	TA	29.453	-103.389	128	35.6	1.73	35.6	0.13	A	BR
628A	TA	29.486	-102.888	136	34.9	1.74	35.1	0.13	A	BR
A04A	TA	48.720	-122.707	110	29.9	1.79	31.4	0.15	A	PB
A04D	TA	48.720	-122.706	43	30.0	1.80	31.9	0.19	A	CS
A05A	TA	48.998	-122.085	161	31.2	1.79	34.0	0.09	A	CS
A06A	TA	49.098	-121.480	64	32.3	1.75	32.8	0.37	A	CS
A07A	TA	49.048	-120.384	128	33.2	1.76	33.9	0.16	A	CS
A08A	TA	48.953	-119.272	137	30.8	1.78	31.6	0.20	A	RM
A09A	TA	48.975	-118.585	138	32.4	1.76	32.9	0.23	A	RM
A10A	TA	48.981	-117.559	123	33.2	1.77	33.9	0.24	A	RM
A11A	TA	48.958	-116.363	154	36.9	1.74	37.0	0.17	B	RM
A12A	TA	48.934	-115.653	229	33.0	1.80	34.9	0.16	A	RM
A13A	TA	48.933	-114.413	161	41.6	1.76	42.2	0.18	A	RM
A14A	TA	48.972	-113.422	52	44.0	1.86	48.0	0.17	C	RM
A15A	TA	48.978	-112.733	140	38.7	1.79	40.0	0.09	A	GP
A16A	TA	48.948	-111.597	223	36.5	1.81	41.0	0.06	A	GP
A17A	TA	48.945	-110.699	126	37.7	1.71	37.4	0.17	B	GP
A18A	TA	48.920	-109.846	107	39.0	1.73	39.0	0.33	B	GP
A19A	TA	48.929	-108.743	71	42.0	1.76	42.6	0.34	A	GP
A20A	TA	48.880	-107.926	76	40.9	1.69	39.5	0.38	B	GP
A21A	TA	48.991	-106.925	71	41.2	1.70	40.9	0.25	B	GP
A22A	TA	48.993	-105.915	53	40.2	1.72	39.8	0.24	C	GP
A23A	TA	48.959	-104.879	64	44.5	1.77	45.7	0.24	C	GP
A24A	TA	48.924	-104.002	53	44.2	1.75	44.9	0.30	C	GP
A25A	TA	48.939	-103.113	97	42.1	1.75	42.9	0.30	C	GP
A26A	TA	48.897	-102.038	71	43.8	1.70	41.0	0.29	C	GP
ADO	CI	34.550	-117.434	36	25.7	1.80	27.3	0.36	C	PB
AHID	US	42.765	-111.100	247	47.1	1.77	47.9	0.04	C	RM
ANMO	IU	34.946	-106.457	1448	38.3	1.70	37.2	0.22	B	BR
ARV	CI	35.127	-118.830	431	39.4	1.73	39.4	0.10	A	PB
AZ45	XM	36.455	-109.082	92	43.1	1.74	43.2	0.18	C	CP
AZ46	XM	36.551	-109.229	105	42.5	1.72	42.1	0.21	C	CP
AZ47	XM	36.636	-109.333	122	42.3	1.79	43.5	0.07	C	CP

AZ48	XM	36.761	-109.539	82	43.4	1.78	44.3	0.11	C	CP
AZ49	XM	36.887	-109.691	146	45.7	1.76	46.8	0.12	C	CP
AZ50	XM	36.978	-109.864	108	37.7	1.71	37.4	0.03	C	CP
B04A	TA	48.057	-123.504	85	35.0	1.79	36.7	0.18	A	PB
B05A	TA	48.264	-122.096	122	27.1	1.76	28.0	0.08	A	PB
B05D	TA	48.264	-122.096	80	29.4	1.86	27.9	0.10	B	PB
B06A	TA	48.518	-121.484	55	35.3	1.66	34.0	0.18	B	CS
B07A	TA	48.461	-120.120	91	33.9	1.65	31.0	0.20	B	CS
B08A	TA	48.358	-119.333	199	28.9	1.76	29.6	0.16	A	RM
B09A	TA	48.423	-118.149	157	31.3	1.75	31.6	0.23	A	RM
B10A	TA	48.299	-117.225	137	31.9	1.78	32.9	0.33	A	RM
B11A	TA	48.437	-116.367	142	33.7	1.77	34.5	0.17	A	RM
B12A	TA	48.469	-115.589	161	38.0	1.80	36.0	0.07	A	RM
B13A	TA	48.374	-114.468	215	37.8	1.71	37.4	0.11	B	RM
B14A	TA	48.361	-113.273	116	37.0	1.69	36.1	0.12	B	RM
B15A	TA	48.313	-112.562	134	38.1	1.74	38.4	0.11	B	GP
B16A	TA	48.413	-111.707	176	38.4	1.78	39.8	0.04	A	GP
B17A	TA	48.292	-110.799	159	38.3	1.73	38.6	0.17	B	GP
B18A	TA	48.394	-109.777	137	38.7	1.76	39.5	0.22	A	GP
B20A	TA	48.439	-108.021	96	34.2	1.82	37.1	0.24	C	GP
B21A	TA	48.428	-107.017	127	44.9	1.68	43.4	0.22	C	GP
B22A	TA	48.301	-105.996	71	40.4	1.73	40.4	0.36	C	GP
B23A	TA	48.464	-104.991	69	44.1	1.77	45.6	0.26	C	GP
B25A	TA	48.272	-103.161	81	47.8	1.81	49.9	0.15	C	GP
B26A	TA	48.376	-102.234	56	42.6	1.81	44.8	0.24	C	GP
BAR	CI	32.680	-116.672	625	38.4	1.77	39.6	0.12	B	PB
BAR	TS	32.680	-116.672	132	38.4	1.77	39.6	0.12	B	PB
BBR	CI	34.262	-116.921	515	34.5	1.75	35.0	0.24	A	PB
BC3	CI	33.655	-115.454	629	24.0	1.81	25.0	0.22	A	BR
BCC	CI	33.575	-117.261	64	31.4	1.75	31.7	0.11	B	PB
BEL	CI	34.001	-115.998	658	27.7	1.77	28.4	0.31	A	BR
BFS	CI	34.239	-117.659	381	29.5	1.85	31.2	0.21	B	PB
BH1C	XV	44.933	-107.766	75	36.1	1.76	36.7	0.15	A	RM
BH1E	XV	44.200	-106.961	98	39.0	1.81	40.8	0.11	A	RM
BH1F	XV	45.275	-106.645	50	36.5	1.74	37.0	0.23	C	GP
BH1G	XV	45.489	-105.863	60	36.9	1.74	37.8	0.24	C	GP
BH1H	XV	44.954	-105.073	57	40.0	1.72	39.9	0.23	C	GP
BH2A	XV	44.686	-108.609	41	48.0	1.77	48.6	0.10	C	RM
BH2C	XV	44.138	-107.828	17	46.5	1.77	47.8	0.22	C	RM
BH2G	XV	44.791	-106.017	28	35.5	1.82	39.9	0.21	B	GP
BH3D	XV	44.417	-107.390	107	37.2	1.79	38.6	0.18	A	RM
BH3E	XV	43.593	-106.893	179	48.8	1.71	48.3	0.07	C	RM
BH3F	XV	44.826	-106.641	37	38.2	1.71	37.7	0.21	B	RM

BH4G	XV	44.191	-105.784	36	42.3	1.80	47.6	0.16	A	RM
BH5G	XV	43.640	-106.030	38	44.9	1.79	46.8	0.16	A	RM
BLA	XG	37.542	-105.575	32	48.5	1.71	48.0	0.08	B	RM
BLUE	XT	40.992	-108.542	27	50.8	1.79	52.6	0.14	C	RM
BMN	US	40.431	-117.222	205	27.8	1.78	28.7	0.27	A	BR
BMO	US	44.853	-117.306	356	28.0	1.84	29.5	0.11	B	ColP
BNLO	TA	37.131	-122.173	100	24.1	1.76	24.6	0.21	A	PB
BOZ	US	45.647	-111.630	957	32.8	1.77	33.7	0.15	A	RM
BTO	XG	40.393	-105.200	58	47.6	1.70	46.7	0.15	B	GP
BUR	XG	39.389	-102.351	21	44.8	1.80	48.2	0.07	C	GP
BW06	US	42.767	-109.558	689	35.2	1.74	35.3	0.11	A	RM
C04A	TA	47.717	-122.972	101	35.4	1.77	35.8	0.19	A	PB
C05A	TA	47.695	-121.689	139	41.5	1.81	44.9	0.12	B	PB
C06A	TA	47.923	-120.894	101	33.9	1.79	34.9	0.16	C	CS
C06D	TA	47.923	-120.894	104	35.1	1.72	34.9	0.21	C	CS
C07A	TA	47.690	-120.061	111	29.1	1.71	28.5	0.24	B	ColP
C10A	TA	47.819	-117.308	173	26.2	1.79	28.2	0.11	C	ColP
C11A	TA	47.840	-116.256	166	27.7	1.87	34.6	0.23	B	RM
C12A	TA	47.704	-115.481	10	36.5	1.70	35.4	0.20	B	RM
C12B	TA	47.709	-115.475	159	36.7	1.69	35.9	0.18	B	RM
C13A	TA	47.680	-114.574	264	32.6	1.79	33.7	0.21	A	RM
C14A	TA	47.769	-113.747	221	38.5	1.70	37.9	0.15	B	RM
C15A	TA	47.775	-112.607	158	43.6	1.79	46.5	0.14	A	RM
C16A	TA	47.801	-111.746	203	44.0	1.76	45.3	0.09	C	GP
C17A	TA	47.633	-110.763	182	39.7	1.72	38.7	0.09	B	GP
C19A	TA	47.734	-109.049	85	43.2	1.77	44.4	0.22	C	GP
C20A	TA	47.713	-108.004	119	48.2	1.68	46.3	0.14	C	GP
C21A	TA	47.826	-107.096	79	48.8	1.66	46.2	0.27	C	GP
C22A	TA	47.746	-105.884	59	42.4	1.76	43.3	0.40	C	GP
C23A	TA	47.803	-105.184	89	45.2	1.72	44.9	0.25	C	GP
C24A	TA	47.530	-104.425	67	50.2	1.75	51.1	0.19	C	GP
C25A	TA	47.712	-103.256	71	45.3	1.75	45.9	0.25	C	GP
C26A	TA	47.826	-102.096	55	36.1	1.93	47.7	0.21	C	GP
CALA	XT	40.113	-108.536	18	56.0	1.74	56.2	0.21	B	BR
CALB	TS	34.143	-118.627	32	28.0	1.85	30.0	0.35	B	PB
CALI	XT	40.365	-108.567	48	51.4	1.80	53.4	0.11	C	RM
CHF	CI	34.333	-118.026	619	28.8	1.90	25.5	0.10	B	PB
CIA	CI	33.402	-118.415	471	23.7	1.70	23.3	0.12	B	PB
CIU	CI	33.446	-118.483	14	23.0	1.65	22.0	0.14	B	PB
CRG	XG	40.540	-107.412	12	47.9	1.82	51.5	0.37	A	RM
CSD	XT	40.436	-108.279	35	44.6	1.73	44.6	0.12	B	RM
CSR	Z2	44.462	-109.861	10	40.1	1.74	40.3	0.09	C	RM
CVS	BK	38.345	-122.458	109	23.5	1.73	23.5	0.15	A	PB

CWC	CI	36.440	-118.080	533	28.9	1.81	31.2	0.22	A	SN
CWC	TS	36.440	-118.080	56	29.1	1.79	31.0	0.24	A	SN
CYF	XH	37.554	-109.866	48	37.3	1.80	38.6	0.09	C	CP
D03A	TA	47.116	-123.771	24	29.1	1.75	29.4	0.12	A	PB
D03D	TA	47.535	-123.089	75	39.0	1.79	39.8	0.18	A	PB
D05A	TA	47.188	-121.989	76	39.8	1.76	40.2	0.12	A	CS
D06A	TA	47.194	-120.844	51	43.4	1.78	42.2	0.10	A	CS
D07A	TA	47.194	-119.973	91	30.3	1.84	31.2	0.09	C	ColP
D08A	TA	47.057	-118.921	185	41.7	1.85	45.9	0.03	A	ColP
D09A	TA	47.062	-118.309	181	44.3	1.90	49.7	0.02	A	ColP
D10A	TA	47.055	-117.276	127	30.1	1.76	31.1	0.19	A	ColP
D11A	TA	47.048	-116.335	106	31.9	1.69	31.3	0.16	B	RM
D12A	TA	47.053	-115.353	165	32.7	1.80	34.0	0.10	B	RM
D13A	TA	47.094	-114.459	160	33.8	1.68	32.4	0.18	B	RM
D14A	TA	47.082	-113.506	200	36.6	1.73	36.6	0.12	B	RM
D15A	TA	47.042	-112.520	209	36.4	1.77	37.4	0.16	A	RM
D16A	TA	47.031	-111.549	154	35.9	1.81	37.1	0.08	C	RM
D17A	TA	47.152	-110.687	195	39.5	1.83	41.4	0.14	B	RM
D18A	TA	47.196	-109.802	149	44.2	1.71	42.2	0.15	B	GP
D19A	TA	47.165	-108.880	157	43.6	1.72	43.2	0.06	B	GP
D20A	TA	47.091	-108.136	105	46.3	1.77	48.2	0.18	A	GP
D21A	TA	47.066	-106.994	48	46.4	1.74	46.8	0.29	C	GP
D22A	TA	47.150	-106.180	76	48.0	1.70	47.0	0.24	C	GP
D23A	TA	47.173	-105.207	74	45.0	1.83	50.2	0.21	C	GP
D24A	TA	47.115	-104.327	91	44.1	1.83	50.5	0.27	C	GP
D25A	TA	47.151	-103.320	70	46.9	1.75	47.4	0.22	C	GP
D26A	TA	47.030	-102.436	48	46.3	1.84	48.0	0.20	C	GP
DAN	CI	34.638	-115.381	1028	27.2	1.65	26.1	0.27	B	BR
DBQ	XG	39.246	-108.176	23	45.1	1.71	43.9	0.19	B	CP
DEC	CI	34.254	-118.334	212	25.7	1.71	25.4	0.15	B	PB
DGMT	US	48.470	-104.196	167	46.3	1.77	47.2	0.24	C	GP
DGR	CI	33.650	-117.009	1176	31.8	1.81	33.3	0.22	A	PB
DGR	TS	33.650	-117.009	197	31.8	1.81	33.3	0.19	A	PB
DJJ	CI	34.106	-118.455	376	27.7	1.65	26.2	0.13	B	PB
DOT	XG	39.777	-106.990	19	47.4	1.71	47.0	0.19	A	CP
DUG	US	40.195	-112.813	916	26.3	1.79	27.3	0.20	A	BR
DVT	CI	32.659	-116.101	195	25.0	1.84	30.6	0.08	C	PB
E03A	TA	46.546	-123.563	72	32.8	1.73	32.8	0.22	B	PB
E05A	TA	46.561	-121.761	79	41.5	1.72	41.2	0.16	B	CS
E06A	TA	46.543	-120.979	57	37.9	1.86	44.8	0.11	A	CS
E07A	TA	46.558	-119.855	178	34.5	1.84	38.7	0.20	B	ColP
E08A	TA	46.491	-119.060	142	31.8	1.78	31.5	0.09	C	ColP
E09A	TA	46.514	-118.146	180	41.3	1.86	45.9	0.00	A	ColP

E10A	TA	46.485	-117.110	140	33.6	1.79	35.0	0.22	A	ColP
E11A	TA	46.356	-116.209	134	30.5	1.78	31.6	0.20	A	ColP
E12A	TA	46.415	-115.571	150	32.1	1.77	32.9	0.22	A	RM
E13A	TA	46.442	-114.188	184	32.3	1.80	34.5	0.20	B	RM
E14A	TA	46.416	-113.493	175	25.6	1.91	33.1	0.17	B	RM
E15A	TA	46.425	-112.641	225	36.4	1.74	36.5	0.05	B	RM
E16A	TA	46.534	-111.676	145	31.5	1.77	32.3	0.17	A	RM
E17A	TA	46.462	-110.858	170	39.1	1.69	38.1	0.10	B	RM
E18A	TA	46.566	-109.914	118	45.9	1.71	45.0	0.17	B	GP
E19A	TA	46.461	-108.786	66	43.7	1.72	43.5	0.22	C	GP
E20A	TA	46.504	-108.130	99	43.2	1.80	45.2	0.13	B	GP
E21A	TA	46.541	-107.076	187	47.6	1.78	49.3	0.10	A	GP
E22A	TA	46.439	-105.949	73	42.2	1.74	42.5	0.23	C	GP
E23A	TA	46.498	-105.306	82	49.5	1.65	47.6	0.14	C	GP
E24A	TA	46.561	-104.307	69	46.1	1.71	45.3	0.30	C	GP
E25A	TA	46.501	-103.401	66	42.0	1.83	46.4	0.31	C	GP
E26A	TA	46.471	-102.462	63	42.0	1.73	42.0	0.28	C	GP
EDW2	CI	34.881	-117.994	672	28.8	1.76	29.2	0.19	A	PB
EDW	CI	34.883	-117.991	27	28.9	1.76	29.3	0.20	A	PB
EGMT	US	48.024	-109.755	363	38.6	1.79	40.6	0.14	A	GP
ELFS	TA	40.618	-120.728	115	35.2	1.81	36.5	0.15	B	BR
ELK	US	40.745	-115.239	848	29.2	1.76	29.7	0.21	A	BR
F03A	TA	45.931	-123.559	36	37.3	1.81	33.4	0.11	A	PB
F04A	TA	45.932	-122.419	105	46.6	1.82	48.4	0.24	A	CS
F05A	TA	45.884	-121.459	69	46.8	1.74	47.2	0.01	C	CS
F05D	TA	45.885	-121.460	51	43.4	1.82	35.8	0.09	A	CS
F06A	TA	45.766	-120.782	98	33.6	1.84	36.5	0.12	A	ColP
F07A	TA	45.895	-119.928	161	34.5	1.73	34.5	0.36	B	ColP
F08A	TA	45.797	-118.777	63	37.1	1.68	35.8	0.12	B	ColP
F09A	TA	45.709	-117.909	98	31.6	1.94	43.4	0.09	C	ColP
F10A	TA	45.973	-117.228	145	44.0	1.70	43.4	0.12	C	ColP
F11A	TA	45.888	-116.155	98	37.5	1.71	37.1	0.11	C	ColP
F12A	TA	45.757	-115.255	232	35.6	1.69	34.9	0.13	B	RM
F13A	TA	45.789	-114.332	185	35.7	1.75	36.1	0.17	A	RM
F14A	TA	45.812	-113.370	93	33.6	1.77	34.2	0.18	B	RM
F15A	TA	45.841	-112.493	207	33.0	1.82	34.3	0.06	B	RM
F16A	TA	45.784	-111.626	156	33.9	1.73	33.9	0.17	A	RM
F18A	TA	45.905	-109.716	137	49.0	1.74	49.4	0.16	A	GP
F19A	TA	45.854	-108.944	103	45.3	1.75	46.0	0.10	A	GP
F20A	TA	45.801	-108.149	120	31.8	1.94	38.4	0.12	B	GP
F21A	TA	45.823	-107.123	91	40.2	1.73	40.2	0.24	C	GP
F22A	TA	45.779	-106.257	83	39.2	1.71	38.6	0.36	C	GP
F23A	TA	45.721	-105.406	66	39.9	1.70	39.3	0.29	C	GP

F24A	TA	45.845	-104.445	60	46.2	1.72	45.7	0.16	C	GP
F26A	TA	45.851	-102.670	85	43.3	1.71	42.7	0.40	C	GP
F27A	TA	45.873	-102.020	72	43.7	1.73	43.7	0.31	C	GP
FA25	XR	47.582	-103.299	41	44.4	1.79	44.6	0.16	C	GP
FA26	XR	48.791	-105.431	36	43.7	1.69	42.8	0.31	C	GP
FA27	XR	49.942	-108.108	24	40.2	1.76	40.9	0.27	C	GP
FMP	CI	33.713	-118.294	340	22.9	1.65	21.7	0.25	B	BR
FUR	CI	36.467	-116.863	423	23.8	1.94	37.3	0.18	B	BR
FWGP	XT	40.964	-108.768	33	50.7	1.77	52.5	0.14	C	RM
G04A	TA	45.206	-122.478	40	32.6	1.79	33.6	0.17	C	CS
G05A	TA	45.242	-121.317	38	44.8	1.71	44.0	0.07	C	ColP
G05D	TA	45.242	-121.317	34	44.8	1.71	44.0	0.05	C	ColP
G06A	TA	45.236	-120.635	137	33.5	1.78	34.1	0.10	B	ColP
G07A	TA	45.266	-119.669	54	39.1	1.78	40.9	0.03	C	ColP
G08A	TA	45.290	-118.960	273	32.9	1.83	35.3	0.13	A	ColP
G09A	TA	45.278	-117.780	162	29.9	1.84	29.9	0.12	C	ColP
G10A	TA	45.292	-117.120	184	33.2	1.80	34.4	0.17	A	ColP
G11A	TA	45.400	-116.268	157	36.8	1.84	39.9	0.12	B	RM
G12A	TA	45.129	-115.326	134	32.3	1.81	34.9	0.11	A	RM
G13A	TA	45.093	-114.233	145	35.6	1.71	35.0	0.12	B	RM
G14A	TA	45.243	-113.460	136	33.5	1.79	34.6	0.22	A	RM
G15A	TA	45.166	-112.489	159	36.1	1.72	35.6	0.14	B	RM
G16A	TA	45.229	-111.805	114	33.8	1.70	33.1	0.28	A	RM
G17A	TA	45.321	-110.740	58	37.8	1.69	36.9	0.25	C	RM
G18A	TA	45.317	-109.563	79	46.5	1.74	46.7	0.12	C	RM
G21A	TA	45.225	-107.207	60	35.4	1.72	35.2	0.16	B	GP
G22A	TA	45.219	-106.292	57	40.4	1.71	39.8	0.35	B	GP
G23A	TA	45.201	-105.391	67	40.2	1.71	39.9	0.23	C	GP
GASB	BK	39.655	-122.716	67	34.2	1.77	34.8	0.27	A	PB
GLA	CI	33.051	-114.827	1368	25.8	1.68	24.9	0.15	B	BR
GLA	TS	33.052	-114.827	141	25.5	1.69	24.9	0.15	B	BR
GMR	CI	34.785	-115.660	616	25.7	1.78	26.5	0.21	A	BR
GOL	US	39.700	-105.371	81	45.8	1.76	46.9	0.13	A	RM
GPO	CI	35.649	-117.662	7	27.6	1.83	29.3	0.31	B	BR
GPO	TS	35.649	-117.662	16	27.7	1.83	29.3	0.23	B	BR
GPSS1	YS	42.500	-123.370	33	41.3	1.78	42.6	0.18	C	PB
GRAN	XT	41.108	-108.642	30	49.4	1.73	49.4	0.17	A	BR
GRA	CI	36.996	-117.366	162	34.5	1.91	39.5	0.28	C	RM
GRM	XG	39.100	-108.130	23	41.5	1.75	41.8	0.24	A	CP
GSC	CI	35.302	-116.806	508	28.2	1.73	28.2	0.13	C	BR
GSC	TS	35.303	-116.808	199	28.6	1.69	28.1	0.13	C	BR
GUN	XG	38.474	-107.056	22	44.5	1.73	44.5	0.20	A	CP
H04A	TA	44.684	-122.186	212	31.8	1.87	33.7	0.07	B	CS

H04D	TA	44.523	-122.738	43	34.1	1.80	35.6	0.13	C	CS
H05A	TA	44.647	-121.227	98	34.0	1.72	33.9	0.17	C	ColP
H06A	TA	44.734	-120.335	109	37.2	1.86	30.2	0.06	A	ColP
H07A	TA	44.591	-119.565	92	36.8	1.65	35.5	0.12	C	ColP
H08A	TA	44.519	-118.670	144	32.6	1.77	33.3	0.11	A	ColP
H09A	TA	44.665	-117.664	184	37.5	1.67	36.6	0.05	C	ColP
H10A	TA	44.589	-116.747	120	30.8	1.71	30.7	0.14	B	ColP
H11A	TA	44.703	-116.013	111	30.4	1.77	31.2	0.21	A	RM
H12A	TA	44.549	-114.855	183	37.5	1.75	37.8	0.21	A	RM
H13A	TA	44.564	-114.255	239	35.7	1.77	36.3	0.12	A	RM
H14A	TA	44.617	-113.367	76	29.5	1.83	32.7	0.19	B	RM
H15A	TA	44.617	-112.644	104	41.8	1.67	40.5	0.15	B	RM
H16A	TA	44.704	-111.248	125	41.8	1.84	44.9	0.16	A	RM
H18A	TA	44.677	-109.664	109	47.7	1.70	46.6	0.14	C	RM
H19A	TA	44.670	-108.986	24	50.6	1.74	50.9	0.13	C	RM
H20A	TA	44.487	-107.999	125	39.6	1.76	40.4	0.06	B	RM
H21A	TA	44.628	-107.042	47	33.7	1.81	36.9	0.16	C	RM
H22A	TA	44.594	-106.352	51	32.8	1.94	40.0	0.15	C	GP
H23A	TA	44.562	-105.401	26	33.8	1.89	41.5	0.21	C	GP
H24A	TA	44.747	-104.552	170	43.4	1.79	44.8	0.05	C	GP
H25A	TA	44.621	-103.598	213	41.5	1.83	44.9	0.13	C	GP
H26A	TA	44.617	-102.774	85	37.5	1.78	38.6	0.20	C	GP
H27A	TA	44.633	-102.077	111	44.3	1.73	44.3	0.13	C	GP
HAST	TA	36.389	-121.551	194	25.9	1.72	25.7	0.17	A	PB
HATC	TA	40.816	-121.461	50	32.6	1.94	35.3	0.18	B	SN
HEC	CI	34.829	-116.335	472	26.8	1.81	27.9	0.28	C	BR
HELL	TA	36.680	-119.023	250	47.3	1.75	47.7	0.08	C	RM
HGTCO	GS	37.107	-104.674	13	40.2	1.82	45.8	0.17	B	GP
HIAW	XT	41.015	-108.734	41	51.0	1.73	51.0	0.13	C	RM
HLD	XG	39.229	-109.140	43	41.3	1.66	40.0	0.07	B	CP
HOPS	BK	38.993	-123.072	40	18.6	1.94	22.8	0.41	B	PB
HUMO	BK	42.607	-122.957	577	39.7	1.65	37.5	0.19	B	PB
HWUT	US	41.607	-111.565	557	26.2	1.77	26.8	0.04	C	RM
I02A	TA	44.004	-123.830	28	33.0	1.83	36.2	0.10	C	PB
I02D	TA	44.106	-123.847	13	34.2	1.82	35.9	0.17	B	PB
I03A	TA	43.973	-123.278	70	39.2	1.94	42.7	0.18	C	PB
I04A	TA	43.794	-122.411	183	34.8	1.87	36.7	0.15	B	CS
I05A	TA	44.163	-121.268	62	31.9	1.82	33.3	0.19	A	ColP
I05D	TA	44.339	-121.340	34	32.9	1.76	33.8	0.12	C	ColP
I06A	TA	43.944	-120.211	138	28.8	1.83	30.7	0.20	A	ColP
I07A	TA	44.082	-119.504	156	31.1	1.90	33.7	0.12	B	ColP
I08A	TA	43.910	-118.569	137	34.1	1.73	34.1	0.13	C	ColP
I09A	TA	43.973	-117.741	198	28.9	1.79	30.0	0.15	A	ColP

I10A	TA	44.086	-116.803	35	44.8	1.84	46.8	0.21	C	ColP
I11A	TA	43.912	-115.958	157	44.2	1.70	43.4	0.01	C	RM
I13A	TA	43.915	-114.117	244	40.0	1.84	48.5	0.06	C	RM
I15A	TA	44.000	-112.485	99	38.6	1.80	40.3	0.19	A	ColP
I16A	TA	43.876	-111.487	169	38.2	1.83	40.2	0.14	C	ColP
I17A	TA	43.920	-110.576	26	36.6	1.82	37.9	0.22	B	RM
I18A	TA	43.701	-109.817	85	40.8	1.69	39.8	0.15	B	RM
I19A	TA	44.036	-108.994	123	49.9	1.73	49.9	0.14	C	RM
I20A	TA	43.950	-108.128	56	53.0	1.74	53.8	0.11	C	RM
I21A	TA	43.812	-107.292	250	56.9	1.73	56.9	0.09	C	RM
I22A	TA	43.892	-106.484	15	57.4	1.88	53.3	0.10	C	GP
I23A	TA	43.960	-105.463	57	40.8	1.79	46.1	0.18	C	GP
I24A	TA	43.859	-104.626	67	41.6	1.77	42.7	0.27	C	GP
I25A	TA	44.020	-103.732	203	45.6	1.75	46.1	0.12	A	GP
I26A	TA	44.031	-102.860	53	31.9	1.78	32.8	0.20	C	GP
I27A	TA	44.069	-102.052	125	26.0	1.92	32.7	0.22	C	GP
IBP	CI	32.661	-116.093	47	26.4	1.80	27.7	0.16	A	PB
IKP	CI	32.650	-116.109	31	22.1	1.94	30.8	0.20	C	PB
IRM	CI	34.157	-115.145	783	26.6	1.78	27.1	0.18	A	BR
ISA	CI	35.663	-118.474	630	37.7	1.73	37.7	0.20	A	SN
ISA	TS	35.663	-118.473	217	37.7	1.73	37.7	0.18	A	SN
ISA	US	35.663	-118.474	27	37.0	1.76	37.7	0.19	A	SN
ISCO	US	39.800	-105.613	883	45.4	1.80	46.8	0.12	A	RM
J03A	TA	43.372	-122.965	72	27.5	1.88	36.8	0.06	C	CS
J04A	TA	43.241	-122.109	19	43.2	1.70	42.6	0.12	C	CS
J05A	TA	43.284	-121.236	55	33.5	1.81	35.3	0.20	A	ColP
J05D	TA	43.285	-121.235	90	33.7	1.80	35.3	0.22	A	ColP
J06A	TA	43.251	-120.153	173	33.0	1.80	34.3	0.20	A	ColP
J07A	TA	43.374	-119.311	109	32.2	1.79	33.3	0.18	A	ColP
J08A	TA	43.358	-118.474	203	31.9	1.76	32.4	0.16	A	ColP
J09A	TA	43.347	-117.754	143	31.6	1.81	33.0	0.17	A	ColP
J10A	TA	43.428	-116.767	171	35.5	1.69	34.9	0.09	B	ColP
J11A	TA	43.415	-115.828	318	34.8	1.82	40.3	0.06	A	RM
J13A	TA	43.398	-114.174	224	37.9	1.79	39.2	0.04	A	RM
J14A	TA	43.323	-113.518	103	37.1	1.78	38.2	0.25	A	ColP
J15A	TA	43.400	-112.433	112	42.1	1.77	43.1	0.12	C	ColP
J16A	TA	43.274	-111.612	129	36.3	1.82	37.9	0.14	A	RM
J18A	TA	43.211	-110.020	119	43.0	1.81	47.9	0.17	C	RM
J19A	TA	43.265	-109.053	98	48.5	1.80	49.9	0.15	C	RM
J20A	TA	43.353	-108.084	48	35.9	1.87	42.6	0.16	B	RM
J22A	TA	43.413	-106.479	184	44.1	1.71	43.6	0.05	C	GP
J23A	TA	43.404	-105.552	60	44.7	1.73	44.7	0.14	C	GP
J24A	TA	43.331	-104.661	36	52.3	1.70	51.3	0.23	C	GP

J25A	TA	43.390	-103.803	203	53.8	1.74	54.2	0.10	C	GP
J26A	TA	43.313	-103.075	112	52.2	1.75	53.1	0.10	C	GP
J27A	TA	43.253	-102.007	68	32.4	1.76	33.1	0.19	C	GP
JCC	BK	40.818	-124.030	48	25.6	1.73	25.6	0.41	A	PB
JCS	CI	33.086	-116.596	434	33.9	1.77	34.9	0.16	A	PB
JNMT	XT	40.459	-108.020	45	54.9	1.79	54.9	0.10	C	RM
JRSC	BK	37.404	-122.239	125	21.1	1.76	21.6	0.03	B	PB
JWM	XT	40.572	-108.604	56	53.5	1.80	23.6	0.12	C	RM
K01A	TA	42.809	-124.469	22	20.9	1.80	21.5	0.27	A	PB
K02A	TA	42.767	-123.490	111	37.2	1.86	39.5	0.11	C	PB
K04A	TA	42.613	-121.731	46	33.8	1.84	35.7	0.25	A	BR
K05A	TA	42.726	-120.893	63	31.7	1.83	33.3	0.20	A	BR
K06A	TA	42.799	-120.251	68	36.6	1.84	44.9	0.22	C	BR
K07A	TA	42.691	-119.247	117	31.4	1.85	33.3	0.26	A	BR
K08A	TA	42.731	-118.486	144	31.7	1.72	31.7	0.10	C	ColP
K09A	TA	42.700	-117.725	145	32.7	1.85	34.3	0.11	A	ColP
K10A	TA	42.778	-116.870	163	33.6	1.93	45.4	0.13	C	ColP
K11A	TA	42.771	-116.032	132	37.2	1.76	37.6	0.19	A	ColP
K12A	TA	42.636	-114.903	147	39.9	1.72	39.8	0.13	B	ColP
K13A	TA	42.649	-114.084	155	36.3	1.78	37.1	0.17	A	ColP
K14A	TA	42.545	-113.176	212	34.5	1.81	38.9	0.24	A	ColP
K15A	TA	42.685	-112.531	138	35.3	1.82	37.1	0.08	A	BR
K17A	TA	42.751	-110.920	83	52.6	1.73	52.6	0.20	C	RM
K18A	TA	42.637	-110.042	46	48.0	1.76	49.5	0.03	C	RM
K19A	TA	42.825	-108.847	208	45.6	1.76	46.3	0.05	C	RM
K20A	TA	42.658	-108.342	137	45.7	1.82	47.6	0.12	C	RM
K22A	TA	42.651	-106.524	451	40.6	1.93	46.9	0.08	C	RM
K23A	TA	42.755	-105.625	176	38.5	1.78	40.3	0.07	C	GP
K25A	TA	42.612	-103.870	51	46.8	1.70	45.7	0.33	C	GP
K26A	TA	42.702	-103.178	83	30.0	1.74	30.3	0.21	C	GP
KCC	BK	37.324	-119.319	289	49.8	1.72	49.5	0.11	B	SN
KIDD	EP	31.772	-106.506	178	31.3	1.81	33.3	0.22	A	BR
KINN	XT	41.180	-108.593	23	44.9	1.65	43.3	0.11	B	RM
KNB	US	37.017	-112.822	220	49.6	1.75	50.5	0.13	A	CP
KRM	XG	40.130	-106.405	21	47.7	1.79	49.1	0.17	A	RM
KSCO	TA	39.011	-102.627	265	40.5	1.73	40.5	0.11	B	GP
L01	XF	41.003	-105.525	31	48.7	1.79	51.0	0.14	A	RM
L03	XF	41.041	-105.555	28	51.5	1.78	53.1	0.13	A	RM
L04A	TA	42.175	-121.891	60	33.6	1.82	36.1	0.16	A	PB
L04D	TA	42.218	-122.305	10	29.6	1.89	34.8	0.11	C	CS
L04	XF	41.061	-105.571	26	51.6	1.76	52.3	0.16	A	RM
L05A	TA	42.047	-120.834	58	34.4	1.75	34.8	0.24	A	BR
L05	XF	41.081	-105.588	26	52.1	1.74	52.4	0.15	A	RM

L06	XF	41.100	-105.606	33	46.7	1.79	50.8	0.11	A	RM
L07A	TA	42.019	-119.340	129	33.6	1.79	34.6	0.25	A	BR
L07	XF	41.120	-105.623	34	48.3	1.78	49.5	0.11	A	RM
L08A	TA	42.190	-118.344	207	30.7	1.82	32.0	0.15	A	BR
L08	XF	41.140	-105.642	35	48.3	1.78	49.5	0.11	A	RM
L09A	TA	42.019	-117.667	106	42.8	1.70	41.9	0.15	B	BR
L09	XF	41.160	-105.657	35	47.9	1.80	50.0	0.12	B	RM
L10A	TA	42.077	-116.471	213	38.7	1.73	38.7	0.19	A	ColP
L10	XF	41.181	-105.671	45	50.7	1.81	52.8	0.08	B	RM
L11A	TA	42.167	-115.754	169	38.7	1.79	39.8	0.18	A	ColP
L11	XF	41.198	-105.693	38	42.0	1.89	52.0	0.14	C	RM
L12A	TA	42.146	-115.016	160	38.4	1.72	38.1	0.21	A	ColP
L12	XF	41.222	-105.706	28	50.3	1.76	51.1	0.12	C	RM
L13A	TA	42.089	-113.944	192	35.2	1.80	40.1	0.27	C	ColP
L13	XF	41.234	-105.729	31	52.1	1.74	52.7	0.11	B	RM
L14A	TA	42.034	-113.240	160	35.8	1.73	35.8	0.13	A	BR
L14	XF	41.260	-105.741	22	49.1	1.76	50.1	0.16	A	BR
L15A	TA	42.004	-112.386	166	34.4	1.81	21.4	0.11	A	RM
L16A	TA	42.015	-111.432	107	37.3	1.70	36.5	0.16	B	RM
L16	XF	41.292	-105.789	25	52.6	1.74	52.9	0.14	C	RM
L17A	TA	42.099	-110.873	87	41.7	1.70	40.9	0.24	C	RM
L18A	TA	41.924	-110.036	83	37.0	1.87	42.3	0.20	B	RM
L19A	TA	42.101	-109.357	34	33.4	1.78	34.9	0.25	C	RM
L19	XF	41.360	-105.826	17	46.5	1.83	48.5	0.18	C	RM
L20A	TA	42.007	-108.340	66	27.2	1.92	34.5	0.26	C	RM
L20	XF	41.379	-105.843	21	45.8	1.94	49.7	0.13	C	RM
L21A	TA	41.964	-107.369	181	45.9	1.73	45.9	0.13	A	RM
L21	XF	41.404	-105.859	18	48.9	1.78	50.4	0.12	C	RM
L22A	TA	42.031	-106.434	181	53.3	1.71	53.0	0.09	C	RM
L22	XF	41.420	-105.879	12	49.8	1.79	51.1	0.15	A	RM
L23A	TA	42.114	-105.701	161	50.5	1.79	51.9	0.06	C	RM
L23	XF	41.440	-105.895	10	47.2	1.66	45.4	0.20	C	RM
L24A	TA	42.043	-104.933	128	52.1	1.68	50.3	0.11	C	GP
L24	XF	41.485	-105.894	8	45.7	1.82	52.5	0.25	B	RM
L25A	TA	42.155	-103.966	55	48.1	1.70	47.1	0.36	C	GP
L26A	TA	42.037	-103.079	76	44.5	1.72	44.2	0.27	C	GP
L27A	TA	42.084	-102.315	74	33.0	1.80	34.9	0.21	C	GP
LAO	US	46.688	-106.223	358	47.4	1.74	47.8	0.25	C	GP
LAVA	TA	38.755	-120.740	253	23.6	1.77	24.5	0.06	C	SN
LGU	CI	34.108	-119.066	430	25.9	1.65	25.1	0.09	B	PB
LIZ	XG	39.355	-104.546	12	45.1	1.69	44.2	0.20	B	GP
LKWY	US	44.565	-110.400	60	44.6	1.71	44.2	0.27	C	RM
LMN	XG	39.416	-103.622	32	44.4	1.70	43.6	0.29	C	GP

LRL	CI	35.479	-117.682	617	29.8	1.76	30.4	0.37	A	BR
LSC	XT	40.533	-108.441	40	53.8	1.80	54.9	0.10	C	RM
LT	US	29.334	-103.667	358	34.8	1.79	36.1	0.19	A	GP
M01C	TA	41.847	-124.122	41	25.0	1.71	25.0	0.16	A	PB
M02C	TA	41.392	-122.854	265	35.2	1.75	35.7	0.20	A	PB
M03C	TA	41.274	-122.122	59	36.0	1.73	36.0	0.16	A	CS
M04C	TA	41.783	-121.839	83	31.3	1.82	33.1	0.21	A	BR
M05C	TA	41.359	-121.146	175	33.8	1.79	34.9	0.18	B	BR
M06C	TA	41.205	-120.477	126	31.4	1.73	31.4	0.16	C	BR
M07A	TA	41.388	-119.171	195	29.3	1.78	30.4	0.23	C	BR
M08A	TA	41.448	-118.379	49	34.3	1.77	35.3	0.19	A	BR
M10A	TA	41.522	-116.540	145	37.0	1.74	37.1	0.16	C	BR
M11A	TA	41.431	-115.791	232	41.9	1.70	41.2	0.04	C	BR
M12A	TA	41.416	-114.915	257	36.4	1.72	36.2	0.17	A	BR
M13A	TA	41.360	-114.165	195	32.9	1.72	32.6	0.22	A	BR
M14A	TA	41.503	-113.347	192	22.4	1.81	23.6	0.09	C	BR
M15A	TA	41.463	-112.448	192	25.2	1.87	26.8	0.12	B	BR
M16A	TA	41.315	-111.630	125	33.0	1.80	34.0	0.11	C	RM
M17A	TA	41.473	-110.666	22	40.9	1.81	42.6	0.30	A	RM
M18A	TA	41.427	-110.067	69	48.1	1.67	46.2	0.22	C	RM
M19A	TA	41.505	-109.157	166	37.3	1.73	37.3	0.13	C	RM
M20A	TA	41.491	-108.187	34	41.5	1.65	35.9	0.30	C	RM
M21A	TA	41.607	-107.364	118	40.0	1.79	41.6	0.16	B	RM
M23A	TA	41.468	-105.722	115	47.6	1.74	47.8	0.11	C	RM
M24A	TA	41.468	-104.825	40	46.0	1.74	46.3	0.23	C	GP
M25A	TA	41.435	-104.055	58	44.5	1.67	42.6	0.29	C	GP
M26A	TA	41.466	-103.143	69	43.8	1.76	44.8	0.36	C	GP
M27A	TA	41.528	-102.387	77	41.9	1.73	41.9	0.23	C	GP
MAYB	XT	40.483	-108.193	33	54.5	1.87	51.2	0.14	B	RM
MB01	XM	33.336	-106.034	38	35.8	1.83	37.8	0.21	A	BR
MB04B	XM	34.071	-106.942	30	36.1	1.65	32.6	0.25	B	BR
MB05	XM	34.664	-108.011	10	32.4	1.76	32.8	0.34	C	CP
MCCM	BK	38.145	-122.880	272	22.3	1.78	22.9	0.19	B	PB
MGP	XG	40.260	-108.780	25	53.1	1.81	55.8	0.10	C	CP
MHTCO	GS	37.128	-104.691	26	42.5	1.77	43.7	0.17	A	GP
MKR	XG	40.033	-107.744	31	50.2	1.76	51.1	0.10	C	RM
MLAC	CI	37.630	-118.836	85	32.6	1.79	34.9	0.24	C	SN
MLAC	TS	37.631	-118.834	38	31.3	1.81	34.9	0.14	C	SN
MNRC	BK	38.879	-122.443	30	26.1	1.78	26.6	0.11	C	PB
MNT	US	31.698	-105.382	533	44.9	1.86	52.5	0.08	C	BR
MNV	US	38.433	-118.153	353	30.9	1.82	31.9	0.28	A	BR
MOD	BK	41.903	-120.303	175	35.1	1.72	34.9	0.18	C	BR
MON	XG	38.531	-107.997	46	48.4	1.75	48.9	0.09	C	CP

MPM	CI	36.058	-117.489	994	30.0	1.75	30.4	0.23	A	BR
MPP	CI	34.889	-119.814	327	28.1	1.83	31.9	0.14	B	PB
MSO	US	46.829	-113.941	468	35.8	1.72	35.7	0.15	B	RM
MST	TA	33.970	-102.772	351	42.1	1.79	43.3	0.19	A	GP
MUR	CI	33.600	-117.195	532	30.2	1.81	31.1	0.14	C	PB
MVCO	US	37.210	-108.499	311	45.4	1.74	45.5	0.22	A	CP
MWC	CI	34.224	-118.058	602	27.5	1.84	33.7	0.14	B	PB
N00	XK	42.461	-107.699	31	44.9	1.87	37.8	0.10	C	RM
N01	XS	46.281	-109.411	51	45.3	1.74	45.6	0.12	C	GP
N02C	TA	40.822	-123.306	90	29.8	1.66	28.6	0.24	C	GP
N02D	TA	40.974	-122.705	99	27.2	1.67	26.1	0.10	C	PB
N02	XS	46.251	-109.205	55	45.7	1.71	44.9	0.13	C	PB
N04	XS	46.205	-108.540	38	46.8	1.71	46.3	0.16	C	GP
N05	XK	41.895	-107.392	39	38.3	1.85	40.7	0.14	C	GP
N05	XS	46.250	-108.300	15	43.9	1.79	49.4	0.24	A	RM
N06A	TA	40.748	-119.835	169	32.6	1.75	32.8	0.21	A	BR
N06	XK	41.800	-107.355	44	45.2	1.68	43.8	0.10	C	RM
N06	XS	46.416	-109.519	39	44.4	1.75	45.2	0.17	A	GP
N07B	TA	40.780	-118.971	232	25.4	1.81	28.1	0.33	C	RM
N07	XS	46.443	-109.236	51	44.0	1.73	44.0	0.15	A	GP
N08A	TA	40.781	-118.134	189	30.0	1.84	31.6	0.16	A	BR
N08	XK	41.623	-107.279	29	46.5	1.69	45.2	0.16	B	RM
N08	XS	46.500	-108.861	13	42.8	1.69	40.9	0.23	B	GP
N09A	TA	40.852	-117.524	247	30.7	1.81	31.9	0.08	A	BR
N09	XS	46.513	-108.591	30	41.1	1.71	40.8	0.20	B	GP
N10A	TA	40.719	-116.508	280	27.0	1.81	27.9	0.12	A	BR
N10	XK	41.452	-107.214	81	47.4	1.68	45.0	0.10	B	RM
N10	XS	46.609	-109.193	30	36.1	1.85	40.8	0.24	B	GP
N12A	TA	40.852	-115.039	165	27.8	1.79	28.5	0.11	B	BR
N12	XS	46.649	-108.650	39	42.3	1.72	42.0	0.25	B	GP
N13A	TA	40.856	-114.204	120	27.0	1.77	27.7	0.16	A	BR
N14A	TA	40.851	-113.187	181	28.1	1.66	26.3	0.32	B	BR
N14	XK	41.079	-107.176	6	49.7	1.81	52.1	0.30	C	RM
N15A	TA	40.890	-112.520	181	26.0	1.65	24.7	0.10	C	RM
N15A	XK	40.998	-107.030	34	50.7	1.70	49.8	0.11	B	RM
N16A	TA	40.887	-111.437	29	32.9	1.82	34.5	0.14	C	RM
N16	XK	40.925	-106.990	77	47.0	1.75	47.9	0.20	A	RM
N17A	TA	40.943	-110.834	16	36.0	1.66	34.6	0.21	C	RM
N19A	TA	40.894	-109.177	187	45.9	1.72	45.7	0.04	C	RM
N20	XK	40.566	-106.879	47	48.6	1.75	49.1	0.19	A	RM
N21	XK	40.453	-106.916	72	49.5	1.75	50.0	0.17	A	RM
N22A	TA	40.802	-106.454	57	48.2	1.74	48.6	0.25	C	RM
N23A	TA	40.895	-105.944	283	51.4	1.70	50.2	0.12	B	RM

N24A	TA	40.827	-104.882	45	43.3	1.75	44.0	0.18	C	GP
N24	XK	40.210	-106.777	25	50.4	1.79	53.0	0.08	C	RM
N25A	TA	40.813	-104.087	65	43.9	1.80	47.2	0.25	C	GP
N25	XK	40.129	-106.699	54	48.0	1.90	51.1	0.13	C	RM
N26A	TA	40.829	-103.222	72	42.0	1.73	42.0	0.29	C	GP
N26	XK	40.050	-106.657	28	50.3	1.75	51.0	0.15	A	RM
NDH	XT	40.371	-108.136	28	57.6	1.69	56.4	0.08	B	RM
NEE2	CI	34.768	-114.619	544	26.0	1.76	26.5	0.24	A	BR
NEE	CI	34.825	-114.599	193	25.6	1.75	25.9	0.32	C	BR
NEE	TS	34.823	-114.596	73	25.2	1.76	25.7	0.38	C	BR
NEW	US	48.264	-117.123	742	32.9	1.74	33.1	0.10	C	RM
NLWA	US	47.392	-123.869	194	24.9	1.68	24.4	0.18	B	PB
NM08	XM	32.199	-103.972	47	39.5	1.84	45.3	0.15	C	GP
NM09	XM	32.326	-104.118	54	40.9	1.82	42.8	0.18	C	BR
NM10	XM	32.473	-104.267	68	41.2	1.75	41.7	0.17	B	BR
NM11	XM	32.584	-104.409	68	42.3	1.73	42.3	0.15	B	BR
NM12	XM	32.683	-104.508	58	42.1	1.72	41.9	0.14	B	BR
NM14	XM	32.907	-104.759	51	48.3	1.85	49.9	0.08	C	BR
NM15	XM	33.014	-104.909	102	54.9	1.76	54.9	0.07	C	BR
NM16	XM	33.174	-105.127	82	46.0	1.83	51.0	0.07	C	BR
NM17	XM	33.257	-105.173	118	44.0	1.82	49.7	0.06	C	BR
NM18	XM	33.403	-105.341	88	45.2	1.78	47.0	0.08	C	BR
NM19	XM	33.491	-105.455	67	40.6	1.81	44.9	0.11	A	BR
NM20	XM	33.605	-105.593	91	40.9	1.79	42.2	0.08	A	BR
NM21	XM	33.733	-105.745	13	40.6	1.80	42.1	0.21	A	BR
NM22	XM	33.840	-105.869	78	38.1	1.80	39.4	0.16	A	BR
NM23	XM	33.950	-106.012	73	38.3	1.74	38.4	0.16	A	BR
NM24	XM	34.047	-106.120	76	37.1	1.77	37.9	0.26	A	BR
NM25	XM	34.167	-106.260	92	35.9	1.78	37.0	0.17	A	BR
NM26	XM	34.263	-106.363	134	35.5	1.74	35.6	0.20	A	BR
NM27	XM	34.386	-106.524	103	34.9	1.76	35.5	0.12	A	BR
NM28	XM	34.540	-106.700	18	35.3	1.79	36.2	0.15	C	BR
NM31	XM	34.849	-107.098	83	38.3	1.70	36.8	0.19	A	CP
NM32	XM	34.981	-107.264	124	39.4	1.73	39.4	0.16	A	CP
NM33	XM	35.111	-107.423	87	41.8	1.72	41.6	0.26	A	CP
NM34	XM	35.269	-107.643	24	42.8	1.77	43.8	0.39	A	CP
NM35	XM	35.345	-107.707	51	43.2	1.68	42.1	0.26	B	CP
NM36	XM	35.445	-107.823	76	42.6	1.75	43.1	0.10	A	CP
NM37	XM	35.577	-108.002	52	42.9	1.78	42.9	0.13	A	CP
NM38	XM	35.702	-108.163	35	42.8	1.65	40.8	0.13	B	CP
NM39	XM	35.793	-108.267	52	45.7	1.65	40.4	0.17	C	CP
NM40	XM	35.945	-108.429	32	45.1	1.72	44.9	0.34	C	CP
NM41	XM	36.035	-108.570	31	43.9	1.71	43.7	0.25	C	CP

NM42	XM	36.148	-108.717	36	44.7	1.72	44.5	0.23	C	CP
NM43	XM	36.250	-108.887	29	46.0	1.73	46.0	0.09	C	CP
NM44	XM	36.421	-108.958	58	41.9	1.69	41.3	0.04	C	CP
O01C	TA	40.140	-123.820	13	26.9	1.65	26.0	0.39	C	PB
O02C	TA	40.177	-122.788	62	27.4	1.73	27.4	0.06	C	PB
O02D	TA	40.177	-122.788	58	28.1	1.71	27.7	0.07	C	PB
O03D	TA	40.295	-121.802	71	26.7	1.65	25.8	0.16	C	PB
O04C	TA	40.320	-121.086	190	38.2	1.65	36.6	0.22	B	SN
O05C	TA	39.962	-120.918	270	35.6	1.73	35.6	0.22	A	SN
O06A	TA	40.165	-119.827	189	30.9	1.76	31.6	0.14	C	BR
O07A	TA	40.161	-118.877	99	30.9	1.65	30.1	0.24	C	BR
O08A	TA	40.290	-118.155	217	29.3	1.73	29.3	0.11	C	BR
O09A	TA	40.170	-117.190	99	31.7	1.84	33.2	0.14	C	BR
O10A	TA	40.292	-116.500	304	28.4	1.84	23.9	0.08	A	BR
O11A	TA	40.131	-115.657	295	32.0	1.71	31.5	0.16	B	BR
O12A	TA	40.268	-114.745	160	28.7	1.74	28.8	0.35	A	BR
O13A	TA	40.131	-113.981	95	35.5	1.77	36.1	0.14	C	BR
O15A	TA	40.281	-112.469	25	29.3	1.70	29.0	0.20	B	BR
O16A	TA	40.207	-111.502	129	33.7	1.81	35.8	0.20	C	RM
O17A	TA	40.195	-110.738	83	40.4	1.75	40.7	0.15	B	CP
O18A	TA	40.265	-110.008	39	41.4	1.67	39.2	0.36	C	CP
O19A	TA	40.298	-109.124	73	54.3	1.70	53.7	0.10	C	CP
O20A	TA	40.135	-108.242	73	49.7	1.72	49.6	0.13	B	CP
O21A	TA	40.215	-107.470	116	54.1	1.76	54.8	0.18	A	RM
O22A	TA	40.162	-106.547	149	50.2	1.76	51.3	0.19	A	RM
O23A	TA	40.211	-105.918	113	42.1	1.78	43.5	0.22	A	RM
O24A	TA	40.123	-105.073	71	45.6	1.76	46.6	0.19	C	GP
O25A	TA	40.113	-104.120	62	43.1	1.75	43.5	0.22	C	GP
OCWA	US	47.749	-124.178	70	27.5	1.83	28.8	0.19	C	PB
ORD	XG	38.531	-103.707	12	43.3	1.78	44.6	0.15	A	GP
ORV	BK	39.555	-121.500	371	37.6	1.75	38.2	0.03	A	PB
OSI	CI	34.614	-118.724	460	28.3	1.85	30.0	0.08	B	PB
P01C	TA	39.469	-123.338	77	22.0	1.88	24.4	0.13	B	PB
P05C	TA	39.303	-120.608	234	39.8	1.82	42.7	0.15	B	SN
P07A	TA	39.540	-118.889	13	37.3	1.66	35.7	0.22	C	BR
P09A	TA	39.552	-117.140	152	28.3	1.83	30.5	0.21	C	BR
P10A	TA	39.620	-116.464	17	27.3	1.81	28.6	0.24	C	BR
P12A	TA	39.473	-114.908	157	28.1	1.78	29.0	0.23	C	BR
P13A	TA	39.455	-114.016	146	25.3	1.79	26.1	0.14	A	BR
P14A	TA	39.591	-113.069	185	28.5	1.79	29.4	0.21	A	BR
P15A	TA	39.571	-112.279	195	30.4	1.75	30.8	0.27	A	BR
P16A	TA	39.609	-111.660	62	38.5	1.74	38.6	0.23	A	CP
P17A	TA	39.473	-110.740	187	45.9	1.75	46.3	0.09	C	CP

P18A	TA	39.628	-110.246	100	48.0	1.72	47.4	0.13	A	CP
P19A	TA	39.633	-108.981	153	47.9	1.75	48.5	0.09	A	CP
P20A	TA	39.500	-108.391	68	40.5	1.81	44.9	0.18	B	CP
P21A	TA	39.524	-107.449	45	41.4	1.89	50.2	0.16	C	RM
P22A	TA	39.595	-106.759	117	49.9	1.71	49.4	0.20	C	RM
P23A	TA	39.374	-105.839	59	39.0	1.81	42.9	0.11	C	RM
P24A	TA	39.514	-104.908	18	42.7	1.74	42.7	0.14	C	GP
P25A	TA	39.513	-104.168	71	44.4	1.71	43.8	0.26	C	GP
P26A	TA	39.560	-103.346	64	44.1	1.69	43.2	0.31	C	GP
PACP	BK	37.008	-121.287	206	22.5	1.78	23.2	0.21	A	PB
PAR	XG	38.350	-108.983	21	42.7	1.79	44.3	0.11	C	CP
PASC	CI	34.171	-118.185	286	27.3	1.80	28.4	0.12	B	PB
PAS	CI	34.148	-118.171	384	25.2	1.80	26.7	0.19	A	PB
PAS	TS	34.148	-118.171	700	25.8	1.78	26.7	0.20	A	PB
PD31	IM	42.767	-109.558	688	36.0	1.70	35.4	0.16	B	RM
PDM	CI	34.303	-114.142	701	26.5	1.77	27.1	0.23	A	BR
PFNP	XL	34.897	-109.866	165	39.1	1.76	39.9	0.13	A	BR
PFO	II	33.609	-116.455	1429	28.5	1.72	28.2	0.20	A	PB
PFO	TS	33.609	-116.455	355	28.5	1.72	28.3	0.20	A	PB
PHL	CI	35.408	-120.546	444	23.5	1.79	24.4	0.21	A	PB
PHWY	IW	41.302	-105.458	422	46.5	1.82	53.2	0.12	B	RM
PKD	BK	35.945	-120.542	97	27.3	1.80	28.7	0.20	A	PB
PLM	CI	33.354	-116.863	917	35.1	1.74	35.4	0.31	A	PB
PMR	XT	41.084	-108.821	36	52.7	1.73	52.7	0.16	C	RM
POW	XT	40.935	-108.421	13	54.8	1.72	54.6	0.13	C	RM
Q08A	TA	38.861	-117.932	225	35.9	1.68	35.1	0.12	B	BR
Q09A	TA	38.834	-117.182	44	34.7	1.87	40.1	0.24	C	BR
Q10A	TA	38.825	-116.400	190	36.9	1.73	36.9	0.32	A	BR
Q11A	TA	38.846	-115.654	172	36.4	1.70	35.7	0.20	A	BR
Q12A	TA	39.040	-114.830	129	35.7	1.75	36.0	0.17	C	BR
Q13A	TA	38.955	-114.020	215	34.5	1.81	37.8	0.22	C	BR
Q14A	TA	38.988	-113.277	202	30.9	1.66	29.5	0.22	B	BR
Q15A	TA	39.000	-112.379	201	30.5	1.80	32.4	0.23	A	BR
Q16A	TA	38.918	-111.172	270	48.6	1.82	54.9	0.12	A	CP
Q18A	TA	39.103	-110.133	115	44.6	1.74	44.8	0.15	A	CP
Q19A	TA	38.955	-109.263	238	44.2	1.74	44.4	0.05	C	CP
Q20A	TA	38.954	-108.296	180	44.6	1.71	43.9	0.07	C	CP
Q21A	TA	38.835	-107.574	196	43.9	1.82	48.5	0.12	C	CP
Q22A	TA	38.863	-106.910	150	44.0	1.81	46.7	0.21	C	RM
Q23A	TA	38.904	-105.834	137	43.1	1.78	44.1	0.15	A	RM
Q24A	TA	38.964	-105.149	277	49.4	1.79	50.9	0.13	A	RM
Q25A	TA	38.915	-104.247	38	46.3	1.74	46.6	0.19	C	GP
Q26A	TA	38.923	-103.520	120	44.8	1.78	45.8	0.10	C	GP

R04C	TA	38.257	-120.936	393	29.6	1.80	32.9	0.03	C	PB
R05C	TA	38.703	-120.076	213	40.0	1.77	41.0	0.17	A	SN
R06C	TA	38.523	-119.451	154	42.1	1.74	42.3	0.10	C	SN
R07C	TA	38.089	-119.047	140	37.2	1.71	36.7	0.34	B	BR
R08A	TA	38.349	-118.106	70	33.8	1.79	34.9	0.38	A	BR
R09A	TA	38.240	-117.072	163	30.8	1.79	30.9	0.11	C	BR
R10A	TA	38.289	-116.302	21	30.5	1.81	31.8	0.30	C	BR
R11A	TA	38.349	-115.585	671	30.8	1.79	32.1	0.16	A	BR
R12A	TA	38.328	-114.608	107	31.1	1.77	31.6	0.23	A	BR
R13A	TA	38.180	-113.969	81	36.4	1.79	37.8	0.29	A	BR
R14A	TA	38.299	-113.021	63	30.0	1.81	31.2	0.32	A	BR
R15A	TA	38.211	-112.277	114	35.3	1.86	37.4	0.19	B	CP
R16A	TA	38.284	-111.483	185	42.6	1.73	42.6	0.07	C	CP
R17A	TA	38.419	-110.711	143	48.6	1.69	47.6	0.04	C	CP
R18A	TA	38.386	-109.894	169	42.0	1.78	43.3	0.12	A	CP
R19A	TA	38.292	-109.261	116	44.0	1.69	42.6	0.10	B	CP
R20A	TA	38.189	-108.379	151	45.7	1.74	45.9	0.16	A	CP
R21A	TA	38.368	-107.550	153	44.7	1.76	46.0	0.22	A	RM
R22A	TA	38.229	-106.756	87	42.8	1.81	44.9	0.27	B	RM
R23A	TA	38.191	-105.826	125	43.6	1.81	49.8	0.11	C	RM
R24A	TA	38.231	-105.107	147	44.9	1.78	46.0	0.18	A	GP
R25A	TA	38.147	-104.283	126	44.9	1.74	45.3	0.12	A	GP
R26A	TA	38.301	-103.447	163	46.6	1.76	47.6	0.13	A	GP
RAIO	IU	46.040	-122.885	22	44.2	1.81	46.1	0.17	C	PB
RCT	CI	36.305	-119.244	370	28.8	1.65	27.9	0.17	C	PB
RENO	XL	33.621	-109.429	109	35.6	1.79	36.7	0.22	A	BR
RKF	XG	38.073	-103.630	12	45.4	1.83	48.9	0.08	B	GP
RLMT	US	45.122	-109.267	451	50.7	1.90	54.4	0.08	C	RM
RPV	CI	33.743	-118.404	566	26.8	1.65	25.9	0.14	B	PB
RRE	XT	41.169	-108.732	31	54.8	1.72	54.4	0.22	B	RM
RRW	XT	41.139	-108.859	23	49.9	1.79	51.5	0.10	C	RM
RR	CI	34.875	-116.997	272	28.9	1.80	30.0	0.38	C	PB
RSSD	US	44.120	-104.036	139	50.4	1.74	50.5	0.07	C	GP
RWWY	IW	41.689	-107.210	208	48.3	1.71	47.8	0.26	B	RM
S01	XK	37.245	-105.463	22	45.0	1.75	45.8	0.22	A	RM
S01	XS	45.183	-109.219	20	47.6	1.73	47.6	0.09	C	RM
S02	XK	37.152	-105.453	12	42.8	1.84	44.3	0.15	C	RM
S02	XS	45.268	-108.769	83	53.1	1.72	52.8	0.12	C	RM
S03	XS	45.384	-109.434	19	42.2	1.71	41.8	0.14	C	RM
S04C	TA	37.505	-121.328	79	31.3	1.66	30.2	0.16	B	RM
S04	XS	45.384	-109.182	25	46.1	1.78	47.7	0.16	B	PB
S05B	XK	36.853	-105.406	39	46.0	1.71	45.4	0.30	B	RM
S05C	TA	37.346	-120.330	349	33.7	1.81	37.7	0.11	C	RM

S05	XK	36.878	-105.400	18	43.7	1.75	44.4	0.27	A	RM
S05	XS	45.414	-108.940	51	45.7	1.79	47.1	0.08	C	PB
S06C	TA	37.882	-119.849	254	34.7	1.68	33.7	0.03	C	RM
S06	XK	36.805	-105.303	33	43.8	1.75	44.4	0.19	A	GP
S06	XS	45.577	-108.608	75	42.6	1.79	44.0	0.05	A	SN
S07	XS	45.574	-109.744	17	41.6	1.73	41.6	0.14	A	GP
S08C	TA	37.499	-118.171	216	36.9	1.78	37.8	0.20	A	RM
S08	XK	36.614	-105.322	42	43.4	1.78	45.0	0.23	A	BR
S09A	TA	37.724	-117.225	186	32.9	1.79	33.9	0.11	A	RM
S09	XK	36.512	-105.301	60	43.2	1.77	44.2	0.18	A	GP
S09	XS	45.557	-109.201	41	49.7	1.74	49.9	0.11	C	BR
S107	XL	41.904	-108.845	24	40.3	1.76	40.8	0.12	C	RM
S109	XL	41.727	-108.918	24	39.0	1.75	39.5	0.17	C	GP
S10A	TA	37.923	-116.595	194	31.1	1.81	32.8	0.26	A	BR
S10	XK	36.439	-105.293	23	37.1	1.71	36.7	0.07	B	RM
S10	XS	45.617	-108.870	46	43.9	1.68	42.6	0.07	B	RM
S111	XL	41.539	-108.849	11	38.1	1.74	38.2	0.24	A	RM
S112	XL	41.458	-108.849	22	37.0	1.81	38.7	0.24	B	GP
S113	XL	41.368	-108.862	20	40.8	1.79	42.0	0.16	B	RM
S116	XL	41.109	-108.808	18	53.4	1.71	52.8	0.19	C	RM
S117	XL	41.016	-108.835	18	52.7	1.74	53.0	0.07	C	RM
S118	XL	40.917	-108.826	17	48.6	1.77	49.6	0.15	C	RM
S11	XK	36.339	-105.282	57	42.2	1.75	42.6	0.17	A	RM
S11	XS	45.579	-108.607	72	39.9	1.82	45.2	0.13	B	RM
S122	XL	40.598	-108.790	24	54.8	1.77	55.8	0.10	C	RM
S125	XL	40.260	-108.769	32	53.2	1.80	54.9	0.17	C	CP
S126	XL	40.189	-108.731	16	50.2	1.77	51.3	0.09	A	CP
S129	XL	39.912	-108.683	13	50.4	1.74	51.0	0.18	A	CP
S12A	TA	37.608	-114.849	127	33.0	1.76	33.6	0.15	C	BR
S130	XL	39.839	-108.774	23	52.7	1.65	50.6	0.15	C	CP
S131	XL	39.748	-108.770	26	52.0	1.76	52.6	0.09	C	CP
S134	XL	39.490	-108.774	18	45.3	1.70	44.9	0.15	A	CP
S135	XL	39.403	-108.816	27	41.8	1.74	41.9	0.17	A	CP
S137	XL	39.212	-108.774	30	40.7	1.74	40.9	0.09	A	CP
S139	XL	39.005	-108.740	34	41.5	1.77	42.4	0.08	A	CP
S13A	TA	37.581	-113.860	211	34.3	1.83	39.0	0.26	A	BR
S13	XK	36.151	-105.260	52	42.9	1.71	42.5	0.19	A	RM
S13	XS	45.745	-109.434	20	49.5	1.83	51.8	0.19	B	GP
S140	XL	38.947	-108.738	41	46.7	1.74	47.0	0.13	A	CP
S141	XL	38.883	-108.760	41	36.0	1.74	36.1	0.11	A	CP
S143	XL	38.686	-108.730	29	45.3	1.75	45.7	0.20	A	CP
S144	XL	38.604	-108.685	16	45.1	1.77	46.3	0.21	A	CP
S14A	TA	37.760	-113.168	114	38.1	1.80	46.2	0.15	C	BR

S14	XK	36.068	-105.231	39	42.7	1.72	42.3	0.29	A	RM
S14	XS	45.786	-109.185	30	54.9	1.70	50.7	0.04	C	GP
S15A	TA	37.676	-112.363	102	42.1	1.83	43.8	0.17	C	CP
S15	XK	35.969	-105.220	18	44.0	1.73	44.0	0.18	A	RM
S15	XS	45.827	-108.818	38	44.8	1.73	44.8	0.10	C	GP
S16A	TA	37.722	-111.596	99	49.1	1.77	49.9	0.18	A	CP
S16	XK	35.875	-105.204	20	44.7	1.76	45.7	0.09	A	RM
S16	XS	45.839	-108.576	38	43.6	1.65	40.9	0.12	B	GP
S17A	TA	37.635	-110.802	124	39.0	1.76	39.7	0.10	C	CP
S17	XK	35.786	-105.187	18	46.4	1.76	47.8	0.10	C	RM
S17	XS	45.800	-108.250	48	41.3	1.79	42.7	0.13	A	GP
S18A	TA	37.690	-109.995	196	40.9	1.79	40.9	0.05	C	CP
S18	XK	35.699	-105.171	37	46.6	1.74	46.8	0.09	A	RM
S18	XS	45.954	-109.498	43	45.2	1.80	50.2	0.12	B	GP
S19A	TA	37.746	-109.137	150	40.5	1.73	40.5	0.10	C	CP
S19	XK	35.596	-105.183	79	41.4	1.79	42.9	0.09	A	RM
S19	XS	46.078	-109.150	66	45.4	1.76	46.1	0.11	A	GP
S20A	TA	37.830	-108.360	122	44.5	1.78	46.1	0.22	A	CP
S20	XK	35.510	-105.217	86	45.3	1.71	44.8	0.11	C	RM
S20	XS	46.062	-108.940	52	46.7	1.71	46.3	0.12	C	GP
S21A	TA	37.662	-107.792	172	43.3	1.79	44.9	0.14	A	GP
S21	XK	35.423	-105.199	58	41.8	1.80	43.6	0.17	A	GP
S21	XS	45.950	-108.600	26	42.8	1.77	43.6	0.18	A	CP
S22A	TA	37.746	-106.829	244	46.7	1.74	46.9	0.23	A	RM
S22	XK	35.318	-105.154	80	41.6	1.76	42.1	0.16	A	GP
S22	XS	46.001	-108.290	26	35.2	1.83	39.5	0.16	B	GP
S234	XL	39.360	-108.152	10	48.3	1.71	47.8	0.22	B	CP
S23A	TA	37.706	-106.002	49	44.6	1.70	43.8	0.28	B	RM
S23	XK	35.246	-105.117	59	42.2	1.73	42.2	0.13	B	GP
S241	XL	38.843	-107.541	13	45.7	1.81	48.4	0.26	B	CP
S24A	TA	37.641	-105.213	102	43.2	1.81	46.9	0.19	A	CP
S24	XK	35.151	-105.057	42	41.2	1.76	41.8	0.16	A	GP
S25A	TA	37.661	-104.435	164	49.6	1.79	51.3	0.12	A	RM
S26A	TA	37.622	-103.471	149	39.9	1.76	40.8	0.16	A	GP
S27A	TA	37.684	-102.898	125	41.8	1.80	43.5	0.18	A	GP
SAO	BK	36.764	-121.447	151	23.9	1.91	26.8	0.11	B	PB
SBC	CI	34.441	-119.715	134	29.2	1.78	30.0	0.13	A	PB
SBC	TS	34.442	-119.713	63	30.2	1.69	29.7	0.16	B	PB
SC58	XR	32.289	-102.548	170	43.9	1.78	45.4	0.11	A	GP
SCZ2	CI	33.995	-119.635	257	32.3	1.75	32.6	0.12	C	PB
SCZ	Gy	36.598	-121.403	414	22.2	1.81	23.6	0.11	B	PB
SDCO	US	37.746	-105.501	405	43.8	1.87	46.2	0.08	B	RM
SDD	CI	33.553	-117.662	137	25.3	1.86	27.1	0.25	B	PB

SDP	CI	34.565	-120.501	10	25.2	1.65	34.8	0.18	C	PB
SGMT	Z2	45.007	-109.992	12	41.2	1.75	41.5	0.17	A	RM
SHO	CI	35.900	-116.275	450	28.0	1.75	28.4	0.26	A	BR
SLA	CI	35.891	-117.283	950	28.0	1.77	28.8	0.32	A	BR
SMCO	IW	39.178	-106.974	221	43.7	1.71	43.3	0.12	C	RM
SMM	CI	35.314	-119.996	95	26.4	1.89	32.2	0.17	B	PB
SNCC	CI	33.248	-119.524	115	27.1	1.60	25.1	0.08	B	RM
SNCC	TS	33.248	-119.524	21	26.2	1.60	24.0	0.10	B	PB
SNFF	Z2	44.153	-109.604	12	39.0	1.74	39.5	0.13	A	RM
SNP11	XE	36.699	-119.312	124	34.2	1.83	39.6	0.09	B	SN
SNP14	XE	37.140	-118.774	118	49.0	1.73	49.0	0.19	A	SN
SNP22	XE	37.011	-119.360	107	52.5	1.89	51.8	0.07	C	SN
SNP23	XE	37.123	-119.214	111	52.1	1.82	54.9	0.12	C	SN
SNP24	XE	37.280	-118.973	55	37.3	1.88	45.9	0.17	A	SN
SNP25	XE	37.359	-118.704	43	39.8	1.71	39.3	0.28	A	SN
SNP34	XE	37.391	-119.063	118	38.3	1.84	43.2	0.18	A	SN
SNP42	XE	37.246	-119.578	39	51.3	1.79	52.7	0.13	A	SN
SNP43	XE	37.413	-119.484	134	42.5	1.88	49.9	0.09	A	SN
SNP51	XE	37.253	-120.058	163	45.1	1.80	49.2	0.06	A	SN
SPR	XG	37.459	-102.640	30	43.1	1.76	43.8	0.11	A	GP
SQRL	XL	32.702	-109.891	46	28.4	1.82	30.0	0.22	A	BR
SUTB	TA	39.229	-121.786	94	39.5	1.70	38.7	0.08	B	PB
SVD	CI	34.106	-117.098	718	31.3	1.90	33.8	0.19	B	PB
SVD	TS	34.104	-117.097	83	31.5	1.88	33.7	0.23	B	PB
SWS	CI	32.945	-115.800	429	25.4	1.73	25.4	0.04	B	BR
T06C	TA	37.007	-119.709	283	43.5	1.93	46.9	0.08	B	SN
T11A	TA	37.241	-115.220	154	31.4	1.77	32.4	0.22	A	BR
T12A	TA	36.726	-114.715	163	31.7	1.71	31.3	0.14	B	BR
T13A	TA	37.020	-113.907	182	36.5	1.77	37.2	0.17	A	BR
T14A	TA	37.062	-113.084	196	45.5	1.81	50.2	0.13	B	CP
T15A	TA	37.018	-112.382	180	51.4	1.74	51.7	0.11	A	CP
T16A	TA	36.984	-111.506	117	42.7	1.75	43.1	0.01	C	CP
T17A	TA	36.997	-110.804	152	43.8	1.66	41.7	0.08	C	CP
T18A	TA	37.136	-109.874	205	41.2	1.83	43.2	0.05	C	CP
T19A	TA	36.830	-109.025	194	42.2	1.81	44.8	0.05	C	CP
T21A	TA	36.991	-107.534	85	44.2	1.85	47.3	0.14	B	CP
T22A	TA	37.014	-106.903	170	50.3	1.73	50.3	0.12	C	CP
T23A	TA	37.036	-106.037	86	43.1	1.80	44.5	0.18	B	RM
T24A	TA	37.074	-105.052	72	45.1	1.75	45.6	0.15	A	RM
T24B	TA	37.062	-105.382	26	41.9	1.80	43.3	0.21	B	RM
T25A	TA	37.139	-104.411	308	40.5	1.76	41.4	0.16	A	GP
T26A	TA	37.175	-103.593	144	37.9	1.81	41.2	0.14	A	GP
T27A	TA	37.061	-102.721	133	42.1	1.82	44.8	0.16	A	GP

T28A	TA	37.120	-102.114	143	41.9	1.76	42.8	0.14	A	GP
TASL	TA	34.945	-106.456	43	39.4	1.68	37.5	0.23	B	RM
TASM	TA	34.945	-106.460	37	39.8	1.67	37.8	0.22	B	RM
TIN	CI	37.054	-118.230	474	32.6	1.71	32.1	0.30	B	BR
TOV	CI	34.156	-118.820	141	26.9	1.68	25.9	0.13	B	PB
TPFO	TA	33.606	-116.454	67	28.7	1.72	28.5	0.22	A	PB
TPNV	US	36.949	-116.249	395	42.8	1.71	42.1	0.13	B	BR
TUC	IU	32.310	-110.785	256	30.3	1.68	29.7	0.13	B	BR
TUC	US	32.310	-110.784	84	30.1	1.69	29.7	0.11	B	BR
TUQ	CI	35.436	-115.924	764	28.1	1.71	27.8	0.22	B	BR
T01	XM	31.423	-103.105	62	41.0	1.83	46.5	0.22	C	GP
T02	XM	31.513	-103.204	22	41.0	1.83	46.1	0.24	C	GP
T03	XM	31.623	-103.324	25	41.5	1.83	46.0	0.15	C	GP
U05C	TA	36.336	-120.120	10	24.9	1.85	26.6	0.31	B	PB
U10A	TA	36.419	-116.330	122	28.7	1.76	29.2	0.30	A	BR
U11A	TA	36.423	-115.383	55	36.8	1.77	37.7	0.27	A	BR
U12A	TA	36.432	-114.539	229	33.5	1.66	32.3	0.14	B	BR
U13A	TA	36.415	-113.965	123	34.7	1.72	34.6	0.08	C	BR
U14A	TA	36.418	-113.180	206	40.0	1.78	41.1	0.20	A	CP
U15A	TA	36.428	-112.291	232	46.2	1.72	46.0	0.14	C	CP
U16A	TA	36.143	-111.130	189	48.2	1.76	48.9	0.09	C	CP
U17A	TA	36.600	-110.662	232	49.2	1.76	50.3	0.05	C	CP
U18A	TA	36.420	-109.870	149	47.3	1.74	47.6	0.11	C	CP
U19A	TA	36.292	-109.208	111	38.5	1.78	39.6	0.11	A	CP
U20A	TA	36.376	-108.520	101	39.7	1.80	43.0	0.17	A	CP
U21A	TA	36.428	-107.658	87	42.9	1.80	44.4	0.13	C	CP
U22A	TA	36.377	-106.855	106	43.4	1.77	44.9	0.17	A	CP
U23A	TA	36.329	-106.192	145	41.8	1.75	42.2	0.13	A	RM
U24A	TA	36.409	-105.278	116	43.2	1.71	42.8	0.17	B	RM
U25A	TA	36.400	-104.408	180	42.3	1.75	42.7	0.16	A	GP
U26A	TA	36.395	-103.744	166	41.6	1.78	42.7	0.11	C	GP
U27A	TA	36.421	-102.825	82	44.1	1.78	45.5	0.16	C	GP
U28A	TA	36.379	-102.224	111	46.6	1.72	46.3	0.15	A	GP
USC	CI	34.019	-118.286	60	35.5	1.66	34.1	0.10	B	PB
USC	TS	34.021	-118.287	9	34.7	1.68	33.7	0.05	B	PB
V03C	TA	36.021	-121.236	76	25.2	1.77	25.8	0.21	A	PB
V04C	TA	35.636	-120.870	124	25.0	1.69	24.3	0.29	C	PB
V11A	TA	35.838	-115.430	241	30.0	1.76	30.4	0.21	A	BR
V12A	TA	35.727	-114.851	230	29.9	1.75	30.3	0.26	A	BR
V13A	TA	35.852	-113.984	164	31.6	1.74	31.6	0.21	A	BR
V14A	TA	35.634	-113.105	222	33.8	1.78	34.5	0.12	C	CP
V15A	TA	35.819	-112.173	208	40.1	1.75	40.7	0.12	A	CP
V17A	TA	35.622	-110.794	109	49.9	1.73	49.9	0.07	C	CP

V18A	TA	35.711	-109.933	106	43.1	1.74	43.3	0.12	C	CP
V19A	TA	35.715	-109.046	218	38.7	1.76	39.6	0.09	A	CP
V20A	TA	35.799	-108.466	75	46.4	1.67	44.0	0.18	C	CP
V21A	TA	35.805	-107.638	96	43.0	1.73	43.0	0.19	C	CP
V22A	TA	35.914	-106.909	123	38.4	1.75	38.8	0.17	A	CP
V23A	TA	35.745	-106.183	37	45.4	1.76	46.2	0.15	A	BR
V24A	TA	35.726	-105.272	153	43.9	1.78	45.3	0.10	B	GP
V25A	TA	35.838	-104.616	171	43.1	1.77	44.1	0.04	A	GP
V26A	TA	35.796	-103.786	141	41.2	1.78	42.5	0.11	B	GP
V27A	TA	35.757	-102.836	107	41.7	1.80	44.8	0.11	A	GP
V28A	TA	35.750	-102.224	152	50.0	1.71	49.0	0.13	C	GP
VCS	CI	34.484	-118.118	775	30.6	1.81	31.9	0.13	A	PB
VES	CI	35.841	-119.085	188	35.9	1.74	36.1	0.27	C	PB
VMCK	XT	41.079	-108.710	28	50.2	1.79	51.0	0.14	C	RM
VMSC	XT	40.928	-108.648	21	53.8	1.69	52.6	0.26	B	RM
VTV	CI	34.561	-117.330	599	29.3	1.79	30.5	0.15	A	BR
VTV	TS	34.567	-117.333	176	29.6	1.77	30.4	0.15	A	BR
W12A	TA	35.301	-114.870	270	27.8	1.83	32.0	0.19	B	BR
W13A	TA	35.099	-113.885	405	27.6	1.78	28.3	0.27	A	BR
W14A	TA	35.213	-113.083	307	31.4	1.82	33.3	0.24	A	BR
W15A	TA	35.179	-112.267	259	35.3	1.86	37.4	0.13	C	CP
W16A	TA	35.095	-111.532	172	39.0	1.84	41.1	0.13	B	CP
W17A	TA	35.079	-110.713	215	45.5	1.77	46.4	0.09	C	CP
W18A	TA	35.118	-109.736	620	38.6	1.78	39.8	0.12	A	CP
W19A	TA	35.112	-109.388	230	40.0	1.79	41.2	0.06	C	CP
W20A	TA	35.126	-108.500	182	37.4	1.73	37.4	0.12	C	CP
W21A	TA	35.117	-107.648	128	36.5	1.75	36.7	0.09	C	CP
W22A	TA	35.072	-106.867	21	29.8	1.93	33.1	0.20	C	BR
W23A	TA	35.160	-106.150	197	40.9	1.73	40.9	0.16	A	BR
W24A	TA	35.211	-105.408	164	41.8	1.71	41.2	0.19	B	GP
W25A	TA	35.218	-104.461	144	38.6	1.83	41.3	0.12	B	GP
W26A	TA	35.089	-103.766	113	36.4	1.83	38.8	0.12	C	GP
W27A	TA	35.064	-103.063	112	41.5	1.78	42.4	0.13	C	GP
W28A	TA	35.257	-102.206	138	45.7	1.78	47.1	0.12	A	GP
WDC	BK	40.580	-122.541	166	26.0	1.72	26.0	0.15	A	PB
WDC	US	40.580	-122.540	70	26.1	1.73	26.1	0.15	A	PB
WENL	BK	37.622	-121.757	26	21.0	1.77	21.3	0.11	C	PB
WIG	XG	40.327	-104.074	15	39.2	1.75	39.7	0.33	C	GP
WSG	XG	37.777	-104.398	10	49.6	1.77	50.3	0.14	B	GP
WUAZ	US	35.517	-111.374	1060	50.0	1.74	50.4	0.10	C	CP
WVOR	US	42.434	-118.637	920	27.6	1.78	29.9	0.19	A	BR
X13A	TA	34.593	-113.830	275	26.1	1.77	26.7	0.15	A	BR
X14A	TA	34.469	-112.891	340	31.2	1.72	31.0	0.18	A	BR

X15A	TA	34.487	-112.237	291	33.4	1.78	34.5	0.26	A	BR
X16A	TA	34.418	-111.441	284	34.9	1.83	36.8	0.13	A	BR
X17A	TA	34.337	-110.806	170	38.0	1.90	40.8	0.12	B	BR
X18A	TA	34.529	-109.950	339	39.0	1.78	40.2	0.10	A	CP
X19A	TA	34.428	-109.290	245	39.4	1.78	40.4	0.11	C	CP
X20A	TA	34.542	-108.498	104	33.7	1.78	34.8	0.27	C	CP
X22A	TA	34.506	-107.010	13	32.0	1.78	32.9	0.25	C	BR
X23A	TA	34.581	-106.188	205	38.3	1.74	38.7	0.13	A	BR
X24A	TA	34.565	-105.435	175	40.0	1.78	41.0	0.06	A	GP
X25A	TA	34.527	-104.662	124	39.7	1.80	41.0	0.13	A	GP
X26A	TA	34.551	-103.810	137	45.0	1.72	44.8	0.13	C	GP
X27A	TA	34.647	-103.097	142	45.3	1.73	45.3	0.16	C	GP
X28A	TA	34.519	-102.197	112	40.1	1.89	42.7	0.07	C	GP
Y101	XC	44.007	-109.992	14	47.6	1.70	45.2	0.09	C	RM
Y12C	TA	33.750	-114.524	657	23.8	1.87	25.9	0.18	B	BR
Y13A	TA	33.814	-113.829	334	28.8	1.74	28.9	0.15	A	BR
Y14A	TA	33.938	-113.005	401	28.0	1.73	28.0	0.16	A	BR
Y15A	TA	33.953	-112.333	197	30.8	1.69	30.4	0.15	B	BR
Y16A	TA	33.880	-111.478	217	29.7	1.71	29.4	0.23	B	BR
Y17A	TA	33.695	-110.844	181	30.4	1.74	30.6	0.20	A	BR
Y18A	TA	33.778	-110.034	193	35.7	1.73	35.7	0.14	A	BR
Y19A	TA	33.957	-109.254	170	31.5	1.80	32.8	0.13	C	BR
Y20A	TA	33.909	-108.377	127	38.7	1.66	36.3	0.39	B	BR
Y20	XC	43.173	-109.996	26	46.2	1.92	49.7	0.17	C	RM
Y21A	TA	34.009	-107.674	88	36.9	1.74	37.0	0.29	A	BR
Y22A	SC	33.937	-106.965	79	34.4	1.71	34.0	0.24	A	BR
Y22A	TA	33.937	-106.965	99	33.7	1.74	33.8	0.21	A	BR
Y22C	TA	34.074	-106.921	30	32.0	1.76	33.3	0.51	C	BR
Y22D	TA	34.074	-106.921	47	31.0	1.78	32.0	0.51	C	BR
Y23A	TA	33.931	-106.055	174	37.3	1.76	38.0	0.20	A	BR
Y24A	TA	33.926	-105.436	172	46.8	1.69	45.7	0.06	C	BR
Y25A	TA	33.923	-104.693	122	46.5	1.82	52.7	0.18	A	GP
Y26A	TA	33.923	-103.825	130	46.1	1.65	41.3	0.09	C	GP
Y27A	TA	33.884	-103.163	141	47.1	1.73	47.1	0.09	B	GP
Y28A	TA	33.909	-102.248	134	43.7	1.78	45.0	0.11	A	GP
Y33	XC	43.231	-108.976	20	54.9	1.79	54.9	0.18	C	RM
Y35	XC	42.569	-108.039	37	39.0	1.73	39.0	0.18	A	RM
Y43	XC	44.453	-109.598	29	47.7	1.72	47.5	0.19	C	RM
Y44	XC	44.102	-109.189	31	48.1	1.70	47.1	0.17	C	RM
Y46	XC	43.596	-108.204	17	57.6	1.81	52.8	0.11	C	RM
Y50	XC	45.153	-108.966	30	47.9	1.79	49.9	0.14	C	RM
Y51	XC	44.770	-108.533	19	45.2	1.76	46.2	0.14	C	RM
Y64	XC	44.106	-107.474	70	38.9	1.77	39.9	0.09	C	RM

YBH	BK	41.732	-122.710	64	36.5	1.94	39.4	0.10	C	PB
YSCF	XT	40.429	-108.430	21	46.5	1.82	48.6	0.13	C	RM
Z13A	TA	33.200	-113.657	118	26.8	1.75	27.1	0.20	A	BR
Z14A	TA	33.363	-112.946	487	26.2	1.77	26.7	0.22	A	BR
Z15A	TA	33.289	-112.158	214	25.6	1.75	25.9	0.28	A	BR
Z16A	TA	33.341	-111.427	230	25.7	1.77	26.3	0.13	A	BR
Z17A	TA	33.297	-110.472	73	29.8	1.75	30.2	0.36	A	BR
Z18A	TA	33.085	-110.036	91	24.5	1.84	29.9	0.25	A	BR
Z19A	TA	33.292	-109.266	144	30.7	1.86	33.1	0.24	A	BR
Z20A	TA	33.113	-108.592	142	34.4	1.73	34.4	0.19	A	BR
Z21A	TA	33.309	-107.671	143	36.0	1.73	36.0	0.27	A	BR
Z22A	TA	33.256	-106.964	148	33.5	1.73	33.5	0.26	A	BR
Z23A	TA	33.262	-106.232	8	32.9	1.82	34.5	0.34	A	BR
Z24A	TA	33.330	-105.365	173	44.0	1.80	47.3	0.10	A	BR
Z25A	TA	33.280	-104.717	181	52.9	1.84	59.9	0.09	C	GP
Z26A	TA	33.272	-103.980	128	43.6	1.81	46.2	0.12	A	GP
Z27A	TA	33.315	-103.215	114	44.3	1.71	43.8	0.06	C	GP
Z28A	TA	33.288	-102.387	103	41.9	1.75	41.9	0.15	C	GP
ZENO	XT	40.603	-108.825	56	56.3	1.79	59.9	0.13	C	RM
ZIZZ	XL	34.262	-109.720	170	38.2	1.91	41.2	0.09	C	BR

BIBLIOGRAPHY

Allmendinger, R. W., J. W. Sharp, D. von. Tish, L. Serpa, L. Brown, S. Kaufman, and J. Oliver (1983), Cenozoic and Mesozoic structure of the eastern Basin and Range province, Utah, from COCORP seismic-reflection data, G*eology, 11*, 532-536.

Ammon, C. J. (1991), The isolation of receiver effects from teleseismic P-wave-forms, *Bull. Seismol. Soc. Am., 81*, 2504–2510.

Anderson, D, L (1989), *Theory of the Earth*, Boston: Blackwell Scientific Publications.

Andrews, M. C., W. D. Mooney, and R. P. Meyer (1985), The relocation of microearthquakes in the northern Mississippi embayment, *J. Geophys. Res., 90*, 10,223-10,236.

Atwater, T., and J. Stock (1998), Pacific-North American plate tectonics of the Neogene southwestern united States: An update, *Inter. Geol. Rev., 40*, 375-402, doi:10.1080/00206819809465213.

Audet, P., M. G. Bostock, N. I. Christensen, and S. M. Peacock (2009), Seismic evidence for overpressured subducted oceanic crust and megathrust fault sealing, *Nature, 457*, doi:10.1038/nature07650.

Bashir, L., S. S. Gao, and K. H. Liu (2011), Crustal structure and evolution beneath the Colorado Plateau and the southern Basin and Range province: Results from receiver function and gravity studies, *Geoch. Geophys. Geosys., 12*, Q06008, doi:10.1029/2011GC003563.

Bateman, P. C. (1988), Constitution and Genesis of the Central Sierra Nevada Batholith, California, *U. S. Geol. Sur. Open File Report: 88-372*, 284.

Benoit, M., A. Aguillón-Robles, T. Calmus, R. C. Maury, H. Bellon, J. Cotten, J. Bourgois, F. Michaud, (2002), Geochemical diversity of late Miocene volcanism in southern Baja California, Mexico: implication of mantle and crustal sources during the opening of an asthenospheric window, *J. Geol., 110*, 627–648.

Blümling, P., and C. Prodehl, (1983), Crustal structure beneath the eastern part of the Coast Ranges (Diablo Range) of central California from explosionseismic and near-earthquake data, *in* Ansorge, J., and Mereu, R.F., eds., *Probing the earth's lithosphere by controlled source seismology: Physics of the Earth and Planetary Interiors, 31*, 313–326.

Bohannon, R. G., and D. G. Howell (1984), Kinematic evolution of the junction of the San Andreas, Garlock, and Big Pine faults, California, *Geology, 10*, 358-363.

Bohannon, R. G., and Parsons, T. (1995), Tectonic implications of post-30 Ma Pacific and North American relative plate motions, *Geol. Soc. Am. Bul., 107,* 937-959.

Borg, L.E. (1989), Petrogenesis of Magee composite volcano, northern California, M. A. thesis, University of Texas at Austin, 128 p.

Borg, L. E., and M. A. Clynne (1998), The petrogenesis of felsic calc-alkaline magmas from the southernmost Cascades, California: Origin by partial melting of basaltic lower crust, *J. Petrology, 39(6),* 1197-1222.

Bostock, M. G., S. Rondenay, and J. Shragge (2002), Multiparameter two-dimensional inversion of scattered teleseismic body waves, 1, Theory for oblique incidence, *J. Geophys. Res., 106,* 30,771-3782.

Braile, L.W., R. B. Smith, G. R. Keller, R. M. Welch, and R. P. Meyer (1974) Crustal structure across the Wasatch Front from detailed seismic refraction studies, *J. Geophys. Res., 79,* 2669–2676, doi:10.1029/JB079i017p02669.

Braile, L. W., R. B. Smith, J. Ansorge, M. R. Baker, M. A. Sparlin, C. Prodehl, M. M. Schilly, J. H. Healy, St. Mueller and K. H. Olsen (1982), The Yellowstone-Snake River Plain seismic profiling experiment; Crustal Structure of the eastern Snake River Plain, *J. Geophys. Res., 79,* 2597-2609.

Braile, L. W., J. Hinze, R. R. B. von Frese and G. R. Keller (1989), Seismic properties of the crust and uppermost mantle of the conterminous United States and adjacent Canada. In: Pakiser, L.C. and W. D. Mooney, eds. Geophysical Framework of the Continental United States, *Mem. Geol. Soc. Am., 172,* 655-680.

Breitsprecher, K., D. J. Thorkelson, W. G. Groome, and J. Dostal, J (2003), Geochemical confirmation of the Kula–Farallon slab window beneath the Pacific Northwest in Eocene time, *Geology, 31,* 351–354.

Brewer, J. A., S. B. Smithson, J. E. Oliver, S. Kaufman, and L. D. Brown (1980), The Laramide orogeny: Evidence from COCORP deep crustal seismic profiles in the Wind River Mountains, Wyoming, *Tectonophysics, 62,* 165-189.

Brewer, J. A., R. W. Allmendinger, L. D. Brown, J. E. Oliver, and S. Kaufman (1982), COCORP profiling across the Rocky Mountains front in southern Wyoming, Part 1, Laramide structure, *Geol. Soc. Am. Bull., 93,* 1242-1252.

Brocher, T.M., P. E. Hart, W. C. Hunter, and V. E. Langenheim (1996), Hybridsource seismic reflection profiling across Yucca Mountain, Nevada—regional lines 2 and 3, *U.S. Geol. Sur.Open-File Report 96-28,* 110 p.

Brown, L. D., P. A. Krumhansl, C. E. Chapin, A. R. Sanford, F. A. Cook, S. Kaufman, J. E. Oliver, and F. S. Schilt (1979), COCORP seismic reflection studies of the Rio Grande rift, *in* Rieker, R. E., ed., *Rio Grande rift, Tectonics and magmatism,* Washington, D. C., Ammerican Geophysical Union, 169-184.

Brueseke, M., W. K. Hart, and K. Shoemaker (2004), Re-evaluating the "Ohywee-Humboldt" eruptive center: Relationship between voluminous middle Miocene silicic volcanism and the Owyhee plateau, *GSA Abstracts with Programs, 36,* 97 p.

Buck, W. R. (1991), Mode of continental lithospheric extension, *J. Geophys. Res., 96,* 20,161-20,178.

Burchfiel, B. C., and G. A. Davis (1981), Mojave desert and environs, *in* Tectonic Development of California, ed. W. G. Ernst, 21-252, Prentice-Hall, Englewood Cliffs, NJ.

Catchings, R. D., and W. M. Kohler, 1996, Reflected waves and their effect on strong shaking during the 1989 Loma Prieta Earthquake, *Bull. Seism. Soc. Am., 86,* 1401-1416.

Catchings, R. D., and W. D. Mooney (1988a), Crustal structure of the Columbia Plateau: Evidence for Continental Rifting, *J. Geophys. Res., 93,* 459-474.

Catchings, R.D., and W. D. Mooney, (1988b), Crustal structure of East-Central Oregon: relation between Newberry volcano and regional crustal structure, *J. Geophys. Res., 93,* 10,081–10,094, doi:10.1029/JB093iB09p10081.

Chan-Whan, O., and J. G. Liou (1990), Metamorphic evolution of two different eclogites in the Franciscan Complex, California, USA, *LITHOS, 25* 41-53, doi:10.1016/0024-4937(90)90005-L

Cheadle, M. J., B. L. Czuchra, T. Byrne, C. J. Ando, J. E. Oliver, L. D. Brown, S. Kaufman, P. E. Malin, and R. A. Phinney (1986), The deep crustal structure of the Mojave desert, California, from COCORP seismic reflection data, *Tectonics, 5,* 293-320.

Chen, J. H., and G. R. Tilton (1982), Application of lead and strontium isotopic relationships to the petrogenesis of granotoid rocks, central Sierra Nevada batholiths, California, *Geol. Soc. Am. Bull., 103,* 439-447.

Chevrot, S., R. D. van der Hilst (2000), The Poisson's ratio of the Australian crust: geological and geophysical implications, *Earth and Planetary Sci. Lett., 183,* 121-132.

Chamberlain, K. R., S. C. Pael, B. R. Frost, and G. Snyder (1993), Thick-skinned deformation of the Archean Wyoming province during Proterozoic arc-continent collision, *Geology, 21,* 1035-1038.

Christensen, N. I. (1996), Poisson's ratio and crustal seismology, *J. Geophys. Res., 101*, 3139-3156, doi:10.1029/95JB03446.

Christensen, N. I., and D. M. Fountain (1975), Constitution of the lower continental crust based on experimental studies of seismic velocities in granulite, *Geol. Soc. Am. Bull., 86*, 227-236.

Clarke, T. J., and P. G. Silver (1993), Estimation of crustal Poisson's ratio from broad band teleseismic data, *Geophys. Res. Lett., 20,* 241-244.

Clynne, M. A. (1990), Stratigraphic, lithologic, and major-element geochemical constraints on magmatic evlution at the Lassen volcanic center, California, *J. Geophys. Res., 95*, 19,651-19,669.

Clynne, M. A. (1993), Geologic studie of the Lassen volcanic center, Cascade Range, California, PhD. Dissertation, University of California, Santa Cruz, 404p.

Cole, R. B., and A. R. Basu (1995), Nd–Sr isotope geochemistry and tectonics of ridge subduction and middle Cenozoic volcanism in western California. *Geol. Soc. Amer. Bull. 107*, 167–179.

Cole, R.B., S. W. Nelson, P. W. Layer, and P. J. Oswald (2006), Eocene volcanism above a depleted mantle slab window in southern Alaska, *Geol. Soc. Am. Bull. 118*, 140–158.

Condie, K. C. (2011), *Earth as an Evolving Planetary System*, Second Edition, Oxford, UK, Elsevier.

Coney, P. J., D. L. Jones, and J. W. H. Mogner (1980), Cordilleran suspect terranes, *Nature, 288,* 329-333.

Cox, C., and G. R. Keller, (2010), Crustal structure of the High Lava Plains of the Pacifi c Northwest—Source seismic and gravity modeling, *American Geophysical Union Fall Meeting 2010*, abs. T41E–07.

Daly. E., D. Keir, C. J. Ebinger, G. W. Stuart, I. D. Bastow, and A. Ayele (2008), Crustal tomographic imaging of a transitional continental rift: The Ethiopian rift, *Geophys. J. Inter., 172,* 1033-1048, doi:10.1111/j.1365-246X-2007.03682.x.

de Voogd, B., L. Serpa, and L. Brown (1988), Crustal extension and magmatic processes: COCORP profiles from Death Valley and the Rio Grande rift, *Geol. Soc. Am. Bull., 100*, 1550–1567.

Dickinson, W. R., and W. S. Snyder (1979), Geometry of subducted slabs related to San Andreas transform, *J. Geol. 87*, 609–627.

du Bray, E. A., and D. A. John (2011), Petrologic, tectonic, and metallogenic evolution of the Ancestral Cascades magmatic arc, Wachington, Oregon, and northern California, *Geosphere, 5(7),* 1102-1133, doi: 10.1130/GES00669.1.

Dueker, K. G., and A. F. Sheehan (1998), Mantle discontinuity structure beneath the Colorado Rocky Mountains and High Plains, *J. Geophys. Res., 103*, 7153–7169.

Eagar, K.C., M. J. Fouch, D. E. James, and R. W. Carlson (2011), Crustal structure beneath the High Lava Plains of eastern Oregon and surrounding regions from receiver function analysis, *J. Geophys. Res., 116*, B02313, doi: 10.1029/2010JB007795.

Egorkin, A. V. (1998), Velocity structure, composition and discrimination of crustal provinces in the former Soviet Union, *Tectonophysics, 298,* 395-404.

Erkan, K., and D. D. Blakcwell (2008), A thermal test of the post-subduction tectonic evolution along the California transform margin, *Geophys. Res. Lett., 35,* doi: 10.1029/2008GL033479.

Erslev, E. A. (2005), 2D Laramide geometries and kinematics of the Rocky Mountain Region, *in* Karlstrom, K. E. and Keller, G. R., eds, *The Rocky Mountain Region-An Evolving Lithosphere: Tectonic,Geochemistry, and Geophysics,* 7-20, American Geophysical Union, Washington, DC.

Faulds, J. E., and R. J. Varga (1998), The role of accomodation zones and transfer zones in the regional segmentation of extended terranes, *in* Fauds, J. E., and Stewart, J. H., *eds*., Accomodation Zones and Transfer Zones: The Regional Segmentation of the Basin and Range Province, *Geol. Soc. Am., Special Paper 323*, 1-45.

Fliedner, M.M., S. L. Klemperer, and N. I. Christensen (2000), Three-dimensional seismic model of the Sierra Nevada arc, California, and its implications for crustal and upper mantle composition, *J. Geophys. Res., 105*, 10,899–10,921, doi:10.1029/2000JB900029.

Frassetto, A., H. Gilbert, G. Zandt, S. Beck, and M. J. Fouch (2006), Support of high elevation in the southern Basin and Range based on the composition and architecture of the crust in the Basin and Range and Colorado Plateau, *Earth Planet. Sci. Lett., 249*, 62-73.

Frassetto, A.M., G. Zandt, H. Gilbert, T. J. Owens, T.J., and C. H. Jones, (2011), Structure of the Sierra Nevada from receiver functions and implications for lithospheric foundering, *Geosphere*, *7*, 898–921, doi: 10.1130 /GES00570.1.

Fuis, G.S., J. J. Zucca, W. D. Mooney, and B. Milkereit (1987), A geologic interpretation of seismic-refraction results in northeastern California, *Geol. Soc. Am. Bull., 98*, 53–65, doi:10.1130/0016-7606(1987)98.

Fuis, G.S., T. Ryberg, N. J. Godfrey, D. A. Okaya, and J. M. Murphy (2001), Crustal structure and tectonics from the Los Angeles basin to the Mojave Desert, southern California, *Geology, 29*, 15–18, doi:10.1130/0091-7613(2001)029.

Furlong, K.P., and S. Y. Schwartz (2004), Influence of the Mendocino Triple Junction on the tectonics of coastal California, *Annu. Rev. Earth Planet. Sci., 32*, 403–433.

Gao, S. S., P. G. Silver, K. H. Liu, and Kaapvaal Seismic Group (2002), Mantle discontinuities beneath Southern Africa, *Geopys. Res. Lett., 29(10)*, 1491, doi:10.1029/2001GL013834.

Gao, S. S., K. H. Liu, and C. Chen (2004), Significant crustal thinning beneath the Baikal rift zone: New constraints from receiver function analysis, *Geophys. Res. Lett., 31*, L20610, doi:10.1029/2004GL020813.

Gao, S. S., and K. H. Liu (2014), Mantle transition zone discontinuities beneath the contiguous United States, *J. Geophys. Res., 119*, 6452-6468, doi:10.1002/2014JB011253.

Gerdom, M., A. M. Tre'hu, E. R. Flueh, and D. Klaeschen, (2000), The continental margin off Oregon from seismic investigations, *Tectonophysics, 329*, 79–97, doi:10.1016/S0040-1951(00)00190-6.

Gilbert, H. J., A. F. Sheehan, K. G. Dueker, and P. Molnar (2003), Receiver functions in the western United States, with implications for upper mantle structure and dynamics, *J. Geoph, Res., 108,* B5, 2229, doi:10.1029/2001JB001194.

Gilbert, H. (2012), Crustal structure and signatures of recent tectonism as influenced by ancient terranes in the western United States, *Geol. Soc. Am., 8*, 1, 141-157, doi:10.1130/GES00720.1.

Gilbert, H., and A. F. Sheehan (2004), Images of crustal variations in the intermountain west, *J. Geophys. Res., 109*, B03306, doi:10.1029/2003JB002730.

Gilbert, H., A. A. Velasco, and G. Zandt (2007), Preservation of Proterozoic terrane boundaries within the Colorado Plateau and implications for its tectonic evolution, *Earth Planet. Sci. Lett, 258*, 237-248.

Gish, D. M, G. R. Keller, and M. L. Sbar (1981), A refraction study of deep crustal structure in the Basin and Range: Colorado Plateau of eastern Arizona, *J. Geophys. Res., 86*, 6029-6038.

Gorman, A. R., R. M. Clowes, R. M. Ellis, T. J. Henstock, G. D. Spence, G. R. Keller, A. Levander, C. M. Snelson, M. J. A. Burianyk, E. R. Kanasewich, I. Asudeh, Z. Hajnal, and K. C. Miller (2002), Deep Probe; imaging the roots of western North America, *Canadian Journal of Earth Sciences, 39(3)*, 375-398, doi:10.1139/e01-64.

Green, A. R. (1977), The evolvution of the Earth's crust and sedimentary basin development, *in* Heacock, J. G. ed., *The Earth's crust: Its nature and physical properties*, AGU, Geophysical Monograph, Washington, D.C.

Hamilton, R. M. (1986), Seismic reflection studies by the U.S. Geological Survey, *in* Barazangi, M., and Brown, L., eds., *Reflection seismology: a global perspective*, American Geophysical Union, Geodynamics Series, 13, 99–106.

Hamilton, W. (1989), Crustal geologic processes of the United States, *in* Pakiser, L. C., and Mooney, W. D., eds., *Geophysical framework of the continental United States, Geol. Soc. Am. Memoir*, 172, 743-781.

Hammond, W. C. (2004), Vertical motion of the Basin and Range, western United States from 10 Years of Campaign GPS, Cahiers du Centre Europeen de Geodynamique et de Seismologie, Proceedings of the workshop: *The state of GPS vertical positioning precision: Separation of earth processes by space geodesy*, ed T. van Dam, 23, 131-136.

Hansen, S., and K. Dueker (2009), P- and S-wave receiver function images of crustal imbrication beneath the Cheyenne Belt in southeast Wyoming, *Seism. Soc. Am. Bull., 99*, 1953–1961, doi: 10.1785/0120080168.

Hansen, S., J. Stachnik, and K. Dueker, (2011), Lithospheric structure of the Colorado Rockies from CREST and TA seismic data, *Geophys. Res. Abs., 13*, EGU2011-13560, 13.

Hauser, E. C., and J. Lundy (1987), COCORP deep reflections: Moho at 50 km (16s) beneath the Colorado Plateau, *J. Geophys. Res., 94*, 7071-7081.

Hauser, E. C., J. Gephart, L. Latham, L. D. Brown, S. Kaufman, J. E. Oliver, and I. Lucchitta (1987a), COCORP Arizona transect: strong crustal reflections and offset Moho beneath the transition zone, *Geology*, *15*, 1103–1106, doi:10.1130/0091-7613(1987)15.

Hauser, E. C., C. Potter, T. Hauge, S. Burgess, S. Burtch, J. Mutschler, R. Allmendinger, L. Brown, S. Kaufman, and L. Oliver (1987b), Crustal structure of eastern Nevada from COCORP deep seismic reflection data, *Geol. Soc. Am. Bull., 99*, 833–844, doi:10.1130/0016-7606(1987)99.

Heacock, G, (1977), *The Earth's crust: Its nature and physical properties*, AGU, Washington D. C.

Henstock, T.J., and A. Levander (2000), Lithospheric evolution in the wake of the Mendocino Triple Junction: structure of the San Andreas fault system at 2 Ma, *Geophys. J. Inter., 140*, 233–247, doi:10.1046/j.1365-246x.2000.00010.x.

Henstock, T.J., A. Levander, and J. A. Hole (1997), Deformation in the lower crust of the San Andreas fault system in northern California, *Science, 278*, 650–653, doi:10.1126/science.278.5338.650.

Henstock, T. J., A. Levander, C. M. Snelson, G. R. Keller, K. C. Miller, A. R. Gorman, R. M. Clowes, M. J. Burianyk, and E. D. Humphreys (1998), Probing the Archean ans Proterozoic Lithosphere of Western North America, *GSA Today, 8,* 1-5.

Hill, D. P., and L. C. Pakiser (1966), Crustal structure between Nevada Test Site and Boise, Idaho, from seismic-refraction measurements, *in* Steinhart, J. S., and Smith, T. J., eds., The earth beneath the continents, *American Geophysical Union, 10*, 391-419.

Hoffman, L.R., and W. D. Mooney (1983), A seismic study of Yucca Mountain and vicinity, southern Nevada; data report and preliminary results, *U. S. Geol. Sur. Open-File Report 83-588*, 50 p.

Hoffman, P. F. (1988), United Plates of America, birth of a craton: Early Proterozoic assembly and growth of Laurentia, *Ann. Rev. Earth and Planetary Sci., 66*, 543-603.

Holbrook, W. S., and W. D. Mooney (1987), The crustal structure of the axis of the Great valley, California, from seismic refraction measurements, *Tectonics,* 1*40*, 49-63.

Holbrook, W. S., D. Gajewski, A. Krammer, and C. Prodehl (1988), An interpretation of wide-angle compressional and shear wave data in southwest Germany: Poisson's ratio and petrological implications, *J. Geophys. Res., 93,* 12,081-12,106.

Holbrook, W.S., T. M. Brocher, U. S. ten Brink, and J. A. Hole (1996), Crustal structure of a transform plate boundary: San Francisco Bay and the central California continental margin, *J. Geophys. Res., 101,* 22,311–22,334, doi:10.1029/96JB01642.

Hole, J. A., T. M. Brocher, S. L. Klemperer, T. Parsons, H. M. Benz, and K. P. Furlong (2000), Three-dimensional seismic velocity structure of the San Francisco Bay area, *J. Geophys. Res., 105*, 13,859– 13,874, doi:10.1029/2000JB900083.

Ichinose, G., S. Day, H. Magistrale, T. Prush, F. Vernon, and A. Edelman (1996), Crustal thickness variations beneath the peninsular ranges, southern California, *Geophys. Res. Lett., 23*, 3095-3098.

Jackson, W. H., S. W. Stewart, and L. C. Pakiser (1963), Crustal structure in the eastern Colorado from seismic-refraction measurements, *J. Geophys. Res., 68*, 5767-5776.

Johnston, S.T., and D. J. Thorkelson (1997), Cocos–Nazca slab window beneath Central America, *Earth Planet. Sci. Lett., 146*, 465–474.

Karlstrom, K.E., and the CDROM Working Group (2002), Structure and evolution of the lithosphere beneath the Rocky Mountains: Initial results from the CD-ROM Experiment, *GSA Today, 12*, 4–10, doi: 10.1130/1052-5173(2002)012.

Karlstrom, K.E., and E. D. Humphreys (1998), Persistent influence of Proterozoic accretionary boundaries in the tectonic evolution of southwestern North America: Interaction of cratonic grain and mantle modification events, *Rocky Mountain Geology, 33*, 161–179.

Karlstrom, K. E, S. T. Whitmeyer, K. Dueker, M. J. Williams, S. A. Bowring, A. Levander, E. D. Humphreys, G. R. Keller, and the CD-ROM Working Group (2005), Synthesis of results from the CD-ROM experiment; 4-D image of the lithosphere beneath the Rocky Mountains and implications for understanding the evolution of continental lithosphere, *in* Karlstrom, K. E., and Keller, G. R., eds., *The Rocky Mountain Region: An Evolving Lithosphere, Geophysical Monograph Series, 154*, AGU, Washington , DC, 10.1029/154GM30, 421-441.

Keach, R. W., J. E. Oliver, L. D. Brown, and S. Kaufman, Cenozoic active margin and shallow Cascades structure: COCORP results from western Oregon, *Geol. Soc. Am. Bull., 101*, 783– 794, 1989.

Keller, G. R. (2013), The Moho of the North America: A Brief Review Focused on Recent Studies, *Tectonophysics,* doi: 10.1016/j.tecto.2013.07.031.

Keller, G. R., R. B. Smith, and L. W. Braile (1975), Crustal structure along the Great Basin-Colorado Plateau transition from refraction studies, *J. Geophys. Res., 80*, 1093-1098.

Keller, G. R., L.W. Braile, and J. W. Schule (1979), Regional crustal structure of the Rio Grande rift from surface wave dispersion measurements, *in* Riecker, R. E., ed., *Rio Grande rift; tectonics and magmatism,* Washington, DC., AGU, Special Publication, 115-126.

Keller, G.R., K. E. Karlstrom, and G. L. Farmer (1999), Tectonic evolution in the Rocky Mountain region: 4-D imaging of the continental lithosphere, *Eos (Transactions, American Geophysical Union), 80*, 493, 495, 498.

Kern, H. (1982), P- and S- wave velocities in crustal and mantle rocks under the simultaneous action of high confining pressure and high temperature and the effect of the rock microstructure, in *High-Pressure Researchers in Geosciences,* edited by W. Schreyer, 15-45, E. Schweizerbart sche, Stuttgard, Germany.

Koulakov, I., E. I. Gordeev, N. L. Dobretsov, V. A. Vernikovsky, S. Senyukov, and A. Jakovlev (2011), Feeding volcanoes of the Kluchevsoy group from results of local earthquake tomography, *Geophys. Res. Lett.s*, *38*, L09305, doi:10.1028/2011GL046957.

Kluth, C. F., and P. J. Coney (1981), Plate tectonics of the Ancestral Rocky Mountains, *Geology, 9*, 10-15.

Langston, C. A. (1977), Corvallis, Oregon, crustal and upper mantle structure from teleseismic P and S waves, *Bull. Seism. Soc. Am., 67,* 713-724.

Langston, C.A. (1979), Structure under Mount Rainier, Washington, inferred from teleseismic body waves, *J. Geophys. Res. 84*, 4749–4762.

Latham, T. S, J. Best, T. Chaimov, J. Oliver, L. Brown, and S. Kaufman (1988), COCORP profiles from Montana plains: the Archean cratonic crust and lower crustal anomaly beneath the Williston basin, *Geology, 16*, 1073-1076.

Leaver, D. S., W. D. Mooney, and W. M. Kohler (1984), A seismic refraction survey of the Oregon Cascades, *J. Geophys. Res., 89*, 3121-3134.

Leitner, B., A. M. Trehu, and H. J. Godfrey (1998), Crustal structure of the northwestern Vizcaino block and Gorda Escarpment, offshore northern California, and implications for postsubduction deformation of a paleoaccretionary margin, *J. Geophys. Res., 103*, 23,795–23,812, doi:10.1029/98JB02050.

Levander, A., T. J. Henstock, A. S. Meltzer, B. C. Beaudoin, A. M. Trehu, and S. L. Klemperer (1998), Fluids in the lower crust following Mendocino Triple Junction migration: active basaltic intrusion? *Geology, 26*, 171–174.

Ligorria, J. P., and C. J.Ammon (1999), Iterative deconvolution and receiver-function estimation, *Bull. Seismol. Soc. Am., 89(5),* 1395-1400.

Liu, K. H., S. S. Gao, P. G. Silver, and Y. Zhang (2003), Mantle layering across central South Africa, *J. Geophys. Re., 108(B11),* 2510, doi:10.1029/2002JB002208.

Liu, K. H., and S. S. Gao (2006), Mantle transition zone discontinuities beneath the Baikal rift and adjacent areas, *J. Geophys. Res., 111,* B11301, doi:10.1029/2005JB004099.

Liu, K. H., and S. S. Gao (2010), Spatial variations of crustal characteristics beneath the Hoggar swell, Algeria revealed by systematic anayles of receiver functions from a single station, *Geochem. Geophys. Geosyst., 11*, Q08011, doi:10.1029/2010GC003091.

Magnani, M.B., A. Levander, K. C. Miller, T. Eshete, and K. E. Karlstrom (2005), Seismic investigation of the Yavapai–Mazatzal transition zone and the Jemez lineament in northern New Mexico, *in* Karlstrom, K.E., and Keller , G.R., eds., *The Rocky Mountain Region: An evolving lithosphere—tectonics, geochemistry, and geophysics,* Washington, D.C., American Geophysical Union Geophysical Monograph 154, 227–238.

McCamy, K., and R. P. Meyer (1964), A correlation method of apparent velocity measurement, *J. Geophys. Res., 69*, 691-699.

McCarthy,J ., S. P. Larkin, G. S. Fuis, R. W. Simpsona, and K. A. Howard (1991), Anatomy of a metamorphic core complex: Seismic refraction/wide-angle reflection profiling in southeastern California and western Arizona, *J. Geophys. Res.., 96*, 12,259-12,291.

McCrory, P. A., D. S. Wilson, and R. G. Stanley (2009), Continuing evolution of the Pacific-Juan de Fuca-Norht America slab window system- A trench-rdge-transform example from the Pacific Rim, *Tectonophysics, 464*, 30-42.

Miller, K.C., G. R. Keller, J. M. Grindley, J. H. Luetgert, W. D. Mooney, and H. Thybo, (1997), Crustal structure along the west fl ank of the Cascades; western Washington, *J. Geophys. Res., 102*, 17,857–17,873, doi:10.1029/97JB00882.

Mitchell, B. J., and M. Landisman (1970), Interpretation of crustal section across Oklahoma, *Geol. Soc. Am. Bull., 81*, 2647-2656.

Moidaki, M., S. S. Gao, K. H. Liu, and E. Atekwana (2013), Crustal thickness and Moho sharpness beneath Midcontinent rift from receiver functions, *Research in Geophysics*, doi: 10.4081/rg.2013.e1.

Mooney, W. D., and C. S. Weaver (1989), Regional crustal structure and tectonics of the Pacific Coastal States; California, Oregon, and Washington, *Geophysical Framework of the Continental United States, Geol. Soc. Amer. Mem. 172,* Boulder, CO, 129-161.

Mooney, W. D., G. Laske, and T. G. Masters (1998), CRUST 5.1: A global crustal model at 5^0x5^0, *J. Geophys. Res., 13*, B1, 727-747.

Morozova, E.A., X. Wan, K. R. Chamberlain, S. B. Smithson, R. Johnson, and K. E. Karlstrom, (2005), Inter–wedging nature of the Cheyenne belt—Archean - Proterozoic suture defi ned by seismic refl ection data, *in* Karlstrom, K.E., and Keller, G.R., eds., *The Rocky Mountain Region: An evolving lithosphere—tectonics, geochemistry, and geophysics*, Washington, D.C., American Geophysical Union Geophysical Monograph 154, 217–226.

Nair, S. K., S. S. Gao, K. H. Liu, and P. G. Silver (2006), Southern African crustal evolution and composition: Constraints from receiver function studies, *J. Geophys. Res., 111***,** B02304, doi:101029/2005JB003802.

Nicolas, A. (1985), Novel type of crust produced during continental rifting, *Nature, 315,* 112-115.

Oliver, J.E., and S. Kaufman (1976), Profiling the Rio Grande rift, *Geotimes, 21,* 20–23.

Olsen, K. H. (1983), The role of seismic refraction data for studies of the origin and evolution of continental rifts, *Tectonophysics, 94,* 349-370, doi:10.1016/0040-1951(83)90024-0.

Olsen, K. H., G. R. Keller, and J. N. Stewart (1979), Crustal structure along the Rio Grande Rift from seismic refraction profiles, *in* Riecker, R. E., ed., *Rio Grande rift: tectonics and magmatism,* Washington, DC, AGU, 127-144.

Owens, T. J., G. Zandt, and S. R. Taylor (1984), Seismic evidence for an ancient rift beneath the Cumberland Plateau, Tennessee: A detailed analysis of broadband teleseismic P waveforms, *Journal of Geophsyical Research, 89,* 7783-7795.

Pakiser, L.C. (1963), Structure of the crust and upper mantle in the western United States, *J. Geophys. Res., 68,* 5747–5756.

Pakiser, L. C. (1985), Seismic exploration of the crust and upper mantle of the Basin and Range province: Boulder, Colorado, *Geol. Soc. Am.,* The geology of North America Centennial Special Volume 1, 453-468.

Pakiser, L. C. (1989), Geophysics of the Intermontane system, *in,* Pakiser, L. C., and Mooney, W. D., *Geophysical framework of the continental United States,* Boulder, Colorado, Geol. Soc. Am. Memoir, 172.

Pakiser, L. C., and J. N. Brune (1980), Seismic models of the root of the Sierra Nevada, *Science, 210,* 1088-1094.

Paine, J. G. (1982), Crsutal structure of volcanic arcs based on physical properties of andesites, volcanoclastic rocks, and inclusions in the Mt. St. Helen lava dome: Seattle, University of Washington, M. S. thesis, 138p.

Parsons, T. (1995), The Basin and Range Province, *in* K. H. Olsen, *Continental rifts: evolution, structure, tectonics,* Elsevier Science B.V., Amsterdam, The Netherlands.

Parsons, T., and M. L. Zoback (1997), Three-dimensional upper crustal velocity structure beneath San Francisco Peninsula, California, *J. Geophys. Res., 102,* 5473–5490, doi:10.1029/96JB03222.

Parsons, T., A. M. Trehu, J. H. Luetgert, K. C. Miller, F. Kilbride, R. E. Wells, M. A. Fisher, E. Flueh, U. S. ten Brink, and N. I. Christensen, (1998), A new view into the Cascade subduction zone and volcanic arc: implications for earthquake hazards along the Washington margin, *Geology, 26,* 199–202, doi:10.1130/0091-7613(1998)026.

Parsons, T., R. E. Wells, A. M. Trehu, M. A. Fisher, E. Flueh, E., and U. S. ten Brink, (1999), Three-dimensional velocity structure of Siletzia and other accreted terranes in the Cascadia forearc of Washington, *J. Geophys. Res., 104*, 18,015–18,039, doi:10.1029/1999JB900106.

Parsons, T., R. J. Blakely, T. M. Brocher, N. I. Christensen, M. A. Fisher, E. Flueh, F. Kilbride, J. H. Luetgert, K. Miller, U. S. ten Brink, A. M. Trehu, and R. E. Wells (2005),Crustal structure of the Cascadia fore arc of Washington, *U.S. Geol. Sur.Professional Paper 1661-D*, 45 pp.

Peng, X. H., ad E. D. Humphreys (1998), Crustal velocity structure across the eastern Snake River Plain and the Yellowstone swell, *J. Geophys. Res., 103*, 7171–7186.

Phinney, R. A. (1964), Structure of the Earth's crust from spectral behavior of long-period body waves, *J. Geoph. Res., 69*, 14, 2997-3017.

Prodehl, C. (1979), Crustal structure of the western United States, *U. S. Geol. Sur.Professional Paper 1034.*

Prodehl, C., and P. W. Lipman (1989), Crustal structure of the Rocky Mountain region, *in*, Pakiser, L. C., and Mooney, W. D., *Geophysical framework of the continental United States*, Boulder, Colorado, Geol. Soc. Am. Memoir, 172.

Purevsuren, U. (2010), Gravity and magnetic analysis of the lithospheric structure of the southern Sierra Nevada and surrounding regions, California and Nevada, *M. S. Thesis*, Springfield, MO.

Ramesh, D. S., R. Kind, and X. Yuan (2002), Receiver function analysis of the North American crust and upper mantle, *Geophys. J. Int, 150*, 91-108.

Roller, J. C. (1965), Crustal structure in the eastern Colorado Plateau province from seismic-refraction measurements, *Bull. Seismol. Soc. Am., 55*, 107-119.

Rondenay, S., M. G. Bostock, and J. Shragge (2002), Multiparameter two-dimensional inversion of scattered teleseismic body waves: III — Application to the Cascadia 1993 data set, *J. Geophys. Res., 106*, 30,795-30,808.

Rumpfhuber, E.-M., and G. R. Keller, (2009), An integrated analysis of controlled and passive source seismic data across an Archean-Proterozoic suture zone in the Rocky Mountains, *J. Geophys. Res., 114*, B08305, doi: 10.1029/2008JB005886.

Rumpfhuber, E.-M., G. R. Keller, E. Sandvol, A. A. Velasco, and D. C. Wilson (2009), Rocky Mountain evolution: Tying continental dynamics of the Rocky Mountains and Deep Probe seismic experiments with receiver functions, *J. Geophys. Res., 114*, B08301, doi:10.1029/2008JB005726.

Ruppert, S., M. M. Fliedner, M.M., and G. Zandt (1998), Thin crust and active upper mantle beneath the southern Sierra Nevada in the western United States, *in* Klemperer, S.L., and Mooney, W.D., eds., Deep seismic probing of the continents, I: general results and new methods, *Tectonophysics, 286,* 237–252.

Saleeby, J. (2003), Segmentation of the Laramide Slab-evidence from the southern Sierra Nevada region, *Geol. Soc. Am. Bull., 115,* 655-668, doi:10.113/0016-7606(2003).

Schultz, A. P., and R. S. Crosson (1996), Seismic velocity structure across the central Washington Cascade Range from refraction interpretation with earthquake sources, *J. Geophys. Res., 10,* 27,899–27,915, doi:10.1029/96JB02289.

Schutt, D. L., K. Dueker, and H. Yuan (2008), Crust and mantle velocity structure of the Yellowstone hot spot and surroundings, *J. Geoph. Res., 113,* B03310, doi:10.1029/2007JB005109.

Severinghaus, J., and T. Atwater (1990), Cenozoic geometry and thermal state of the subducting slabs beneath western North America, *in* Wernicke, B.P. (Ed.), *Basin and Range Extensional Tectonics Near the Latitude of Las Vegas, Nevada*. Geol. Soc. Am. *Memoir, 176,* 1-22.

Sheehan, A. F., G. A. Abets, H. Jones, and A. L. Lerner-Lam (1995), Crustal thickness variations across the Colorado Rocky Mountains from teleseismic receiver functions, *J. Geophys. Res., 100***,** B10, 20, 391-20,404.

Sheehan, A.F., C. H. Jones, M. K. Savage, S. Ozalaybey, and J. M. Schneider (1997), Contrasting lithospheric structure beneath the Colorado Plateau and Great Basin: initial results from Colorado Plateau — Great Basin PASSCAL experiment, *Geophys. Res. Lett.s 24*, 2609–2612.

Sheriff, R. E., and L. P. Geldart (1993), *Exploration Seismology*, 2nd ed., Cambridge Univ. Press, New York.

Sinno, Y.A., P. H. Daggett, G. R. Keller, P. Morgan, and S. H. Harder (1986), Crustal structure of the southern Rio Grande rift determined from seismic refraction profiling, *J. Geophys. Res., 91,* 6143–6156.

Sloss, L. L. (1988), Tectonic evolution of the craton in Phanerozoic time, *in* Sloss, L. L., ed., *Sedimentary Cover - North America Craton; U. S.,* Boulder, Colorado, Geol. Soc. Am., The Geology of North America, D-2.

Smith, R.B., M. M. Schilly, L. W. Braile, J. Ansorge, J. L. Lehmann, M. R. Baker, C. Prodehl, J. H. Healy, St. Mueller, and R. W. Greensfelder (1982), The 1978 Yellowstone–eastern Snake River Plain seismic profiling experiment: Crustal structure of the Yellowstone region and experiment design, *J. Geophys. Res., 87*, 2583–2596, doi:10.1029/JB087iB04p02583.

Smithson, S.B., J. A. Brewer, S. Kaufman, J. E. Oliver, and C. A. Hurich, C.A. (1979), Structure of the Laramide Wind River uplift, Wyoming, from COCORP deep reflection data and from gravity data, *J. Geophys. Res., 84*, 5955–5972, doi:10.1029/JB084iB11p05955.

Snelson, C.M., T. J. Henstock, G. R. Keller, K. C. Miller, and A. Levander (1998), Crustal and uppermost mantle structure along the deep probe seismic profile, *Rocky Mountain Geology, 33*, 181–198, doi: 10.2113/33.2.181.

Snelson, C. M., G. R. Keller, K. C. Miller, H. M. Rumpel, and C. Prodehl (2005), Regional crustal structure derived from the CD-ROM 99 seismic refraction/wide-angle reflection profile: the lower crust and upper mantle. In: Kalstrom, K.E., Keller, G.R. (Eds.), *The Rocky Mountain Region: An Evolving Lithosphere, Geophysical Monograph Series, 154*, AGU, Washington , DC, 10.1029/154GM30.

Spieth, M. A., D. P. Hill, and R. J. Geller (1981), Crustal structure in the northwestern foothills of the Sierra Nevada from seismic refraction experiments, *Bull. Seism. Soc. Am., 71*, 1075–1087.

Stewart, S. W. (1968), Preliminary comparison of seismic travel-times and inferred crustal structure adjacent to the San Andreas fault in the Diablo and Gabilan Ranges of central California, *in* Dickinson, W.R., and Grantz, A., eds., *Proceedings of Conference on Geologic Problems of the San Andreas Fault System*, Stanford University, School of Earth Science, 218–230.

Taber, J. J, and B. T. R. Lewis (1986) Crustal structure of the Washington continental margin from refraction data, *Bull. Seism. Soc. Am., 76*, 1011-1024.

Tarkov, A. P., and V. V. Vavakin (1982), Poisson's ratio behavior in various crystalline rocks: Application to the study of the Earth's interior, *Phys. Earth Planet. Inter., 29*, 24-29.

Thatcher, W., G. R. Foulger, B. R. Julian, J. Svarc, E. Quilty, and G. W. Bawden (1999), Present-Day Deformation Across the Basin and Range Procince, Western United States, *Science, 283*, 1714 p.

Thiruvathukal, J. V., J. W., Jr. Berg, and D. F. Heinrichs (1970), Regional gravity of Oregon, *Geol. Soc. Am. Bull, 81*, 725-738.

Thybo, H., and C. A. Nielsen (2008), Magma-compensated crustal thinning in continental rift zones, *Nature, 457*, 873-876.

Tre'hu, A. M., I. Asudeh, T. M. Brocher, J. H. Luetgert, W. D. Mooney, J. L. Nabelek, and Y. Nakamura (1994), Crustal architecture of the Cascadia forearc, *Science, 266*, 237– 243.

Varga, R. J. (1993), Rocky Mountain foreland uplifts: product of a rotating stress field or strain partitioning?, *Geology, 21,* 1115-1118, doi:10.1130/0091-7613(1993)021.

Walter, A.W., and W. D. Mooney (1982), Crustal structure of the Diablo and Gabilan Ranges, central California: a reinterpretation of existing data, *Bull. Seism. Soc. Am., 72,* 1567–1590.

Warren, D. H. (1969), A seismic-refraction survey of crustal structure in central Arizona, *Geol. Soc. Am. Bull., 80,* 257-282.

Warren, D. H. (1981), Seismic-refraction measurements of crustal structure near Santa Rosa and Ukiah, California, *in* McLaughlin, R.J., and Donnelly-Nolan, I.M., eds., *Research in The Geysers–Clear Lake Geothermal Area, Northern California*, U.S. Geol. Sur.Professional Paper 1141, 167–181.

Warren, D. H., and J. H. Healy (1973), The crust in the conterminous United States. *Tectonophysics 20,* 203–213.

Wells, R. E., D. C. Engebretson, P. D., Jr, Snavely and R. S. Coe (1984), Cenozoic plate motion and the volcano-tectonic evolution of western Oregon and Washington, *Tectonics, 3,* 275-294.

Wernicke, B., R. Clayton, M. Ducea, C. H. Jones, S. Park, S. Ruppert, J. Saleeby, J. K. Snow, L. Sqires, M. Fliedner, G. Jiracek, R. Keller, S. Klemperer, J. Luetgert, P. Malin, K. Miller, W. Mooney, H. Oliver, and R. Phinney (1996), Origin of high mountains in the continents: the southern Sierra Nevada, *Science, 271,* 190–193, doi:10.1126/science .271.5246.190.

Wernicke, B., G. J. Axen, and J. K. Snow (1988), Basin and Range extensional tectonics at the latitude of Las Vegas, Nevada, *Geol. Soc. Am. Bull., 100,* 1738-1757.

Wilson, J. M., and G. S. Fuis (1987), Data report for the Chemehuevi Vidal, and Dutch Flat lines: PACE seismic-refraction surveys, southeastern California, and western Arizona, *U.S. Geol. Surv. Open File Rep., 87-86,* 75 p.

Wilson, J. M., J. McCarthy, R. A. Johnson, and K. A. Howard (1991), An axial view of a metamorphic core complex: Crustal structure of the Whipple and Chemehuevi Mountains, southeastern California, *J. Geophys. Res., 96,* 12,293-12,3111.

Wilson, D. R., R. Aster, J. Ni. S. Grand, M. West, W. Gao, W. S. Baldridge, and S. Semken (2005), Imaging the seismic structure of the crust and upper mantle beneath the Great Plains, Rio Grande Rift, and Colorado Plateau using receiver functions, *J. Geophys. Res., 110,* B05306, doi:10.1029/2004JB003492.

Wilson, D.S., P. A. McCrory, and R. G. Stanley (2005), Implications of volcanism in coastal California for the deformation history of western North America, *Tectonics, 24*, 22.

Wolf, L. W., and J. J. Cipar (1993) ,Through thick and thin: A new model for the Colorado Plateau from seismic refraction data from Pacific to Arizona Crustal Experiment, *J. Geophys. Res., 98*, 19,881-19,894.

Xu, L., S. Rondenay, and R. D. van der Hilst (2007), Structure of the crust beneath southeastern Tibetan Plateau from teleseismic receiver functions, *Physics of Earth and Planetary Interiors, 165*, 176-193.

Yang, Y, and M, Liu (2009), Crustal thickening and lateral extrusion during the Indo-Asian collision: A 3D viscous flow model, *Tectonophysics, 465*, 128-135.

Yuan, H., K. Dueker, and J. Stachnik (2010), Crustal structure and thickness along the Yellowstone hot spot track: Evidence for lower crustal outflow from beneath the eastern Snake River Plain, *Geochem. Geophys. Geosys., 11*, doi:10.1029/2009GC002787.

Zandt, G., and C. J. Ammon (1995), Continental crust composition constrained by measurements of crustal Poisson's ratio, *Nature, 374*, 152-154.

Zandt, G., S. C. Myers, and T. C. Wallace (1995), Crust and mantle structure across the Basin and Range-Colorado Plateau boundary at 37^0N latitude and implications for Cenozoic extensional mechanism, *J. Geophys. Res., 100*, 10,529-10,548.

Zhu, L., and H. Kanamori (2000), Moho depth variation in Southern California from teleseismic receiver functions, *J. Geophys. Res., 105***,** B2, 2969-2980.

Zucca, J.J., G. S. Fuis, B. Milkereit, W. D. Mooney, and R. D. Catchings (1986), Crustal structure of northern California from seismic-refraction data, *J. Geophys. Res., 91*, 7359–7382, doi:10.1029/JB091iB07p07359.

VITA

Uranbaigal Purvsuren was born in Ulaanbaatar, Mongolia. She completed high school at Ulaanbaatar, Mongolia in 1994 and continued her studies at Mongolian University of Science and Technology (MUST), graduated in 1999 with a Bachelor of Science degree in Exploration Geophysics. She worked as a lecturer at MUST. In 2006, she joined Missouri State University and received a Master degree in Geospatial Sciences in 2010. She started her Ph.D. study at Missouri University of Science and Technology under the supervision of Dr. Stephen S. Gao and Dr. Kelly. H. Liu. She received a PhD in Geophysics in December of 2014.